8-12-2016

Optical Property Enhancement And Characterization Of Fluorescent Protein Based Intracellular Calcium Probes

Demesheka Goolsby
dgoolsby1@gsu.edu

OPTICAL PROPERTY ENHANCEMENT AND CHARACTERIZATION OF FLUORESCENT PROTEIN BASED INTRACELLULAR CALCIUM PROBES

by

DEMESHEKA GOOLSBY

Under the Direction of Jenny J. Yang PhD

ABSTRACT

Calcium (Ca^{2+}), a crucial effector for many biological systems, has been associated with diseases such as cardiovascular disease, Alzheimer's, Parkinson's, cancer, and osteoporosis. It is important to develop calcium sensors to measure intracellular Ca^{2+} dynamics at various biological and pathological states. Our lab has engineered such probes by designing a Ca^{2+} binding site into fluorescent proteins such as Enhanced Green Fluorescent Protein (EGFP) and mCherry. In this thesis, we aim to improve optical properties and metal binding properties of green EGFP-based sensor CatchER and mCherry based red sensors by site-directed mutagenesis and protein engineering, various spectroscopic methods and cell imaging. The green EGFP-based sensor CatchER, with a Ca^{2+} binding pocket charge of -5, displays the greatest affinity for Ca^{2+} and has the greatest fluorescence intensity change with Ca^{2+} when compared to its variants with a less negative binding pocket charge. In addition, we have also designed several SR/ER targeting CatchER variants using Ryanodine receptor and Calnexin transmembrane domains. These constructs were shown to display a strong presence in the SR/ER lumen and further designed for

a new luminal orientation. Further, we have shown that the optical properties of two red calcium sensors can be significantly improved by modifying the local environment of the chromophore.

INDEX WORDS: Fluorescence, mCherry, EGFP, Calcium imaging, Fluorescence spectroscopy, Fluorescence lifetime

OPTICAL PROPERTY ENHANCEMENT AND CHARACTERIZATION OF FLUORESCENT PROTEIN BASED INTRACELLULAR CALCIUM PROBES

by

DEMESHEKA GOOLSBY

A Thesis Submitted in Partial Fulfillment of the Requirements for the Degree of

Master of Science

in the College of Arts and Sciences

Georgia State University

2016

OPTICAL PROPERTY ENHANCEMENT AND CHARACTERIZATION OF FLUORESCENT PROTEIN BASED INTRACELLULAR CALCIUM PROBES

by

DEMESHEKA GOOLSBY

Committee Chair: Jenny Yang

Committee: Dabney Dixon

Donald Hamelberg

Electronic Version Approved:

Office of Graduate Studies

College of Arts and Sciences

Georgia State University

May 2016

DEDICATION

I would like to dedicate this thesis to my family and friends, especially my parents Anthony and Marilyn Goolsby. They have been a tremendous support to me both emotionally and financially during my academic career. Being the first in my family to go to college has not been the easiest because it was a different endeavor to us but they have been extremely helpful in every way, and I cannot express my love and gratitude enough. The list of things they've done is a heavy one: provided rides to and from bus stops and campus, letting me use their cars for days on end, providing monetary help when things were tight, listening when I needed to vent about an experiment and a stressful schedule, providing a laugh when I desperately needed, dropping whatever they were doing to come to my aid, coming to rescue me during the "snowpocalypse" of 2014, and being an all-around strong force of encouragement that I desperately needed. I love and thank them both eternally for who they are and what they do for me. I am also thankful to my siblings AJ, Anthonette, and Marvin for continuing to push me and cheer me on since we were kids.

I also thank my many close friends who have been a great support as I've gone through school and used me as an inspiration to push themselves further in their careers. My childhood friends Robyn, Jennifer, and Javahnda, have created a lifelong bond of support that seems impenetrable. My high school friends Lauren and Christa have continued to be there for jokes and Applebee's nights long after high school was over. My Furman University friends Geena, Lauryn, Samantha, Shanikque, and Desmond have constantly kept tabs on my progress and given advice at the most opportune times. My work friends Brittany, Jessica, Samuel, Krystal, and Tracey, encouraged me by using me as personal encouragement. They have all been a blessing in my life that I am so thankful for and consider them the family members God let me choose.

ACKNOWLEDGEMENTS

All of the work for this project was done under the direction of Dr. Jenny J. Yang. I want to take this time to thank her for taking me into her lab as an undergraduate and continuing to direct me into my masters. She has an upbeat personality and great amount of excitement that is contagious and encouraging. She has always told me about my potential with a fine tone and relentlessly pushed me to come as close to meeting it as possible. She has also been very patient with me during the times when I felt discouraged and reiterated the importance and purpose in everything I was doing. I know she will continue to push me toward my potential even after I graduate, and I do sincerely appreciate her for what she has done and what she will continue to do for me.

During my time in the lab I have received an enormous amount of help from lab mates past and present. I would like to thank Florence Reddish and Dr. You Zhuo, who were my mentors on the sensor project. They were both wonderful and patient with me as I learned over the last four years. I would also like to thank Dr. Alice Zhang and Cassandra Miller, two members of the CaSR project in our lab. Cassie and Alice were a great help to me in troubleshooting problems I had and helped me think from a different perspective. Jilma Phillips and Lillia Tran were my two undergraduate mentees. Having them learn under me allowed me to develop training and mentoring skills that I had not had the opportunity to learn otherwise. I would also like to thank the other members of our lab Dr. Jie Feng, Corrie Purser, Anvi Patel, Mani Salarian, Rakshya Gorkhali, Juan Zou, Shanshan Tan, Rose Auguste, Chaky Muankaew, Dr. Shenghui Xue, Dr. Fan Pu, Snow Liu, Dr. Jingjuan Qiao, Li Zhang, Oluwatosin Ibhagui, Leng Yueshuang, and Dr. Yanyi Chen for not only helping me in the lab but for becoming like another family to me

TABLE OF CONTENTS

LIST OF TABLES

LIST OF FIGURES

1 Introduction

1.1 Calcium Signaling and Calcium Dynamics

Calcium (Ca^{2+}) metal ions play a fundamental role in many of the biological functions of the body. As a second messenger[1], it induces the release of neurotransmitters[2] in the synapse of neurons, stimulates contraction of smooth and skeletal muscle[3], regulates metabolism, initiates fertilization[4], mediates protein folding, activates cell proliferation, and commences gene transcription among other roles. Ca^{2+} concentrations vary among the organelles of a cell as well as among different cell types for the various Ca^{2+} functions. Ca^{2+} concentrations can be as low as 10^{-7}-10^{-6} M in the cytosol to 10^{-3} M in the extracellular region. The sarcoplasmic/endoplasmic reticulum (SR/ER) of the cell acts as the storehouse for Ca^{2+} and has a 10^{-4}-10^{-3} M Ca^{2+} concentration. The dynamics of Ca^{2+} movement throughout the cell differ depending on the signal process and the various Ca^{2+} binding proteins involved.

Many Ca^{2+} binding proteins are present at various cellular locations to maintain the Ca^{2+} homeostasis and to control calcium dynamics. For example, Ca^{2+} channels and pumps are present at different cellular locations to modulate calcium levels and transport Ca^{2+} response to signaling. As shown in Figures 1.1 and 1.2, Ca^{2+} pumps such as the plasma membrane calcium ATPase (PMCA) and sodium-calcium exchanger (NCX) in the cell membrane and the sarco/endoplasmic reticulum (SR/ER) calcium ATPase (SERCA) in the SR/ER membrane pump Ca^{2+} out of the cytosol to ensure a low concentration of free cytosolic Ca^{2+} at sub μM range. In the cytosol, calmodulin, a ubiquitous Ca^{2+} trigger protein, binds Ca^{2+} upon increase of free Ca^{2+} levels. It has a large Ca^{2+}-dependent conformational change and in turn, regulates various biological processes inside the cell. Within the SR/ER, there are chaperone and Ca^{2+} binding proteins such as calnexin, calreticulin, and calsequestrin[5] that assist in buffering Ca^{2+} in this cellular compartment.

Depending on the cell type, the ryanodine receptor (RyR1 or 2) and the inositol 1,4,5-triphosphate receptor (IP_3R) in the membrane of the SR/ER are Ca^{2+} channels release the SR/ER Ca^{2+} at mM upon response to corresponding signal molecules such as ryanodine or IP_3. The channel and rate of Ca^{2+} transport vary depending on the receptors and stimulus used as well as the cell type itself. In excitable cells, voltage-gated Ca^{2+} channels are the primary source of signal transduction through the use of action potentials to release Ca^{2+} into the cytosol, for example in excitation-contraction coupling of muscle cells and excitation-transcription coupling in neuron cells. This process can take 1-5 ms in skeletal muscle and neuron cells and up to 100 ms in smooth muscle cells in the heart. Ca^{2+} release also occurs as a result of calcium-induced calcium release[6] (CICR) where the release of lipid messenger inositol 1,4,5-trisphosphate (IP_3) after hormone stimulation induces the release of Ca^{2+} from the SR/ER through IP_3R, an event that occurs in 10-60 seconds. The released Ca^{2+} goes on to induce Ca^{2+} release from the SR/ER through the RyR, taking 1-5 seconds.

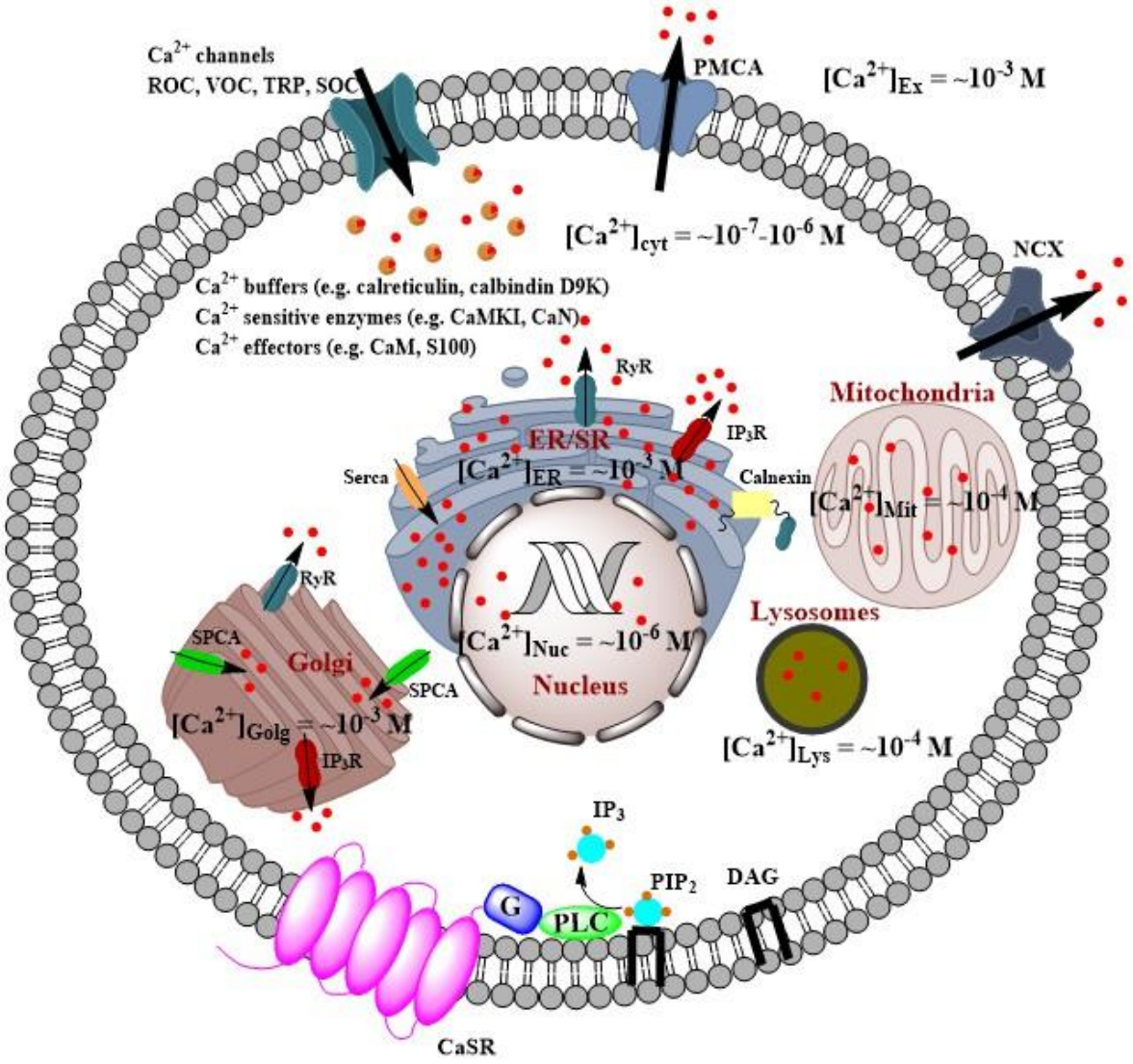

Figure 1-1 Dynamics of Ca^{2+} inside the cell

The intracellular Ca^{2+} dynamics vary. Ca^{2+} flows into the cell through Ca^{2+} channels and pumps on the plasma membrane such as the sodium-calcium exchanger (NCX) and plasma membrane calcium ATPase (PMCA). The cytosolic calcium concentration is maintained by buffer proteins such as calreticulin and calnexin. Biological functions that use Ca^{2+} as a second messenger for their signal transduction pathways are triggered by increased cytosolic Ca^{2+}. This increase comes from Ca^{2+} release from the Ca^{2+} storage organelle SR/ER by either hormone activation (IP_3R activation by IP_3 produced by G protein receptor activation) or calcium-induced calcium release (increased calcium in the cytosol activates the ryanodine receptor). Ca^{2+} is present in other organelles to assist with their function, post-translational protein modification in the Golgi, breakdown enzymes of the lysosomes, DNA transcription in the nucleus, and function of mitochondrial enzymes.

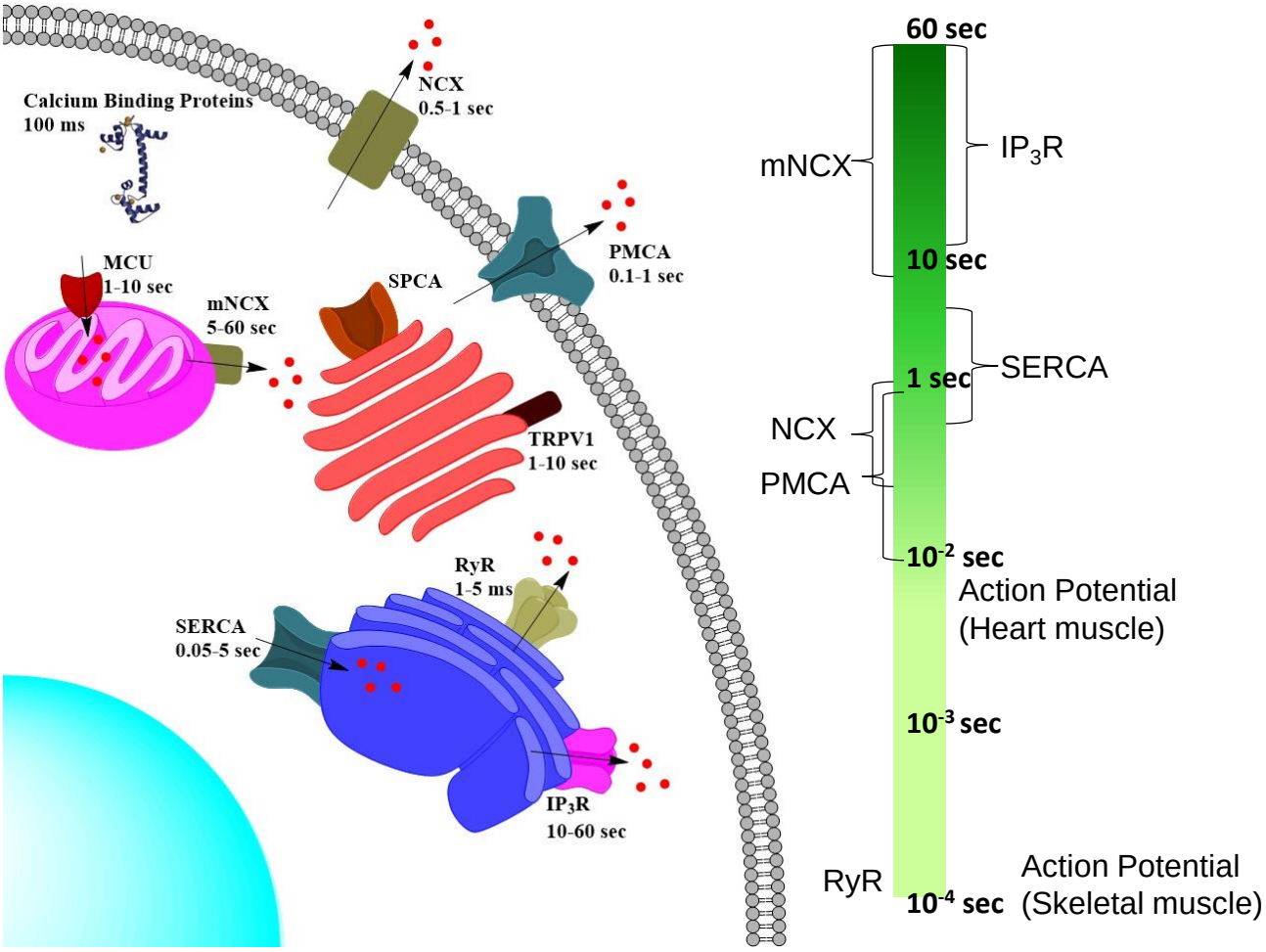

Figure 1-2 Gating and uptake of intracellular Ca^{2+}

The rate of Ca^{2+} release varies by channel and Ca^{2+} binding protein. The Ca^{2+} binding proteins in the cytosol such as calmodulin have very quick binding (100 ms), faster than the Ca^{2+} flow out of the cell via PMCA activation (0.1-1 s) and NCX activation (0.5-1 s). The fastest kinetics are seen in the SR/ER where Ca^{2+} is released quickly via the RyR (1-5 ms) and the IP_3R (10-60 s) and pulled in quickly through SERCA (0.05-5 s).

1.2 Importance for Monitoring Calcium Dynamics

Since Ca^{2+} has been found to play a role in many different biological processes, disruptions to its homeostasis have been correlated with many diseases. For example, many heart and skeletal diseases, such as cardiac hypertrophy, arrhythmia, malignant hyperpyrexia, and CPVT, have mutations of the ryanodine receptor, IP_3R, and SERCA pump. Such mutations can negatively affect the expression levels and function of these channels which impair basal calcium in the ER and the calcium release.

The dysfunction of Ca^{2+} release of the SR/ER has been found in cases of Alzheimer's disease[7], heart disease, Huntington's disease[8], and diabetes among others. The release of Ca^{2+} as a second messenger from the SR/ER to the cytosol, by either an action potential or Ca^{2+}-induced calcium release (CICR), activates a number of biological pathways such as muscle contraction in muscle cells and neurotransmitter release in the neurons. Malfunction of these channels, which can be due to mutations in or expression of the channels and pumps, can cause irregular Ca^{2+} movement and concentrations in the cell. These diseases have created a pressing need for an accurate way to measure Ca^{2+} concentrations, changes, and movements throughout the cells via the development of calcium sensors.

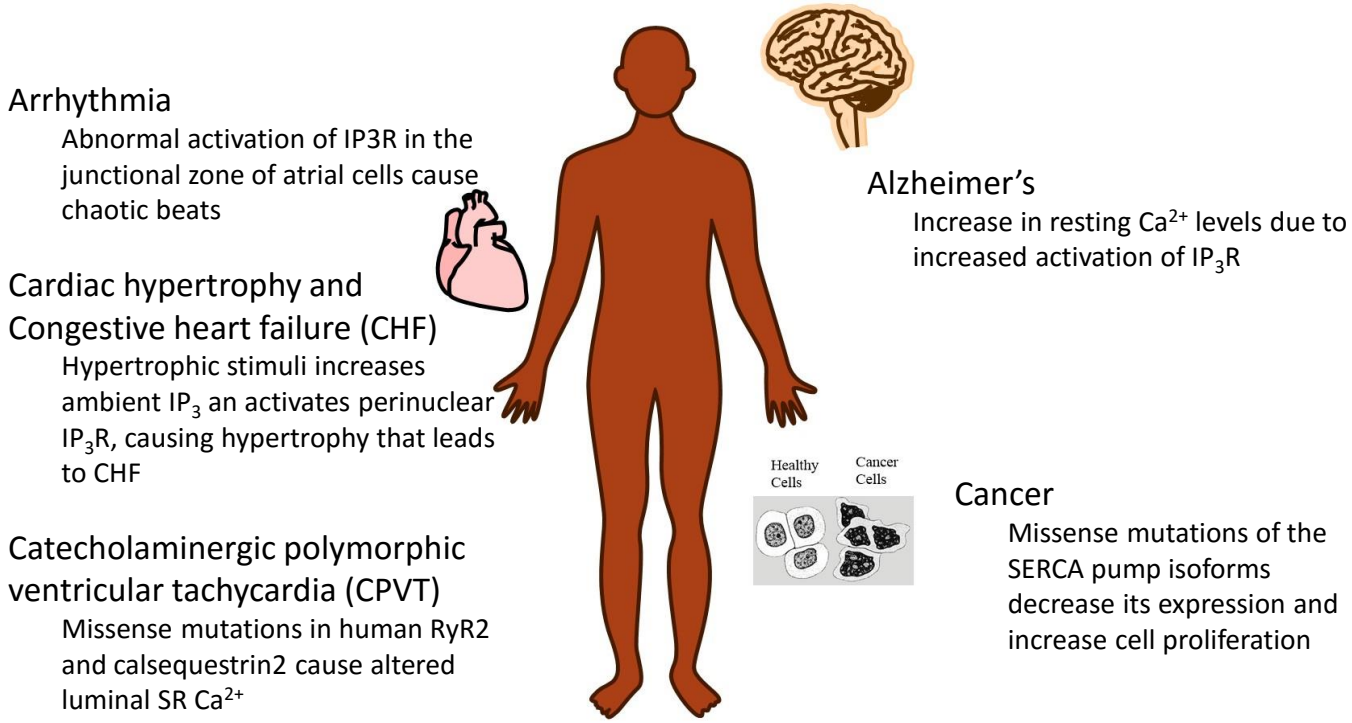

Figure 1-3 Diseases of the SR/ER

Mutations in the SR/ER Ca^{2+} pumps and channels can cause decreased/increased protein expressed, improper folding, or irregular function. These abnormalities with the channels can cause changes in the basal cytosolic Ca^{2+}, SR/ER Ca^{2+}, or rate of Ca^{2+} transport which will then disrupt the signal transduction pathways in which Ca^{2+} acts as a messenger.

1.3 Fluorescence Spectroscopy and Criteria for Intracellular Calcium Probes/Indicators

There has been considerable growth in the field of intracellular Ca^{2+} probe development for use in measuring the Ca^{2+} dynamics inside the cell. The use of fluorescence spectroscopy has become widely utilized for this goal. Fluorescence occurs when a highly aromatic species, called a fluorophore, transitions through its various vibrational states. Photons from visible light hit a fluorophore at a particular wavelength and bring it from a stable low energy state to a high energy state, a process that occurs on a femtosecond timescale. The species then undergoes vibrational relaxations in picoseconds followed by a nanosecond return to the low energy ground state which releases a photon at a longer wavelength. The field of Ca^{2+} indicator development utilized the fluorescence process where binding of Ca^{2+} causes a change in fluorescence intensity.

Fluorescence imaging is a very powerful technique to monitor cellular calcium response. Due to the pioneering work by Dr. Roger Tsien, the cellular imaging field started with the development of cell permeable intracellular Ca^{2+} dyes such as Fura-2 AM for use in measuring the Ca^{2+} dynamics inside the cell[9-14]. Figure 1-3 shows that fluorescence occurs when a fluorophore or chromophore undergoes vibrational relaxations in picoseconds followed by a nanosecond return to the low energy ground state which releases a photon at a longer wavelength. This process was used in the development of Ca^{2+} indicators and dyes where binding of Ca^{2+} causes a change in fluorescence intensity.

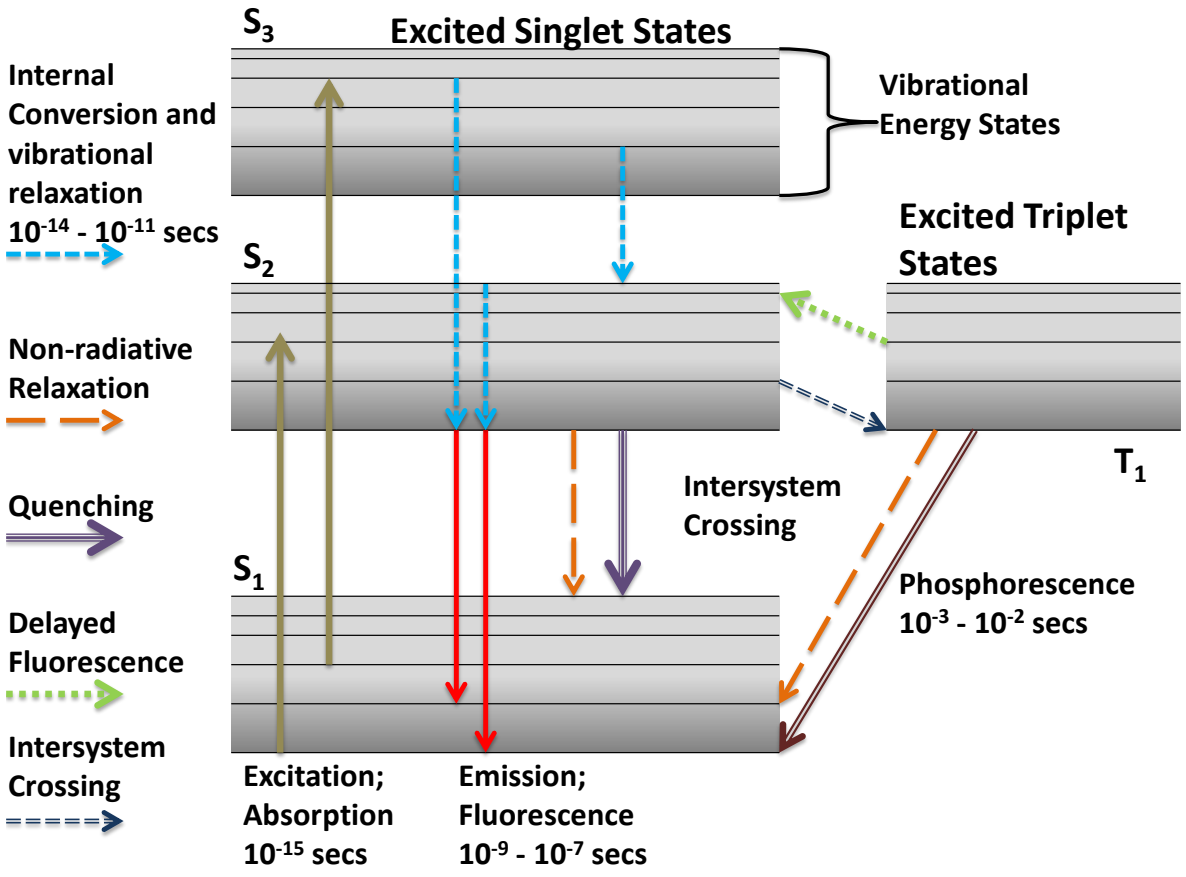

Figure 1-4 Jablonski Diagram
When energy is applied to a chromophore compound, this chromophore will absorb the photon energy and go from a low energy ground state to a high energy excited state. The excited compound can go through a number of vibrational and internal conversion energy states before returning to the lowest level excited state. From the lowest level excited state, the compound can then enter a triplet state for phosphorescence, undergo intersystem crossing, or emit off the photon energy as fluorescence.

A good fluorescent Ca^{2+} indicator must fulfill a number of criteria for biological use. First, it should have good optical properties such as strong fluorescence at an ambient body temperature of 37 ˚C. Second, it must bind Ca^{2+} with the necessary K_d that is close to the target environment, such as the SR/ER of 1 mM. Third, it should exhibit a large calcium-dependent fluorescence change (large dynamic range) of fluorescence, preferably a ratiometric change. Such a signal change should have a 1:1 binding that is required for quantitative measurement. Third, it should exhibit good Ca^{2+} binding kinetics with fast on and off rates. Fourth, it needs to exhibit structural

stability at the ambient body temperature of 37 ˚C and pH insensitivity. It should also ideally have minimal interaction with other target proteins in the intracellular environment.

There are currently two classes of fluorescent Ca^{2+} indicators used: synthetic Ca^{2+} indicating dyes and genetically encoded Ca^{2+} indicators (GECIs). To be used in biological studies, a fluorescent Ca^{2+} indicator must first correctly fold with full chromophore formation at 37 °C. The indicator should also display a Ca^{2+}-induced change in its fluorescence intensity that is independent of any pH-induced change and should have favorable optical properties. The Ca^{2+} binding affinity of the indicator should be in the appropriate range for the desired environment and be selective over other metals. The indicator should also maintain limited interactions between with other biological molecules in this environment to prevent deactivation.

1.4 Synthetic Ca^{2+} indicating dyes

Figure 1-4 shows that 1,2-**b**is(o-**a**mino**p**henoxy)ethane-N,N,N’,N’-**t**etra**a**cetic acid (BAPTA) is a non-fluorescent Ca^{2+} chelating polycarboxylic acid that has a higher specificity for Ca^{2+} than EGTA and EDTA. BAPTA was used to derive the commonly used fluorescent chemical indicators, often referred to as dyes, used today for intracellular Ca^{2+} measurement. These compounds come in three different forms: salts, dextran conjugates, or acetoxymethyl (AM) esters.

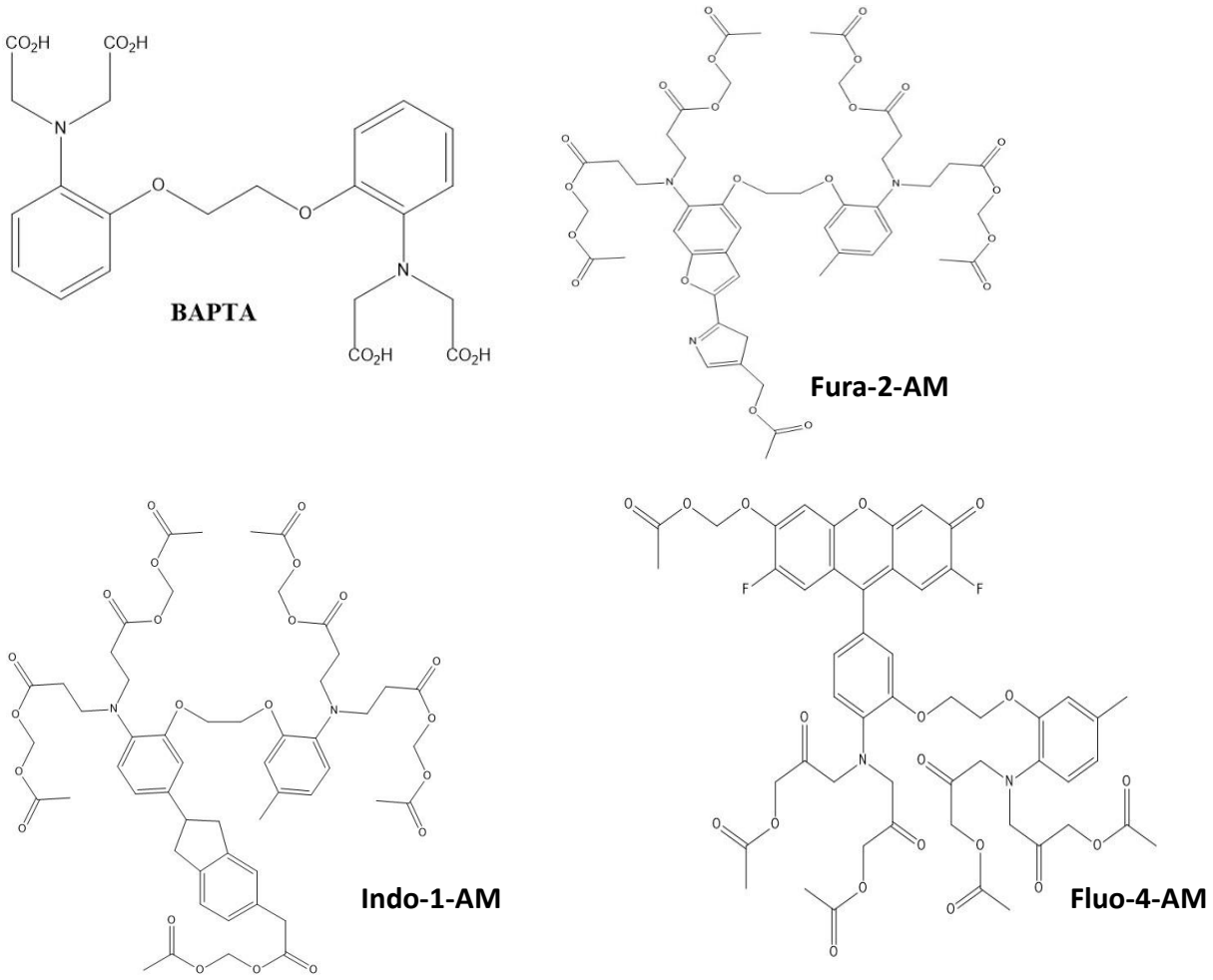

Figure 1-5 Synthetic Ca2+ dyes

Structure of Ca^{2+} chelator BAPTA and derivatives Fura-2-AM (K_d = 145 nM; λ_{ex} = 340/380 nm), Indo-1-AM (K_d = 230 nM; λ_{em} = 405/485 nm), and Fluor-4-AM (K_d = 345 nM; λ_{em} = 520 nm).

The AM ester form of these compounds can be loaded into the cell within minutes of incubation. A major setback of the calcium dyes is that they are very hydrophilic, tend to compartmentalize, and leak out or get pumped out of the cell after a short time. These features make them difficult to use for longer term experimentation. Their dextran conjugates have some improvement in the compartmentalization and leaking problem. The AM ester fluorescent dyes were designed for easy cell loading. These dyes are hydrophobic and readily diffuse through the

membrane into the cell with the addition to culture media. Once inside esterases cleave off the AM groups to trap the dye inside which accumulates in high concentration inside the cell.

The synthetic dyes have many advantages. In addition to their simpler methods of loading, there is a broad range of affinity choices. Some dyes have a high affinity for use in the cytosol and others have a low affinity for use in the intracellular compartments. The dyes also display pH insensitivity and photostability. There is also the choice of ratiometric dyes that have a shift in the excitation or emission upon Ca^{2+} binding or single excitation/emission dyes. The vast selection of dyes also allows for more equipment choices as far as microscope and light source. As far as disadvantages, aside from the compartmentalization and diffusion problems, the dyes lack targeting capabilities and also have some buffering effect. The second class of indicators, the GECIs, addresses these setbacks.

1.5 Fluorescent Proteins (FP)

The second class of Ca^{2+} sensors is the **G**enetically **E**ncoded **C**alcium **I**ndicators or GECIs[15]. These indicators are only composed of amino acids, so the Ca^{2+} binding capabilities are determined by mutagenesis. Naturally, fluorescent proteins (FPs) such as green fluorescent protein (GFP) and discosoma (DsRed) are used as templates (Figure 1-6).

Green fluorescent protein[16, 17] (GFP) is a 238 amino acid β-barrel protein isolated from the jellyfish *aequeora Victoria*. Through the center of the barrel runs a large α-helix that holds the p-hydroxybenzylideneimidazolinone fluorophore comprised of residues Ser65-Tyr66-Gly67. These residues autocyclize to make the fluorescent chromophore that possesses a major and minor excitation peak at 395 nm and 475 nm respectively and a single emission peak at 508 nm. A mutation at residue 65 from serine to threonine gave the enhanced green fluorescent protein (EGFP) which loses the major 395 nm excitation while having a 6-fold increase in the minor

excitation which red shifts to 488 nm. This version is noticeably brighter than the wild-type version. Further mutations to the chromophore have yielded the blue, cyan, and yellow variants, commonly used to biosensor engineering.

DsRed[18] is another β-barrel fluorescent protein found in discosoma coral (Figure 1-6). Unlike GFP, DsRed forms tetramers that can loosely come together to form octamers. The Gln66-Tyr67-Gly68 chromophore undergoes the same autocyclization reaction with an extra dehydrogenation step that extends the conjugation into the backbone and shifts the chromophore from green to red during maturation. DsRed provides the possibility of a pH insensitive probe with deeper skeletal tissue penetration but because of the tetramer formation and a 12-hour maturation time cannot be readily used for biological studies. Many mutations have been carried out through the use of a random library to make a monomeric version of DsRed without losing the optical properties. Some of the key mutations include the Q66M/T/C to the chromophore and mutations to neighboring residues 41, 62, 64, 67, 83, 163, 195, 197, and 213[19].

The mFruits fluorescent proteins were generated by Tsien et al.[20] and are a series of monomeric FPs with different colors. mCherry is one of the mFruits that is widely for biological tagging and sensor engineering because of its low chromophore pKa of ~4.0 and maturation time of 15 minutes. We also use mCherry and EGFP to develop a red and green calcium sensor (chapter 2 and 3). The key determinants that contribute to the optical properties of fluorescent proteins are essential for creating Ca^{2+} sensors. This question will be addressed in chapter 2.

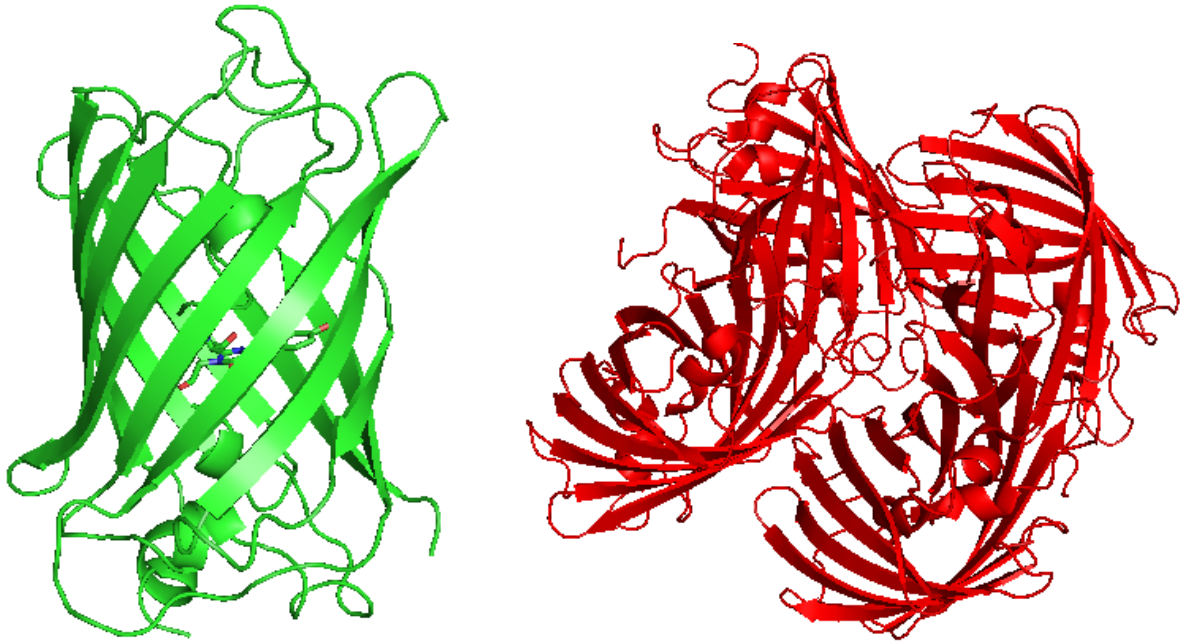

Figure 1-6 Fluorescent proteins GFP and DsRed
Tertiary structure of FPs GFP (λ_{ex} = 396/470 nm, λ_{em} = 504 nm) and the tetrameric DsRed (λ_{ex} = 558 nm, λ_{em} = 583 nm).

1.6 Calcium Binding Proteins

Calcium binding properties are important for creating calcium sensors. Figure 1.7 shows several common calcium binding motifs in calcium binding proteins. For example, calcium binding sites in the C2 domain are formed by discontinuous calcium binding residues. The C2 domain contains approximately 130 amino acid residues folded into eight β-sheets and three loops. These domains are capable of binding Ca^{2+} and phospholipids, with the binding of the later improving the affinity for Ca^{2+} by up to 1000 fold in some cases. These domains do not show any substantial conformational changes upon Ca^{2+} or phospholipid binding, have a significant sequence distance between chelating residues, and are capable of binding to other targets.

The EF-hand domain shown in Figure 1-7, also referred to as the helix-loop-helix domain, contains approximately 30 amino acid residues. Proteins with EF-hand motifs commonly present as pairs of 2, 4, 6, or more EF-hands that cooperatively bind. The critical loop region contains the

predominantly negatively charged residues that hold a single Ca^{2+} in the pentagonal bipyramid binding coordination. For example, calmodulin and troponin C contain 4 EF-hand motifs in two domains. Both proteins exhibit big conformational change upon calcium binding. Some proteins with this domain do not exhibit conformation changes upon Ca^{2+} binding while others such as calmodulin have structural changes for regulation purposes. The EF-hand motif is the most commonly used Ca^{2+} binding motif for engineering biosensors[15, 21, 22]. The troponin C (TnC) is a specialized Ca^{2+} binding protein that closely associates with troponin I and troponin T in the troponin complex. TnCs only known function is regulating muscle contraction in skeletal and cardiac muscle. The protein is not found natively in the cytosol but can be expressed without aggregation in various cells.

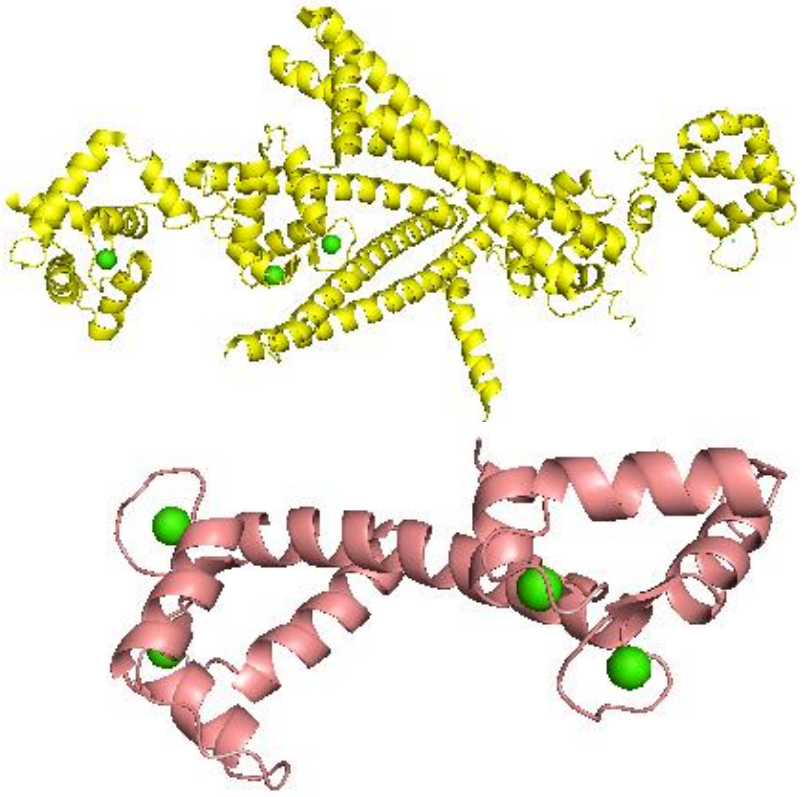

Figure 1-7 Commonly used Ca^{2+} binding domains
Ca^{2+} loaded Troponin C (yellow) and Calmodulin (pink) proteins with the Ca^{2+} molecules (green) residing in the EF-hand motifs of each protein.

1.7 Genetically Encoded Calcium Indicators (GECIs)

There are several methods for engineering GECIs pioneered by Persechini and Tsien. Earlier and common GECIs were created by utilizing Förster Resonance Energy Transfer (FRET) for their fluorescence measurement[23, 24]. This technique uses two fluorophores in proximity to each other where the excited energy of one is transferred the other. The Cameleon series of GECIs are one example of a FRET pair using blue (BFP) and green fluorescent proteins for the fluorophores and calmodulin with one of its binding peptides M13 as the Ca^{2+} binding motif [15, 23]. Early versions of BFP were not suitable for biological use due to strong absorbance in the UV range, so the second generation of Cameleons was made using cyan (CFP) and yellow (YFP) fluorescent proteins[14, 15, 23]. YFP was further improved by mutagenesis to create pH insensitive versions named Citrine and Venus. The use of circular permutated (cp) versions of Venus, a mutant where the N and C terminals are linked together, and a new N and C terminals are made elsewhere on the protein, displayed more than a five-fold change in the emission fluorescence of the sensors. Although these sensors provided excellent optical properties and high Ca^{2+} affinities, the use of calmodulin as the Ca^{2+} binding motif causes problems in the sensors because of its role in signal transduction[1, 23, 25, 26]. For example, the high number of native calmodulin in the cell binding to the peptide in the sensor and the calmodulin in the sensor binding to other target proteins in the cell deactivate the sensor[15, 23]. One attempt to eliminate these interactions involved making a series of FRET pair sensors were made using troponin C as the Ca^{2+} binding motif[27, 28].

The first generation of FRET pair biosensors made using TnC were similar to the Cameleons in that they used CFP and Citrine but there is no binding peptide used with TnC like the M13 used with calmodulin. CFP was later substituted with Cerulean to optimize the brightness of the proteins. Engineering the C-terminal of the EF-hands within the backbone also eliminated

FRET detectable Mg^{2+} binding with the exchange of a slightly decreased Ca^{2+} affinity. Further mutations to eliminate low-affinity lobes of the biosensor gave the Tn-XXL, a biosensor that will remove the need for earlier generation TnC based FRET sensors[15].

Baird et al. discovered that GFP could withstand large insertions without disruptions to the protein structure or destruction of fluorescence, setting the stage for work to create single fluorophore sensors[29]. Substituting the residue 145 tyrosine in YFP with the sequence for calmodulin gave Camgaroo. With Ca^{2+} binding the sensor experienced an absorbance spectrum change where the dominant peak changes from being the 400 nm peak to the 490 nm peak. The 400 nm is consistent with the protonated form of the YFP chromophore, implying that the Ca^{2+} encouraged the deprotonation of the chromophore in Camgaroo. Unfortunately, this sensor displayed large pK_a changes from 10.1 in the Ca^{2+} free form to 8.9 in the Ca^{2+} loaded form. This pH change along with the poor visibility at basal Ca^{2+} levels and less than ideal Ca^{2+} K_d made it difficult to use. The second generation Camgaroo-2 was improved for visibility but not for the other characteristics.

Three biosensors, the pericams, were made using a circular permutated version of YFP by fusion of the M13 peptide to the new N-terminal and calmodulin fused to the new C-terminal. Flash pericam has an 8-fold increase with Ca^{2+} binding, ratiometric pericam has a change in the excitation wavelength with Ca^{2+} binding, and inverse pericam, which is bright in its resting state, and has a decrease in fluorescence with Ca^{2+} binding.

Substituting the YFPcp backbone for a GFPcp with calmodulin on the C-terminal and M13 on the N-terminal gave one of the most used GECI G-CaMP. Ca^{2+} binding to G-Camp increased the chromophore ionization as shown by the decrease and increase in the 400 nm and 490 nm excitation wavelengths respectively. This biosensor possesses a high affinity for Ca^{2+} but is dim

and slow to mature at 37 °C. Maturation was improved in G-CaMP1.6, GCaMP2, and further in G-CaMP3, the most optimized of the single fluorophore biosensors.

Campbell et al. did a colony based screening of G-CaMP3 to find the variants with the greatest Ca^{2+}-dependent change. Three proteins were chosen to make up the GECO series which exhibit high Ca^{2+} affinities and fluorescent increases with Ca^{2+}. Making the Y66H mutation creates the BFP chromophore to the sensor, dubbed B-GECO. Replacing the cpGFP in the GECO1.1 with a cp variant of mApple created a red version of the sensor named R-GECO. B-GECO and R-GECO are pH insensitive compared to GECO, and the longer wavelength of R-GECO allows for deeper tissue penetration.

Table 1-1 Commonly used Genetically Encoded Calcium Indicators

Subcellular Compartment	Green	Cyan	Yellow	Red
Intracellular (0.1-1 µM)	GCaMP (K_d=0.5 µM) G-GECO (K_d=0.6-1.2 µM)	B-GECO (K_d = 0.2-0.5 µM) YC3.6 (K_d = 0.3 µM) TN-XXL (K_d=0.8 µM)	Flash pericam (K_d=0.7 µM)	R-GECO (K_d=0.5 µM)
Golgi		YC3.3 (K_d=4.4 µM)		
Lysosome				
Mitochondria/ Nuclear envelope (1-10 µM)		Cameleon-2 (K_d = 0.07; 11 µM) YC4.6 (K_d = 0.06, 14.4 µM)	Ratiometric pericam (K_d=1.7 µM); Camgaroo -2 (K_d=5.3 µM)	
ER/SR (0.2-1 mM)	CatchER (K_d= 190 µM) G-Cepia1er (K_d=672 µM) GEM-Cepia1er (K_d=558 µM)	D1ER (K_d = 0.8, 60 µM) Cameleon-4 (K_d = 0.083, 700 µM)		R-Cepia1er (K_d=565 µM)

These insertions of CaM variants allowed the GECIs in use today to provide a less toxic option compared to the synthetic dyes with the capability for targeting to different organelles. However, the limited range of Ca^{2+} K_ds, large bulky size and pH sensitivity observed in the GFP-based sensors limit these targeting capabilities. One of the limitations of such constructs is the complexed pH dependence. With these sensors, the change in fluorescence intensity with Ca^{2+} binding resembles the change with environmental pH. This sensitivity is also shown with the neutral chromophore pK_a values of these sensors. The pH insensitive red and blue versions are one way to combat the setbacks. Our lab is working to engineer Ca^{2+} biosensors using a different approach.

1.8 Gaps for Calcium Sensor Rapid Kinetics Challenges

To understand the relationship between Ca^{2+} and the diseases it has been associated with the entire signal cascade needs to be measured. This measurement requires Ca^{2+} probes with fast kinetics to measure the beginning and ending traces. Many signals, such as those from Ca^{2+} sparks require deconvolution to obtain the intrinsic signals. Ca^{2+} transients from high-frequency action potentials require similar analysis and can end up missing peaks in the beginning or the end of the trace.

Currently, the synthetic dyes such as Fluor-5-N possess fast off rates but are limited with their use due to their high affinity for Ca^{2+} and their lack of targeting capabilities which only allow them to measure up to 80 nm from a channel. The GECIs containing the EF-hand motifs from calmodulin and troponin C can be targeted for microdomain measurement but possess slow on rates due to the global structure conformation changes that occur upon Ca^{2+} binding. This cooperative binding prevents them from capturing the rapid Ca^{2+} release from the SR/ER. There

is currently work being done to improve the targeting of the synthetic dyes, but the need for a Ca2+ indicator with fast kinetics still exists.

1.9 Design and Engineering of Calcium Sensors in the Yang Lab

Rather than using two or more coupled EF-hand motifs or native EF-hand proteins to insert into fluorescent proteins for single fluorophore or FRET paired Ca^{2+} sensors, the Yang group uses a very different approach. We aimed to Ca^{2+} sensors by the addition of a single Ca^{2+} site into fluorescent proteins. In early work pioneered by Zou et al. we grafted a single Ca^{2+} EF-hand binding motif into EGFP to create a protein called G1[22]. This protein displays an absorbance spectra resembling the wild type GFP with peaks at 398 nm and 490 nm, indicating a neutral and anionic form of the chromophore contributing to the fluorescence. It also displays fast Ca^{2+} binding kinetics at 398 nm, a millimolar binding affinity, and a selectivity for Ca^{2+}. The addition of Ca^{2+} induces and increase in absorbance at 398 nm and a decrease at 490 nm. This trend is also present in the fluorescence spectra of these wavelengths.

Later, April Ellis and Shen Tang designed a non-native Ca^{2+} binding site into a fluorescent protein. We hypothesize that the addition of a Ca^{2+} binding site on the surface of the FP near the chromophore environment will lead to a Ca^{2+}-dependent fluorescence change. Using an algorithm to predict the location on the FP for the site as well as what residues to use as ligands, we used site-mutagenesis to create the GFP-based CatchER[30]: a low-affinity Ca^{2+} sensor with fast kinetics and a longer fluorescence lifetime that is useful for measuring Ca^{2+} dynamics in the SR/ER.

In the process of creating CatchER, four variants of increasing binding pocket charge were created: D8 with a -2 charge, D9 with a -3, D10 with a -4, and CatchER (D11) with a -5. With these variants, some questions about the electrostatic effects of a *de novo* Ca^{2+} binding site was

raised. These included inquiring about what effects to the protein's tertiary structure, the UV-vis and fluorescence spectra, the biophysical properties, and the fluorescence intensity.

Red pH insensitive Ca^{2+}-binding proteins R-Catcher (MCD1) and R-CatchER´ (MCD15), were developed using the same methods with mCherry as the template by Dr. You Zhuo. Modifications are readily being made to improve the fluorescence dynamic range and SR/ER membrane targeting of our sensors. The challenges and limitations of these sensors, such as the low quantum yield, low fluorescence dynamic range, and lack of color, will be addressed in chapter 2.

1.10 Overview of this thesis

This thesis serves to outline the work done on design, optimization, and application of fluorescent protein-based intracellular calcium (Ca^{2+}) sensors. Chapter 1 introduces the role of Ca^{2+} in the body including the concentrations, dynamics, and kinetics before leading to the diseases associated with Ca^{2+} and presents the need for tools to measure the intracellular Ca^{2+} dynamics.

Chapter 2 describes the work on optimizing a red pH insensitive sensor for its fluorescence properties and chromophore maturation. We hypothesize that manipulating the ionization of the chromophore to increase the pK_a will be key to achieving the desired fluorescence intensity and the increased Ca^{2+}-induced change in fluorescence intensity. The problem to address with this work is whether we can manipulate the sensitive area of the chromophore to create an optimized sensor that will fold well and display a Ca^{2+} dependent change in fluorescence.

Chapter 3 describes the work done to analyze our method of Ca^{2+} binding pocket development by observing the effect of increasing electrostatic interactions in our green CatchER

variants. CatchER is used for measurement of the high Ca^{2+} concentrations in the SR/ER. The problems addressed are whether a *de novo* site can successfully be engineered in a fluorescent protein with a desired binding affinity and optical properties.

Chapter 4 discusses the work done to target CatchER specifically to the membrane of the SR/ER and anchor it there with an orientation toward the cytosol. The major problem is whether we can successfully target our sensor to a particular region of the SR/ER to allow for local Ca^{2+} dynamic measurements rather than global ones. Key challenges faced with this is whether the cytosolic Ca^{2+} concentrations in these local regions can reach concentrations high enough for our sensors to capture their signal and if a truly cytosolic-facing sensor can be made using tags that initiate protein translation within the ER. This work sets out to answer these questions. Chapter 5 discusses the significance of this work and the impact it will have to further Ca^{2+} research.

2 Optimization of mCherry Based Ca^{2+} Binding Proteins as Calcium Sensors

2.1 Introduction

2.1.1 Calcium dynamics at low pH and the unmet need for a pH insensitive sensor

As discussed in Chapter 1, there are extensive studies on the Ca^{2+} dynamics and content in the cytosol and SR/ER of the cell where concentrations and pathways of Ca^{2+} are well known. Gradually more and more research is also being done to study the Ca^{2+} dynamics of the more acidic organelles such as the endosomes, lysosomes, and Golgi apparatus. It is known that these organelles have Ca^{2+} stores and even possess some Ca^{2+} dependent pathways for cell function, but little is known about the specifics of these pathways.

The endolysosomal system is involved in degradation of various macromolecules and micromolecules in the cells for either recycling or removal from the cell. The synthesis of the

lysosomes begins with endocytosis of the plasma membrane to form an endosomal vesicle. As this vesicle matures to an endosome and finally a lysosome, the luminal pH continues to decrease. The final pH of a lysosome is typically 4.5-5.5. A relationship between Ca2+ signaling and the function of lysosomal enzymes has been made after Ca2+ channels and pumps have been found in the membrane of the lysosome. Some metabolic diseases are found to be connected to deficiencies in these enzymes.

More is known about the Ca^{2+} flow in and out of the Golgi apparatus. The Golgi is involved in synthesis and packaging of proteins meant for the lysosomes, plasma membrane, SR/ER, and secretory vesicles. Studies have shown that the pH in the Golgi is not homologous throughout but rather increases from the cis-Golgi network (CGN) close to the ER membrane to the trans-Golgi network (TGN) on the far side of the Golgi. After being synthesized in the SR/ER proteins are transported to the CGN and continue through the Golgi for posttranslational modifications and secreted to their appropriate destinations from the TGN. The CGN has Ca^{2+} uptake mediated by the SERCA pump of the SR/ER and secretory pathway Ca^{2+}-ATPase (SPCA) whereas only the SPCA is dominant at the TGN. The main difference between these two pumps is that SPCA functions to transport Mn^{2+} equally as Ca^{2+}. IP_3R found on the Golgi membrane indicate that it may be a poorly IP_3-sensitive Ca^{2+} store to complement the SR/ER high IP_3-sensitive Ca^{2+} store. As with the lysosomes the luminal Ca^{2+} of the Golgi helps regulate the posttranslational enzymes and diseases such as Hailey-Hailey have been connected to dysfunction of the Ca^{2+} pump and Golgi enzymes.

The interest in studying these Ca^{2+} dynamics of these organelles is halted by the lack of measurement tools. The majority of the commonly used GECIs utilized for intracellular Ca^{2+} measurement make use of EGFP and its derivatives as the template because of the brightness and

high fluorescence quantum yield of these proteins at ambient temperatures. While these sensors possess the appropriate optical properties, the chromophore pK_as are in the 6.5-7.5 range, making these sensors pH sensitive. It is this pH sensitivity that prevents the use of these indicators for measuring calcium dynamics in the endolysomes and Golgi. Thus, there is an unmet need for a pH insensitive Ca^{2+} sensor to assist in these studies.

2.1.2 Red fluorescent protein as a scaffold for design of a pH insensitive calcium sensor

mCherry, the red monomeric derivative of DsRed, is a potential candidate for a scaffold to design calcium sensors that are insensitive to low pH due to its low chromophore pK_a value. As discussed in Chapter 1.6 Figure 1-5 the red fluorescent protein DsRed comes from *Discosoma sp*., a type of soft coral. It has a β-can tertiary structure just like GFP with a Q66-Y67-G68 chromophore located in the center α-helix of the β-can. This chromophore extends into the backbone adding to the conjugation and giving the excitation and emission spectra a red shift compared to that of GFP. Unlike GFP and its derived proteins, DsRed forms a tetramer which hinders it from being used as a Ca^{2+} indicator in biological systems. A series of mutations by Tsien et al. led to the monomeric red fluorescent protein mCherry with a Q66M mutation to the chromophore to improve maturation time. mCherry excites and emits at 587 nm and 610 nm respectively. The longer wavelength of this protein allows for high tolerance to photobleaching and deeper tissue penetration allowed by the longer wavelength, and shorter chromophore maturation time make mCherry a good candidate for Ca^{2+} probing. Table 2-1 summarizes the pKa values for fluorescent proteins. The pK_a of mCherry is 4.0 making it insensitive to pH around 5-6.5 in the endolysosomes and Golgi.

Table 2-1 Commonly used fluorescent proteins

Protein	λex	λem	pK_a
Cerulean	433 nm	475 nm	4.7
mOrange	548 nm	562 nm	6.5
EGFP	488 nm	507 nm	6.0
EYFP	514 nm	527 nm	6.9
mCherry	587 nm	610 nm	4.5

2.1.3 Creation of the MCDx Sensors

A previous graduate student in the lab, Dr. You Zhuo (Joy) devoted her studies to engineering Ca^{2+} probes using mCherry. She looked to utilize the H-bond network of the M66-Y67-G68 mCherry chromophore. Using crystal structure 2H5Q, the potential H-bonds that help stabilize the chromophore in the β-barrel were determined as shown in Figure 2-1. The tyrosyl of the chromophore was found to directly H-bond with the side chains of S146 and Q163. Indirect H-bonds to E144, the only main chain interaction to chromophore interaction, and I197 are made through S146. The nitrogen of the imidazolinone ring of the chromophore is involved in an H-bond network with E215, Q42, S69-K70, the carbonyl of the imidazolinone, R95, and Q64. The thioether sulfur of the chromophore also has an H-bond interaction with the side chain amide of Q213. A potential Ca^{2+} binding site was to be engineered by creating an area of high negative charge potential using aspartate and glutamate residues.

All possible Ca^{2+} binding sites in mCherry and red protein mKate were predicted using the program MUG. The sites were engineered using site mutagenesis PCR. The primers designed were no more than 45 base pairs long with t_m values for annealing in the 45-55 °C range and a

GC content of less than 70%. The vectors used were prsetb for bacterial expression and pcdna3.1 for mammalian expression. A Histidine-tag was placed at the N-terminal of the bacterially expressed DNA for purification. To target the sensor to the ER, the ER retention tag KDEL was placed at the C-terminal and the ER targeting sequence of calreticulin was fused at the N-terminal. The specific mutations made are shown in Table 2-1**.**

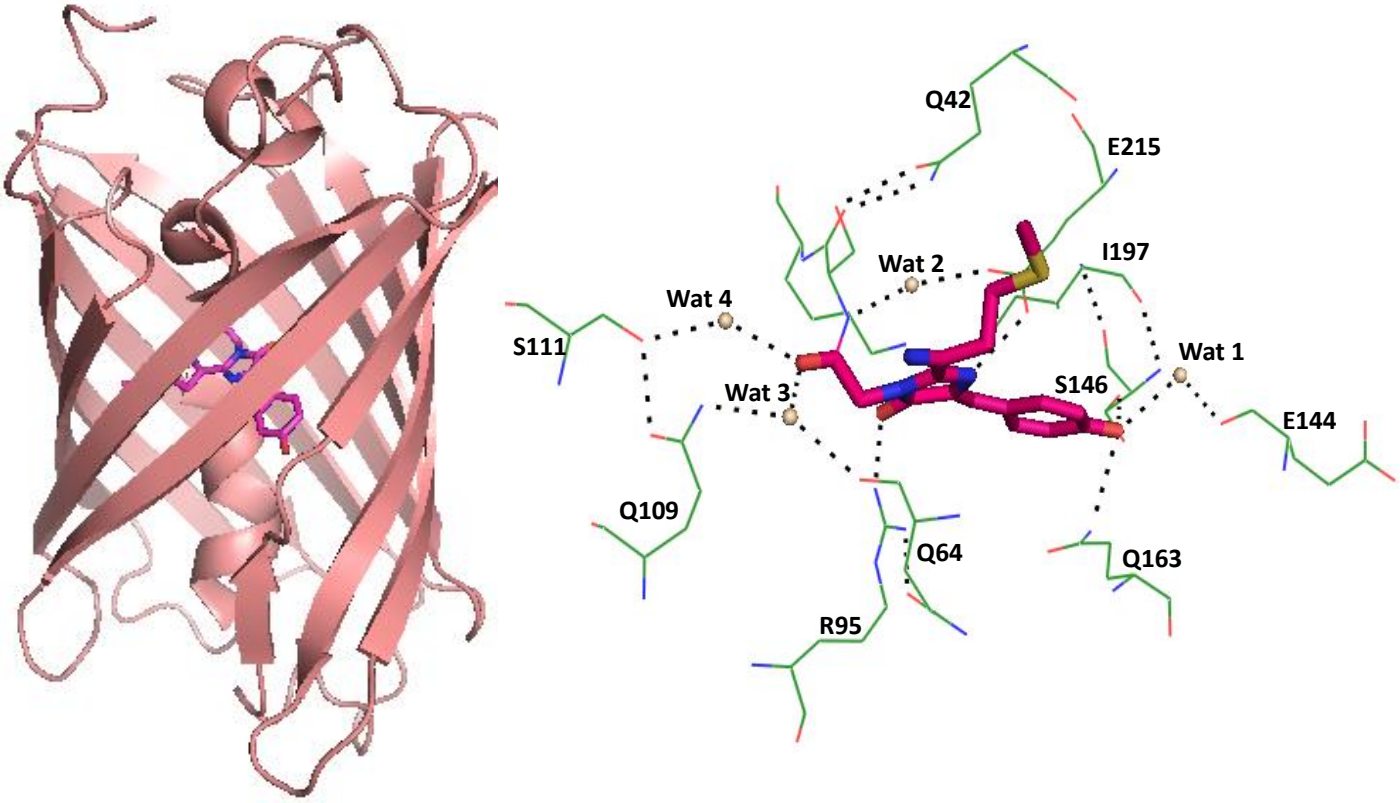

Figure 2-1 mCherry structure and H-bond network

2H5Q crystal structure of mCherry (left) and mCherry chromophore environment (right) with the bonds of predicted H-bond network shown as dotted lines.

As shown in Table 2-2, of the seven sites made, the MCD1 group maintains the red color and displayed an increase in fluorescence upon Ca^{2+} binding. The quantum yield, extinction coefficient, and chromophore pK_a of MCD1 is lower than that of mCherry. MCD14 and MCD15 were made to optimize MCD1 for expression in mammalian cell lines. These proteins have similar

quantum yield and extinction coefficients to MCD1 with pK_a values closer to mCherry. The major setback for these sensors was the small fluorescence dynamic range. Although the proteins were responding to Ca^{2+} binding with a K_d of 0.1, 0.09, and 0.5 for MCD1, MCD14, and MCD15 respectively, the change in fluorescence from the Ca^{2+} free form to the Ca^{2+} saturated form was small.

In this chapter, we set out to improve the dynamic range and optical properties of our red sensors by further manipulating the H-bond network of the chromophore. We will first examine the formation of the RFP chromophore to identify which residues play a crucial role in this process. We will then observe the effect of making multiple mutations to residue 163 in our sensors, which interacts with the phenolate ion of the chromophore, has on the protein expression and optical properties. We will then look at the Ca^{2+}-induced changes and Ca^{2+} affinity of the proteins. Lastly, we will determine what other changes can be made in the chromophore environment to improve the MCD1x Ca^{2+} sensors further.

Table 2-2 First generation MCDx variants and mutations

Position	Design Strategy	Clones	Mutations
Pocket 1	Influence the H-bonds formed between the chromophore tyrosyl and WAT1-E144 backbone, S146 side chain. Modification around MCD1 is to modify the Ca^{2+} binding affinity and the optical properties.	MCD1	A145E/N196D/K198D/R216E
		MCD14	MCD1 + R220E
		MCD14Y	197Y + MCD14
		MCD14YS	197Y/199S + MCD14
		MCD15	MCD14 + D198E
		MCD16	MCD14 + S147D
		MCD17	MCD14 + I197T/K198E/L199S/D200A
		MCD18	MCD14 + K198E/D200A
		MCD19	MCD1 + D198E
		MCD110	MCD15 + L199S
		MCD111	MCD15 + D196E
		MCD112	MCD1 + E220Q
Pocket 2	Influence the H-bonds formed between the chromophore tyrosyl and WAT1-E144 backbone.	MCD2	K198D/Y214E/R216E
		MCD22	N196E/Y214E/R216E
		MCD23	MCD2 + D200E
		MCD24	MCD2 + D200Q
		MCD25	MCD2 + D200N
		MCD26	MCD2 + E216D
Pocket 3	Influence the H-bonds formed between the chromophore tyrosyl and Q163 side chain.	mcEE	R164E/K166E
		mcP4	G142E/R164E/K166E
		mcP5	R164E/K166E/H172E
Pocket 4	Influence the H-bonds formed between the chromophore and Q109 and R95. (Figure 2.1)	mcP6	K92E/T108E
Pocket 5	Insert the EF-hand away from the chromophore.	MCIN1	153^154 (Insertion is between residue 153 and 154.Same as below)
Pocket 6	Insert the EF-hand near the chromophore tyrosyl.	MCIN2	135V^142G
		MCIN3	142G^147S
		MCIN4	143W^147S
Pocket 7	Mount the calcium binding site in cp-mKate in the corresponding location as MCD1 and CatchER.	cp-mKate_149-148	Corresponding to mKate
		cp-mKate_168-167	A142E/R198E/V216E
		cp-mKate_189-188	
		cp-mKate_154-153	

Table 2-3 Optical properties of MCD1x Ca^{2+} binding proteins

Protein	λex	λem	K_d (mM)	Extinction coefficient (M^{-1} cm^{-1})	Quantum yield		Protein brightness		pK_a	
				Apo/Holo	Apo	Holo	Apo	Holo	Apo	Holo
mCherry	587 nm	610 nm	___	72,000	0.22		0.16		4.5	
MCD1	587 nm	610 nm	0.1 ± 0.03	64,000	0.17	0.24	0.11	0.15	3.6	5.0
MCD14	587 nm	610 nm	0.085 ± 0.004	67,000	0.20	0.22	0.13	0.15	4.4	4.8
MCD14	587 nm	610 nm	0.48 ± 0.08	65,000	0.21	0.24	0.14	0.16	4.4	4.6

Data courtesy of Dr. You Zhuo. All error not listed held a value of 0.01

2.2 Materials and Methods

2.2.1 Primer Preparation

Primers were ordered from Integrated DNA Technologies (IDT). The primers were designed to be 30-40 base pairs long with GC content of no more than 60%. The primer powder was spun down, and elution buffer was added based on its concentration to make a 100 μM concentration stock. The stock was diluted to 30 μM for experimental use with elution buffer.

2.2.2 PCR Sample Preparation and Process

The PFU polymerase kit from Promega was used for site mutagenesis. A 50 μL solution was made by adding five microliters of 10X PFU polymerase buffer with $MgSO_4$, 0.1-0.2 mM of two millimolar dNTPs, 1.5-2.25 mM of 25 mM $MgSO_4$, four microliters of 20 ng template DNA, one microliter of each 30 μM primer, one microliter of the PFU polymerase, and the rest sterile ddH_2O to a PCR tube. The program was run for 25 cycles.

2.2.3 Ligation, Inoculation, and Sequencing

Site mutated samples amplified with Pfu polymerase PCR were incubated with one microliter of DpnI at 37°C for one hour. After incubation, the sample was transformed into XL-gold E. coli cells. This strain of E. coli allows for DNA ligation inside the cell. One microliter of the DNA was added 50 μL of the competent cells. The solution was mixed and left on ice for 30-90 minutes. The mixture was then placed in a 42 °C water bath for exactly 45 seconds. Following this heat shock step, the mixture was placed back on the ice for two minutes before adding 200 μL of nutrient rich XYZ media and incubating at 37°C for 30-90 minutes. Following incubation, 200 μL of the solution was spread on an ampicillin-treated agar plate and left to incubate overnight at 37°C.

The plate was retrieved after 16-18 hours of incubation, and multiple colonies were inoculated for DNA amplification. Ten microliters of ampicillin were added to ten milliliters of LB media in a 50 mL falcon tube for each colony selected. A single colony was added to this solution using an inoculation loop, and the solution was left to shake at 37°C overnight. After 16-18 hours of incubation, the DNA was amplified using QIAprep miniprep kit as directed. The DNA obtained was sent for sequencing to Genewiz Inc. Samples with the correct sequence were expressed and used for further study.

2.2.4 Transformation, Expression, and Purification in E. coli

mCherry-based proteins were in the prsetb vector for the bacterial expression carried out in the rosetta gammi E. coli competent cell line. To 50 μL of the competent cells 0.5-1 μL of plasmid was added. The solution was mixed and left on ice for 30-90 minutes. The mixture was then placed in a 42 °C water bath for exactly 90 seconds. Following this heat shock step, the mixture was placed back on the ice for two minutes before adding 50 μL of LB media and

incubating at 37 °C for 30-90 minutes. Following incubation, 50 μL of the solution was spread antibiotic treated agar plate and left to incubate overnight at 37 °C.

The next morning the transformation plate was retrieved from the incubator. Ten milliliters of LB was treated with ten microliters of 100mg/mL ampicillin. A single colony from the transformation plate was added to the LB-antibiotic solution using an inoculation loop. The inoculate solution was left to shake at 37° C overnight. After 16-18 hours of incubation, the solution was retrieved for expression. One liter of LB media was prepared for every ten milliliters of inoculate with the one milliliter of 100mg/mL ampicillin.

Two one-milliliter samples of the antibiotic-media solution were taken for optical density (O.D) blanks. The ten milliliter inoculate sample was then added to the flask, and a one-milliliter sample was taken for an O.D. reading (600 nm). The sample was placed in a refrigerated shaker to shake at 30 ° C. One milliliter of the sample was taken approximately every hour until the O.D. reached 0.6. Once and O.D. of 0.6 was reached, 200 μL of one molar IPTG was added to induce expression of the polymerase and the temperature was lowered to 25 °C. The cell pellet collected before inoculation was saved for SDS-PAGE analysis. Approximately two more O.D. readings were taken, and the solution was left to shake overnight. The following morning one last O.D. reading was taken, and the cell pellet saved for SDS-PAGE analysis of the post-induction sample. The cell pellet from the full solution was collected by centrifugation (7000 rpm for 36 minutes) and frozen until ready to purify.

The proteins were purified using a fast protein liquid chromatography (FPLC) instrument by General Electric (GE). The cell pellets were suspended in approximately 20 mL of extraction buffer (20 mM Tris, 100 mM NaCl, 0.1% Triton; pH 8.0) and vortexed to mix. The solution was sonicated for six rounds of 30 pulses to lyse the cells and then centrifuged at 17,000 rpm for 36

minutes. The supernatant was filtered using a 0.45 mm Whatman filter before being injected onto the nickel loaded five milliliter HiTrap chelating column. The Histidine-tagged protein was bound to the nickel coating the column while the impurities were washed away with buffer A (40 mM K_2HPO_4, 10 mM KH_2PO_4, 250 mM NaCl; pH 7.4). The protein was eluted off using an increasing concentration of buffer B (buffer A with 0.5 imidazole). The imidazole was removed using a 120 mL gel filtration column with ten millimolar Tris (pH 7.4). The purified protein was concentrated and stored appropriately for future use.

2.2.5 Transfection in Mammalian Cells

The protein was placed in the pcdna3.1 vector for mammalian expression. *In vivo* studies were carried out in C2C12 mouse myoblast cells and HEK293 cells. The cells were cultured in high glucose DMEM buffer with 10% fetal bovine serum (FBS). The transfection reagent used to deliver the plasmid into the cell was Lipofectamine 2000. A one microgram DNA to three microliters Lipofectamine 2000 ratio was used for mCherry based protein transfection. One milliliter of transfection solution was prepared for every slide of cells being transfected. Two tubes of 0.5 mL OPTI were prepared. The Lipofectamine 2000 was added to one and the DNA to the other. The solutions were left to sit for approximately one minute at room temperature. The DNA solution was then added in its entirety to the lipofectamine solution. After using a pipette to mix the solution was centrifuged for five seconds and placed in a dark, room temperature drawer to incubate for five minutes.

For HEK293 cells, the cells were previously split to the imaging slides and left to reach 40% confluency before transfection. The cells were rinsed with Hank's Balanced Salt Solution (HBSS) before adding four milliliters of OPTI buffer. After the incubation time has lapsed the transfection solution was added dropwise to the dish and left to incubate at 37 °C for four hours.

The buffer was then changed to fresh DMEM and the cells left for 36-48 hours to allow protein expression.

For C2C12 cells, the cells were split just before transfection. During the incubation time, the cells were rinsed with HBSS and digested in trypsin to split. The cells were transferred to the coverslips with three milliliters of DMEM buffer and one milliliter of OPTI buffer. After the incubation time has lapsed the transfection solution was added dropwise to the dish and left to incubate at 37 °C for 24 hours. The buffer was then changed to fresh DMEM and the cells left for 36-48 hours to allow protein expression.

2.2.6 Ca^{2+} Titration

A Ca^{2+} titration was performed to solve for the dissociation constant (K_d) and determine the Ca^{2+} binding affinity of the proteins. One milliliter of a 10 μM protein sample was prepared in 10 mM Tris buffer (pH 7.4) with 2 μM EGTA. The absorbance spectrum was taken before experimentation to observe the calcium free apo form absorbance. A fluorescence spectrum was taken at the 587 nm excitation wavelength using the fluorometer. Fifty micromoles of Ca^{2+} were added to the solution, and another fluorescence spectrum was taken at the excitation wavelength. This step was repeated as the Ca^{2+} concentration was slowly increased in the solution to ten millimolar. An absorbance spectrum was taken at the end of the experiment to observe the calcium saturated holo form absorbance. The maximum value of each spectrum at the wavelength of emission was normalized with Eq. 2.1. The normalized data was graphed as normalized fluorescence versus wavelength (nm) and fitted with Eq. 2.2 to obtain the K_d. In the equations, F is the fluorescence, A is the absorbance, F_0 is the lowest fluorescence value with no Ca^{2+}, F_{max} is the greatest fluorescence value at Ca^{2+} saturation, p is the protein being analyzed, and r is the reference protein.

$$f = \frac{F - F_{\min}}{F_{\max} - F_{\min}} = \frac{[P]_T + [Ca^{2+}]_T + K_d - \sqrt{([P]_T + [Ca^{2+}]_T + K_d)^2 - 4[P]_T[Ca^{2+}]_T}}{2[P]_T} \quad \textbf{Eq. 2.1}$$

$$f = \frac{(m_0 * m_1)}{(m_0 + m_2)}; m_1 = 1; m_2 = 1 \quad \textbf{Eq. 2.2}$$

2.2.7 Chromophore pKa

The pK_a of the chromophore was determined by taking fluorescence spectra of the protein in various pH conditions. A ten micromolar protein sample was made in 12 different pH buffers, outlined in Table 2-3, with two micromolar EGTA and incubated overnight at 4 °C. The next day the pH of each sample was determined using a pH meter to observe the calcium free apo form pH. A fluorescence spectrum was taken at the 587 nm excitation wavelength using the fluorometer. The protein was saturated with ten micromolar Ca^{2+}, and the fluorescence spectrum was taken again. The pH of each sample was determined using a pH meter to observe the calcium saturated holo form pH. The data was normalized with the Eq. 2.3. The normalized data was graphed as the normalized fluorescence versus pH and fitted with Eq. 2.4 to obtain the chromophore pK_a of the apo and holo forms.

Table 2-4 Buffers used for pKa determination

Buffer	Concentration (mM)	pH
Sodium Acetate (NaOAc)	500	2.0
(NaOAc)	10	3.0
(NaOAc)	10	3.5
(NaOAc)	10	4.0
2-(N-morpholino)ethanesulfonic acid (MES)	10	5.0
(MES)	10	5.5
(MES)	10	6.0
piperazine-N,N′-bis(2-ethanesulfonic acid) (PIPES)	10	6.5
(PIPES)	10	7.0
2-Amino-2-hydroxymethyl-propane-1,3-diol (Tris)	10	7.4
(Tris)	10	8.0
(Tris)	10	9.0

$$Y = \frac{Y_{\min} \times 10^{-pH} + Y_{\max} \times 10^{-pKa}}{10^{-pH} + 10^{-pka}} \quad \textbf{Eq. 2.3}$$

$$Y = \frac{1}{1 + \exp^{-\frac{(m0-m1)}{m2}}}; m1 = 1; m2 = 1 \quad \textbf{Eq. 2.4}$$

2.2.8 Quantum Yield and Extinction Coefficient

The quantum yield (Φ) and extinction coefficient (ε) are measures of the fluorescence efficiency and light absorption strength respectively of a species. The quantum yield was determined by preparing the protein at five different concentrations (15 μM, 20 μM, 25 μM, 30 μM, and 35 μM) in ten millimolar Tris buffer (pH 7.4) with two micromolar EGTA. The wild-type protein was also prepared at five different concentrations (5 μM, 10 μM, 15 μM, 20 μM, and 25 μM) in ten millimolar Tris buffer (pH 7.4) with two micromolar EGTA as a control and for

calculations. The fluorescence spectra of the wild-type and apo protein form were obtained at 587 nm excitation using a fluorometer. The absorbance spectra of both were also obtained using UV-vis. Ten microliters of one molar Ca^{2+} were added to the protein sample for a final Ca^{2+} concentration of ten millimolar. The fluorescence and absorbance spectra of the holo protein form were obtained the same as the apo form. The maximum value of fluorescence at the 610 nm emission wavelength was graphed versus the maximum value of absorbance at the 587 nm excitation wavelength for each protein to obtain the fitted line slope. This value along with the literature quantum yield of the template reference protein was used in Eq. 2.5 to calculate the quantum yield.

$$\Phi_p = \Phi_r \times \frac{\frac{F_p}{A_p}}{\frac{F_r}{A_r}} \qquad \textbf{Eq. 2.5}$$

$$\varepsilon_{p\,587nm} = \varepsilon_{r\,455nm}\left(\frac{A_{p\,587nm}}{A_{p\,455nm}}\right) \qquad \textbf{Eq. 2.6}$$

$$B = \varepsilon \times \Phi \qquad \textbf{Eq. 2.7}$$

The extinction coefficient was determined using an alkali denaturation assay. The protein was prepared at five different concentrations (15 μM, 20 μM, 25 μM, 30 μM, and 35 μM) in ten millimolar Tris buffer (pH 7.4) with two micromolar EGTA. The template protein was also prepared at five different concentrations (5 μM, 10 μM, 15 μM, 20 μM, and 25 μM) in ten millimolar Tris buffer (pH 7.4) with two micromolar EGTA. The absorbance spectra of the apo

protein form and holo protein form, as well as the absorbance spectra of the wild-type protein, were acquired. The proteins were then unfolded to expose the chromophore by adding 0.1 M sodium hydroxide (NaOH). After mixing the absorbance of each was taken again. To obtain the fitted line slope the maximum absorbance value of the folded protein was graphed versus the maximum absorbance value of the denatured protein. This slope along, with the literature extinction coefficient value for the template protein chromophore at the maximum absorbance in the denatured form, was used in Eq. 2.6. The quantum yield and extinction coefficient can be utilized further to determine the brightness of the protein as shown in Eq. 2.7.

2.2.9 Fluorescence Dynamic Range

The dynamic range is a measurement of the fluorescence intensity change from the apo to the holo form of our proteins. This characteristic was determined *in vitro* using the apo and holo fluorescence data from the Ca^{2+} titrations and *in vivo* using cultured cells transfected with ER-tagged protein as described in section 2.2.5. For the *in vivo* determination, the coverslip containing the transfected cells, as outlined in section 2.2.5, was rinsed three times with 1.8 mM Ca^{2+} Ringers buffer (145 mM NaCl, 2.5 mM K_2HPO_4, 1 mM $MgSO_4$, 10 mM HEPES buffer, 10 mM glucose, 1.8 mM Ca^{2+}; pH 7.4) and mounted for imaging using the Leica microscope at 40X magnification. After ideal cells were found and focused, the experiment was carried out at 550 nm excitation in KCl rinse solution (125 mM KCl, 25 mM NaCl, 10 mM HEPES buffer, 0.2 mM $MgCl_2$; pH 7.25). The cell walls were first permeated using 0.01% saponin. After rinsing the saponin away with KCl rinse, one micromolar EGTA was added to empty the ER of Ca^{2+}. The cells were rinsed once more with KCl rinse and then saturated with ten millimolar Ca^{2+}. The peak data was analyzed using Eq. 2.8 to determine the dynamic range.

$$DyR = \frac{F_{max}}{F_0} \qquad \textbf{Eq. 2.8}$$

2.3 Results

2.3.1 Strategy for Optical Property Optimization

2.3.1.1 DsRed-like Chromophore Formation

The MCD1x Ca^{2+} binding proteins made from mCherry maintain the low chromophore pK_a and long wavelength emission that the wild type has but exhibit a decrease in the quantum yield and extinction coefficient. The dynamic range of the proteins is also very small compared to our green CatchER and other published Ca^{2+} probes (Zhuo, 2014). For the proteins to be used successfully as an intracellular probe, these characteristics must be optimized. We hypothesize that this can be done by influencing the ionization of the chromophore based on our knowledge in designing green calcium indicator CatchER (Tang et al., PNAS). It is imperative to understand the chromophore and its formation to achieve this goal.

It is known that the chromophore forms after the protein properly folds, but the mechanism for chromophore formation in red FPs like DsRed and its variants is actively being investigated. Many theories for this mechanism have been hypothesized. It was originally believed that the extended conjugation of the red chromophore in DsRed and other red FPs involved an anionic GFP-like green intermediate (Gross et al., 2000)[31] after a mixture of green and red color was observed in mature DsRed samples. The immature green chromophore was believed to have formed after the chromophore cyclization and first oxidation step and would yield the mature red chromophore following a second oxidation step. This theory was later challenged as the oxidation to the red chromophore was believed to involve a carbanion state which would be energetically

unfavorable from the anionic GFP-like green intermediate. The anionic GFP-like intermediate is instead believed to be an endpoint form[32, 33].

It was then proposed that the mechanism to the red chromophore involved a branched mechanism[33-35]. On one path is the GFP-like chromophore endpoint and on the other the red chromophore via a blue chromophore intermediate. The blue intermediate, absorbing around 400 nm, would be capable of creating the carbanion state needed to extend the π-system conjugation to make the red chromophore.

Mechanism studies, as well as work to monomerize the tetrameric DsRed by Campbell et al., have uncovered crucial residues for chromophore formation. These residues work in different ways to encourage the protein folding and chromophore formation. Campbell et al. reported three "hot spots" that play a role in the chromophore maturation. The first of these involves the chromophore sidechain residue Q66, N42, and V44 in DsRed. Residues 42 and 44 were found to improve the maturation time of the protein by influencing the conformation of Q66. The second hot spot contained the sidechain of residue 163 being influenced by V175, F177 and possibly I161[20]. In DsRed and its derivatives, residue 163 interacts directly with the phenolate in the chromophore. Different residues, whether it be a lysine (DsRed), glutamine (dimer2), or methionine (mRFP1) in that position[20, 32] were found to cause different polarizations, shifting the electron density of the chromophore and encouraging formation.

The third hot spot was thought to be the most sensitive. It contained the K70 sidechains and the adjacent S197 and T217 sidechains. Having a positively charged residue in position 70 was found to be crucial for chromophore formation because it delocalizes the oxygen in the imidazolinone ring and encourages its negative charge[20, 34]. Having a larger polar residue in position 197 such as threonine or tyrosine would allow H-bonding with the chromophore and

improve its maturation[32]. Conservative mutations to these residues were crucial intermediates to mRFP1 and have strong effects on the fluorescent properties (Campbell et al., 2002).

Residues that do not interact directly with the chromophore have also been found to play significant roles in the chromophore formation. Mutations V71A and L150M to mRFP1 are in one of the hydrophobic pockets close to hot spot three and are thought to influence the chromophore by causing subtle packing rearrangements[20]. Verkhusha et al. found that small residues at position 71 are preferred after the introduction of V71M halted the chromophore at the GFP-like endpoint likely, because the larger residue displaces K70 toward the chromophore and quickly deprotonate the phenolate. Residue K83 also influences the orientation of residue L70. Mutations of K83 in DsRed to large nonpolar residues in the mFruits (K83L in mCherry and mStrawberry and K83F in mOrange) causes a position shift of K70 that is likely one reason for the red shift in the mFruits[36]. This residue is also crucial for the folding of monomeric reds after L83K mutations to mCherry and mStrawberry disrupted protein folding. The interaction of K70 and E148, a necessary interaction in the absence of the AC interface of the DsRed tetramer, is credited for the folding.

The protein environment is also important for successful chromophore formation. All of the proposed mechanisms for chromophore formation involve oxidation and dehydration steps, none of which involve any outside enzymes but instead occur with the aid of neighboring residues in certain ionic states. These steps can only be carried out fully and efficiently in the proper pH conditions. The temperature is also important for chromophore formation. While many FPs are being engineered to express at ambient body temperature for biological studies, there are still some chromophores that do not efficiently form in that range. Another factor that can affect the chromophore formation is the cell strain used to express the protein. Not all cell lines can express FPs so that they fold properly and without proper folding, the chromophore will not form.

2.3.1.2 Design of Optimized Next Generation MCD1x

We hypothesize that manipulating the ionization of the chromophore is key to optimizing the optical properties of the red sensors. Using the knowledge of which residues are pivotal to the chromophore formation, we began non-random mutagenesis. Our first approach was to make multiple mutations to residue 163. This residue is located in hot spot two and interacts directly with the chromophore[20]. Residue 163 was also found to play a role in the sensing mechanism of the R-GECO2 sensor reported by Campbell et al[37]. In DsRed and other monomeric variants this residue is either lysine or methionine, but in mCherry, it has been mutated to glutamine. This glutamine carried over into our sensors. The mutations Q163M, Q163K, Q163E, Q163L, Q163I, and Q163N were made to MCD15, and the Q163M mutation was made into MCD1.

Table 2-5 Design of Q163 Mutants

Mutation	Rationale
Q163M	Recovered mutation from mRFP1; present in other mFruit proteins
Q163K	Recovered mutation from DsRed
Q163I	Non-aromatic Hydrophobic residue structural isomer of Leu
Q163L	Non-aromatic Hydrophobic residue; structural isomer of Ile
Q163E	Charged residue; -CH_2 longer than Gln
Q163N	-CH_2 shorter than Gln

Our second approach was to make other chromophore sensitive residue mutations based on a sequence comparison of mCherry with other second generation monomers: mOrange, mStrawberry, mBanana, and mTangerine. These mFruits were made from mRFP1 in a similar fashion to mCherry. The different mutations made gave the different optical properties among the mFruits as outlined in Figure 2-2. mOrange and mBanana were chosen because they both possess

high quantum yields as well as a pH sensitivity similar to those in GFP and its variants. mOrange also has a high extinction coefficient. mStrawberry is considered a medium between mCherry and mOrange with a high extinction coefficient and relatively fast maturation time but has a low quantum yield similar to mCherry. mTangerine has a slightly higher pK_a than mCherry but shows a decrease in all other optical properties.

In choosing residues to mutate any residues that interact with the chromophore directly but have been previously seen to cause a decrease in optical properties when mutated, such as K70, were left alone. Residues in proximity to those were instead chosen. Six mutations total were chosen: S62T and Q64N from mStrawberry, I197E from mBanana, and A175S, L83F, and T41F from mOrange. Residues I197 and L83 sit in hot spot three[20] and interact indirectly with the chromophore through K70. Residue 197 also sits between two of our Ca^{2+} binding pocket residues: 196 and 198. Residue A175 sits in hot spot two and interacts with the chromophore indirectly through Q163. Residue T41 is a neighbor residue to hot spot one where Q42 interacts with M66 in the chromophore. Residue 64 does not interact with the chromophore directly but has been found to contribute to changes in photostability in a mutant of mOrange in combination with residue 163, 99, and 97 (Shaner et al, 2008)[38] and plays a role in the chromophore formation of orange DsRed variants (Subach et al, 2012)[39]. Residue 62 is mentioned for creating stability for the chromophore in mStrawberry along with residue 64 without direct interaction with the chromophore. As of this thesis the T41F mutant in MCD1 has been successfully cloned.

Table 2-6 Fluorescent properties of DsRed and the first and second generation variants

Fluorescent Protein	λ_{ex} (nm)	λ_{em} (nm)	Extinction Coefficient ($M^{-1}cm^{-1}$)	Quantum Yield	Brightness %DsRed	pK_a	$T_{0.5}$ for maturation at 37 ˚C	$T_{0.5}$ for bleach
DsRed	558	583	75000	0.79	100	4.7	~10 h	ND
T1	555	584	38000	0.51	33	4.8	<1 h	ND
Dimer2	552	579	69000	0.69	80	4.9	<2 h	ND
mRFP1	584	607	50000	0.25	21	4.5	<1 h	6.2
mHoneydew	487/504	537/562	17000	0.12	3	<4.0	ND	5.9
mBanana	540	553	6000	0.70	7	6.7	1h	1.4
mOrange	548	562	71000	0.69	83	6.5	2.5 h	6.4
dTomato	554	581	69000	0.69	80	4.7	1 h	64
tdTomato	554	581	138000	0.69	160	4.7	1 h	70
mTangerine	568	585	38000	0.30	19	5.7	ND	5.1
mStrawberry	574	596	90000	0.29	44	<4.5	50 min	11
mCherry	587	610	72000	0.22	27	<4.5	51 min	68

2.3.2 Expression and Purification

The cell pellets collected after expression of the 6 Q163 mutants in MCD15 are shown below in Figure 2-2 and compared to MCD15 without any mutation and mCherry. All proteins were expressed as outlined in 2.2.4. Mutants Q163K and Q163E appear to have lost all red color. Mutants Q163I and Q163L appear to have a light pink and purple color respectively. Mutants Q163N has a very faint pink color that can be seen against a white background. Mutant Q163M shows the brightest deep red color as well as more collected pellet than the other mutations.

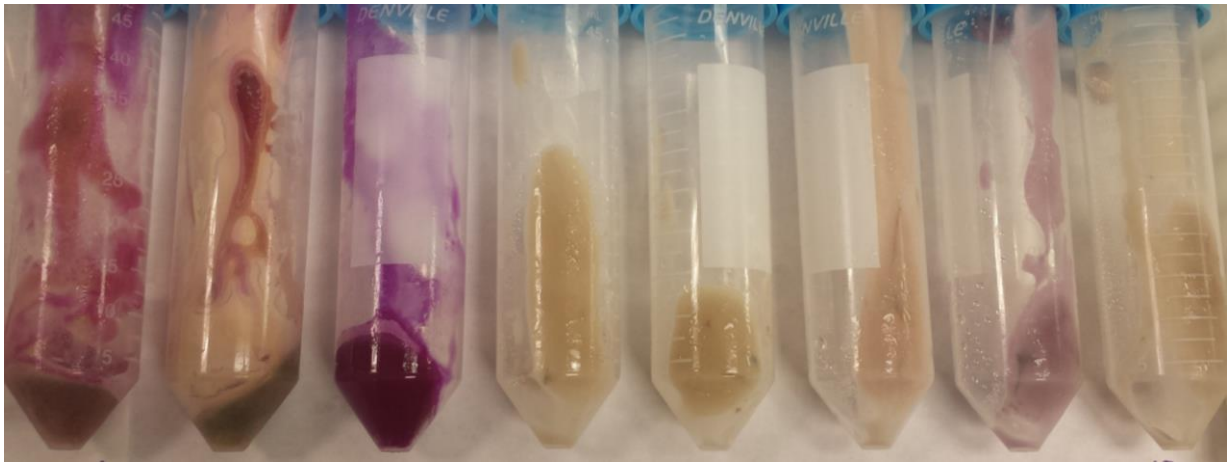

Figure 2-2 Expressed MCD15 Q163 mutants

Cell pellet collected after Rosetta Gammi expression of residue 163 mutants in MCD15 template as outlined in section 2.2.4.

Figure 2-3 shows the chromatograms from the gel filtration step of purification for proteins MCD1 Q163M, MCD15 Q163M, MCD15 Q163L, and MCD15 Q163I. The protein samples were collected from the second blue peak circled in brown. The first blue peak circled in red is currently being investigated. It was noted that this peak appears to increase in size with decrease in protein color and quantity.

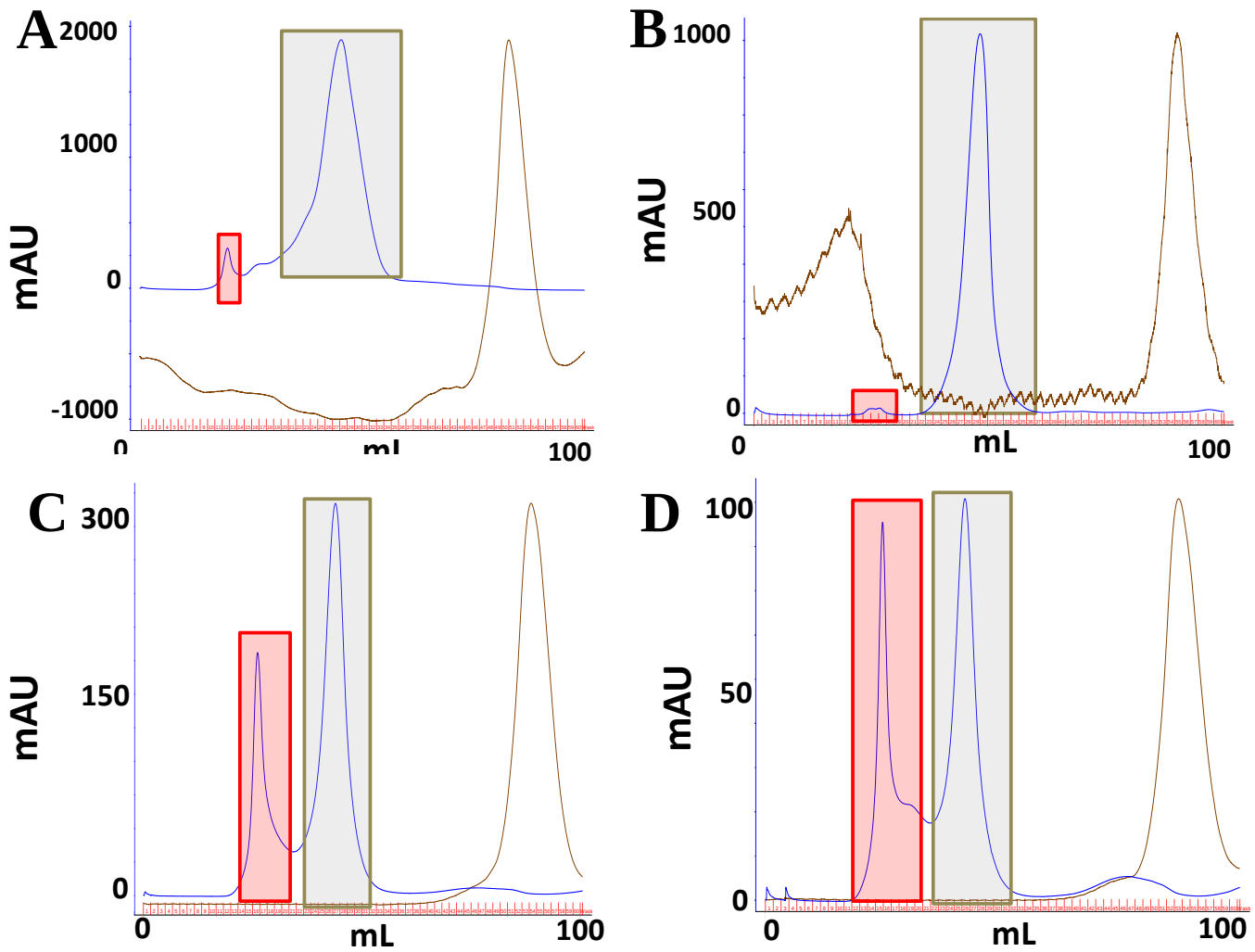

Figure 2-3 Gel filtration FPLC chromatograms

MCD1 Q163M (A), MCD15 Q163M (B), MCD15 Q163L (C), and MCD15 Q163I (D) purification chromatograms after gel filtration using Sephacryl S300 column using 10 mM Tris buffer (pH 7.4). The UV of the protein is the blue spectrum with two peaks while the imidazole removed from the samples is shown in the brown spectrum with the single peaks. The mature protein peak is circled in brown while unknown peak one is circled in read.

Figure 2-4 shows the SDS-PAGE analysis of the peaks seen in the Figure 2-3 chromatograms for the MCD15 mutants. The MCD15 Q163M mutant only displayed a band for peak two. Q163I showed a faint band for peak one that appeared to be the same size as the protein in peak two. Q163L has the same bands as Q163I, with the peak one band being stronger for this mutant.

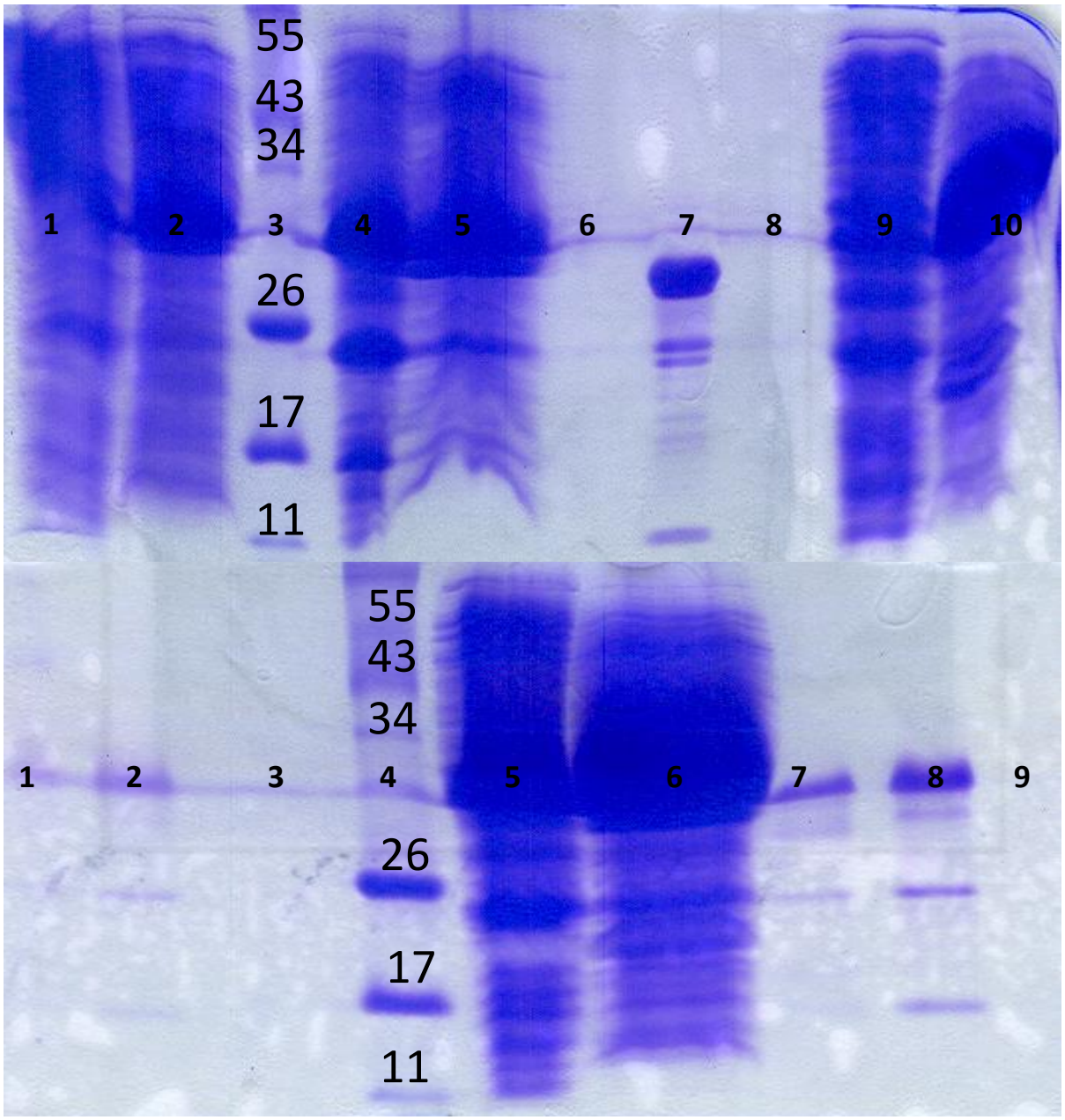

Figure 2-4 SDS-PAGE of gel filtration samples

SDS-PAGE gel (10%). Samples were dissolved in SDS buffer and heated to 100 ˚C for 10 minutes. Protein band present at 29 kDa. Top Gel: MCD15 sonicated supernatant (1), MCD15 sonicated pellet (2), protein ladder (3), MCD15 Q163M sonicated supernatant (4), MCD15 Q163M sonicated pellet (5), MCD15 Q163M gel filtration peak 1 (6), MCD15 Q163M gel filtration peak two (7), MCD15 Q163M gel filtration peak three (8), MCD15 Q163I sonicated supernatant (9), MCD15 Q163I sonicated pellet (10). Bottom Gel: MCD15 Q163I gel filtration peak one (1), MCD15 Q163I gel filtration peak two (2), MCD15 Q163M gel filtration peak three (3), protein ladder (4), MCD15 Q163L sonicated supernatant (5), MCD15 Q163L sonicated pellet (6), MCD15 Q163L gel filtration peak one (7), MCD15 Q163L gel filtration peak two (8), MCD15 Q163L gel filtration peak three (9).

Figure 2-5 shows the native protein gel for the peak one samples from gel filtration of the Q163M mutants compared with the pure protein and the mCherry template. The purpose of this gel was to examine the folded structure to see if the unknown gel filtration peak could be an oligomer. The mCherry protein in lane two appears to form multiple oligomers but does not appear in the monomer form. The sensors and their mutants, however, appear mostly in the monomer form with double bands around 29 kDa. MCD1 Q163M does show a light band in the possible dimer size region.

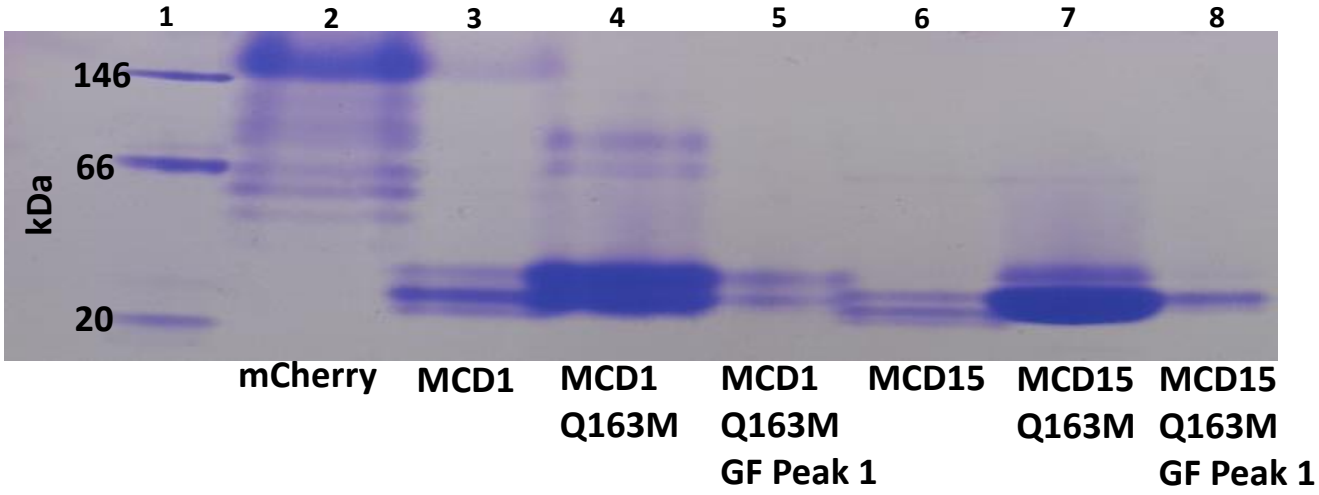

Figure 2-5 Native protein gel of gel filtration samples

NativePAGE™ Novex 14-16% protein gel. Samples were prepared and loaded as specified in manufacturer protocol and run at 150V for 120 minutes. LC075 ladder (1), mCherry pure (2), MCD1 pure (3), MCD1 Q163M pure (4), MCD1 Q163M gel filtration peak 1 (5), MCD15 pure (6), MCD15 Q163M pure (7), MCD15 Q163M gel filtration peak 1 (8).

Figure 2-6 shows the purified MCD1 and MCD15 proteins in quartz cuvettes in the apo form. The proteins were prepared in 5 μM concentrations. The chromophore environment based on crystal structure 2H5Q are shown below with the binding pocket residues and residue 163.

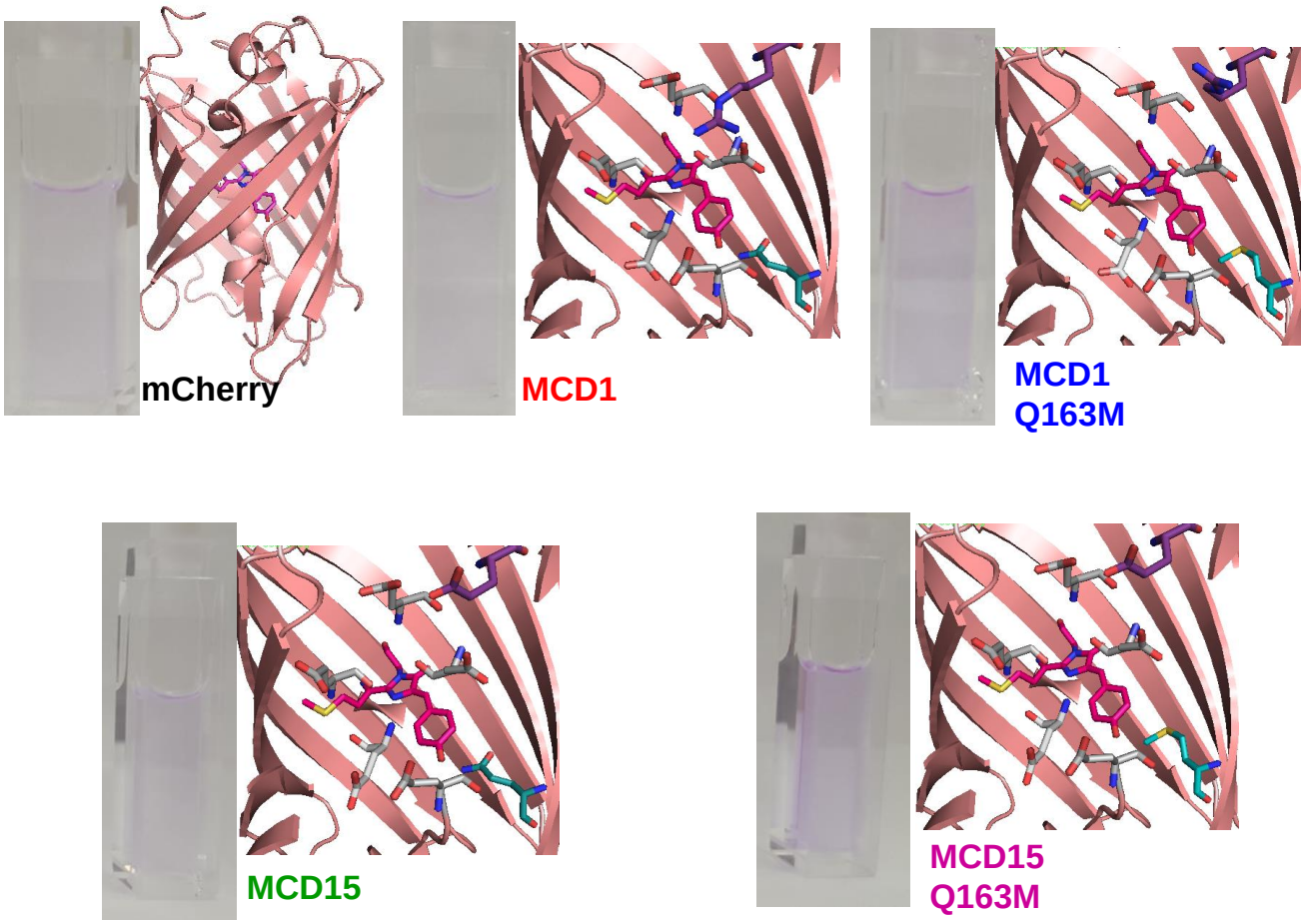

Figure 2-6 Purified MCD1x proteins

The tertiary structure of mCherry (2H5Q) shown with purified mCherry. (5 μM protein in 10 mM Tris; pH 7.4). The purified MCD1x mutants are shown with the binding pocket region for each protein and residue 163 (5 μM protein in 10 mM Tris; pH 7.4).

2.3.3 Effect of Q163M Mutation on Protein Optical Properties

Figure 2-7 shows the absorbance and fluorescence spectra of MCD1 and MCD15, with and without the Q163M mutation, compared to mCherry after expression in rosetta gammi bacteria cells. The Q163M mutation appears to cause a slight 3 nm shift in the chromophore absorbance from 587 nm to 590 nm. A small absorbance peak appears at ~505 nm in the Q163M mutant proteins. There also appears to be a 5 nm shift in the emission peak from 610 nm to 615 nm with the Q163M mutation. The mutation recovers lost absorbance and fluorescence

intensities in both proteins, with MCD1 Q163M having a higher absorbance and fluorescence than mCherry.

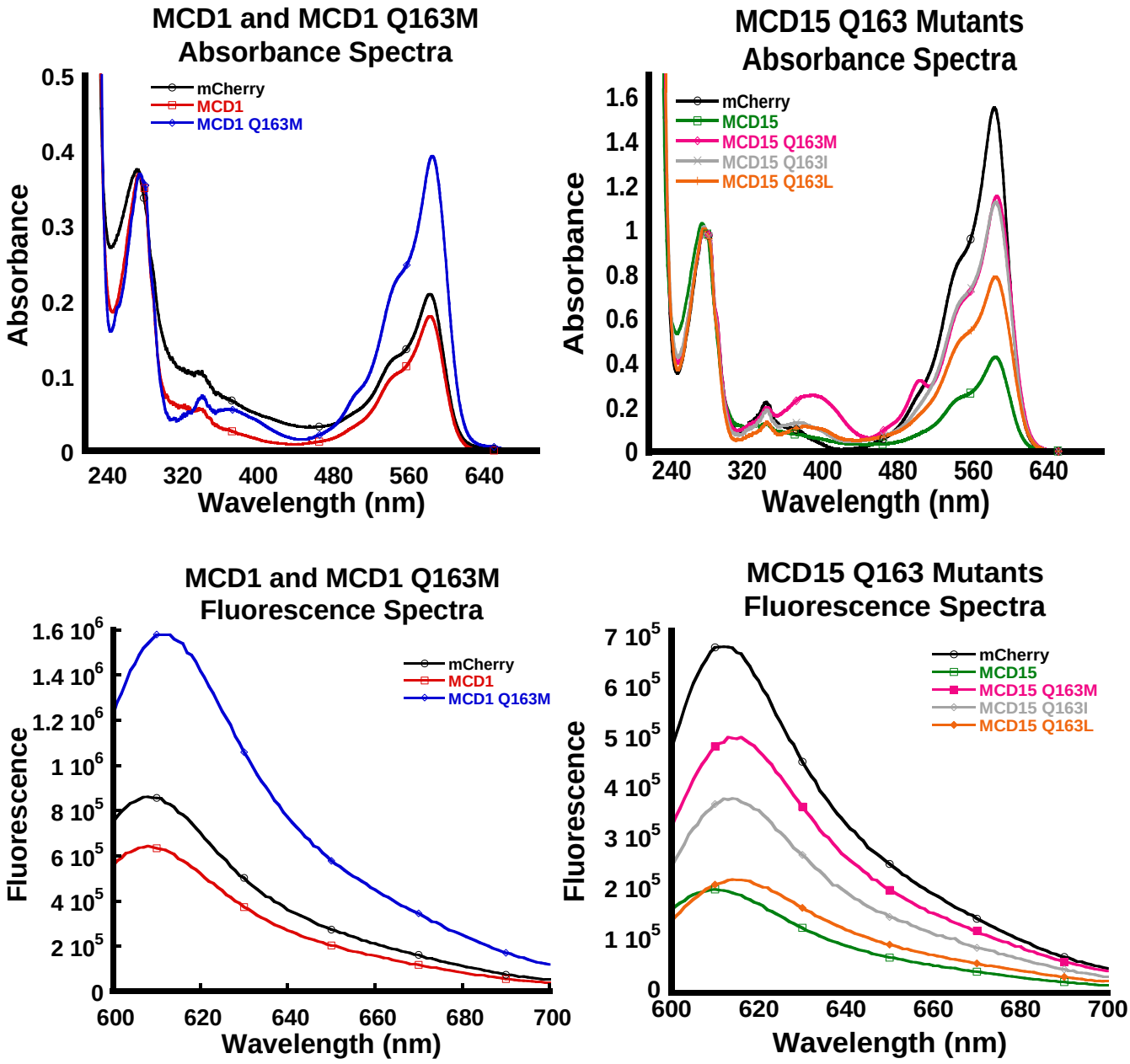

Figure 2-7 Q163 Mutation Effect on UV-VIS and Fluorescence Spectra

Protein samples were prepared at 10 μM concentration in 10 mM Tris (7.4 pH). A blank Tris buffer sample was used for the background in UV-VIS. The slit widths of the fluorometer were set using mCherry.

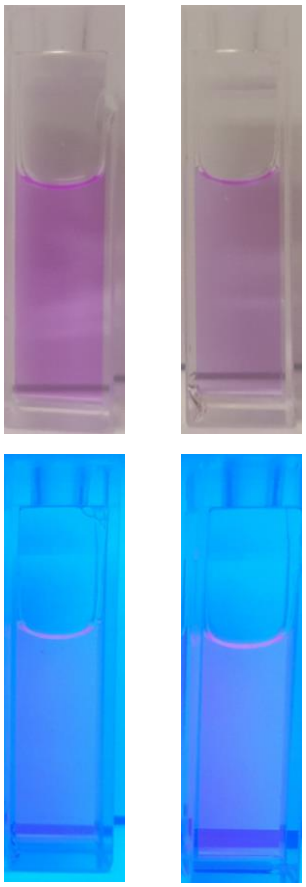

Figure 2-8 Pure mCherry and MCD15 Q163M

Pure mCherry (left) and MCD15 Q163M (right) in quartz cuvettes. The proteins were introduced to a long wave UV light source (bottom). Proteins were prepared at 20 mM concentration in 10 mM Tris buffer (pH 7.4) with 2 μM EGTA.

Figure 2-9 shows the ImageJ analysis of the proteins transfected into C2C12 mouse myoblast cells. As with the fluorescence seen in bacterially expressed protein, the fluorescence intensity increases with the Q163M mutation and MCD1 Q163M is the most intense of the 5. MCD15 displayed very low fluorescence and poor transfection.

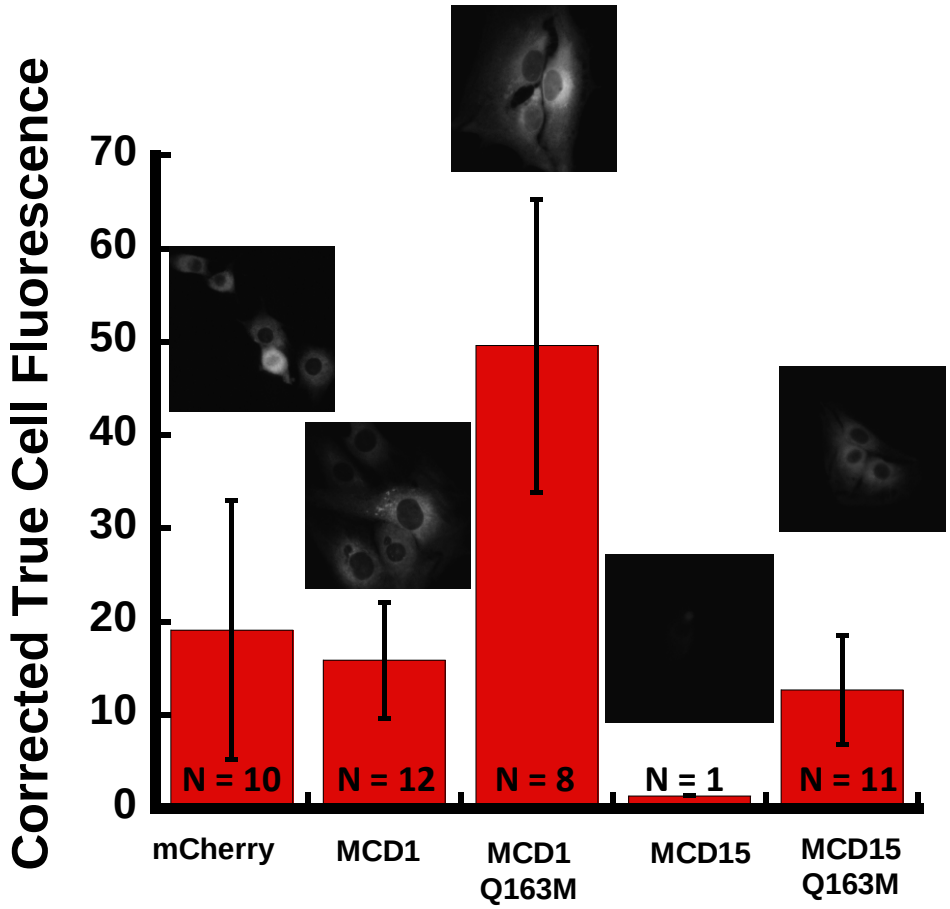

Figure 2-9 True Protein Fluorescence in C2C12 Mammalian Cells

The C2C12 cells were transfected with protein as outlined in section 2.2.5. Images were analyzed using ImageJ software to determine the true cell fluorescence.

Figure 2-10 displays the extinction coefficient values and quantum yield values that have been determined as shown in 2.2.8. MCD1 Q163M displays the greatest extinction coefficient, recovering the loss brought by the Ca^{2+} binding pocket. The quantum yield has yet to be determined but is expected to maintain the trend of increased optical properties. MCD15 Q163M thus displays the greatest quantum yield value.

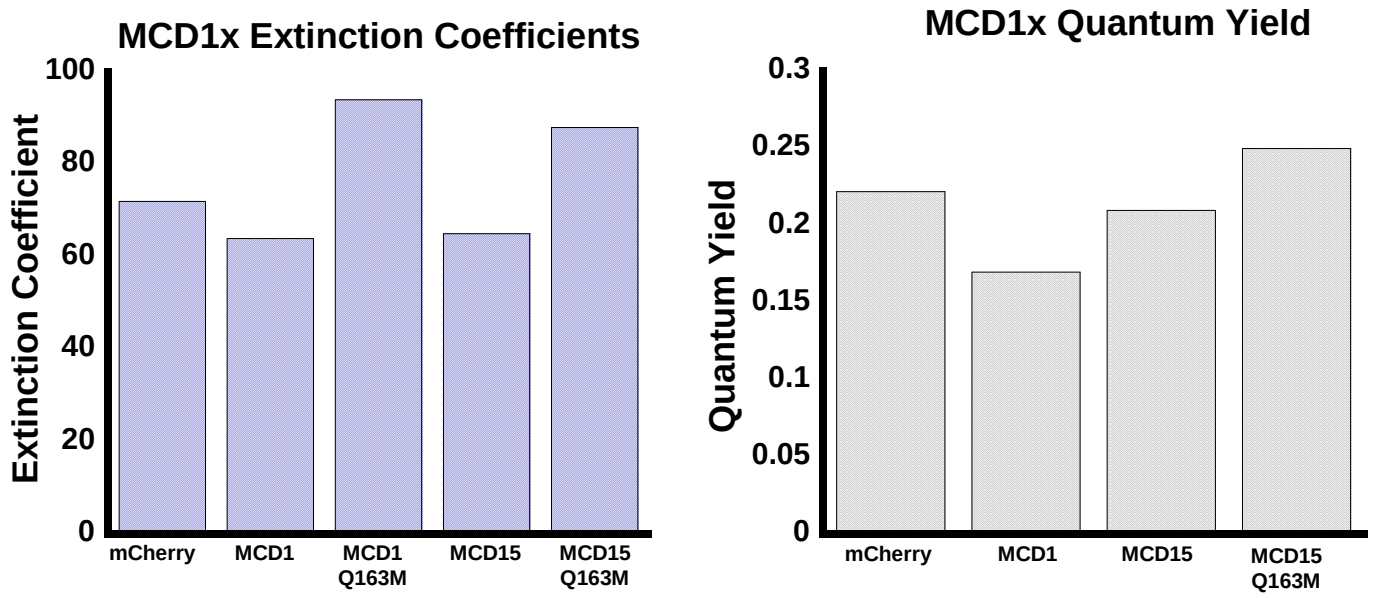

Figure 2-10 Optical Properties

The extinction coefficient and quantum yield of the proteins were determined as outlined in section 2.2.8. Samples were prepared in 10 mM Tris buffer (pH 7.4) at five different concentrations. Experiments were done in duplicate. Slit widths were set using the sample with the greatest fluorescence intensity. St Dev < 0.02

2.3.4 Chromophore pK_a

Figure 2-11 shows the data for the pKa determination for MCD15 Q163M. Graphs A and B show the raw fluorescence data for the protein in environment pH from 2 to 9 for the apo and holo protein form respectively. Graph C displays the normalized data from A and B, apo in red and holo in blue, to give the chromophore pK_a.

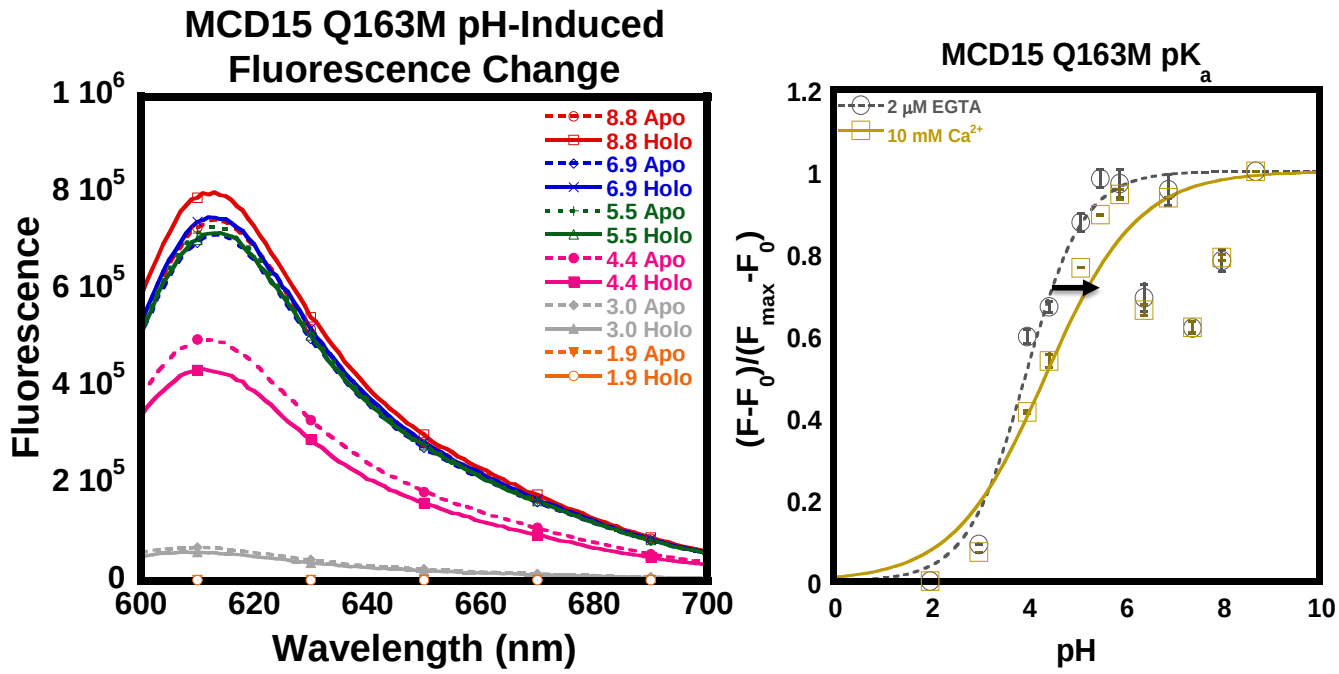

pK$_a$	Apo	Holo
	4.4 ± 0.3	3.9 ± 0.3

Figure 2-11Chromophore pKa of MCD15 Q163M

The protein sample was prepared as outlined in 2.2.7. The experiment was done in duplicate. Fluorescence spectra of the protein in the apo (dashed) and holo (solid) form in various pH conditions. Normalization of these data points with apo (gray dashed) and holo (gold solid) gives the pH profile and the chromophore pK$_a$. The pK$_a$ values for the chromophore are listed in the figure table.

2.3.5 Ca^{2+}-Induced Effect on Optical Properties

In figure 2.12 the Ca^{2+}-induced changes to the absorbance and fluorescence spectra are shown. There does not appear to be any change in the chromophore absorbance peak at 587 nm with Ca^{2+}, but the peak at 505 nm does increase with increasing Ca^{2+} concentrations. The fluorescence change with the 163M mutation appears to be the same as the fluorescence with 163Q. However, 163lI shows a noticeable increase in fluorescence.

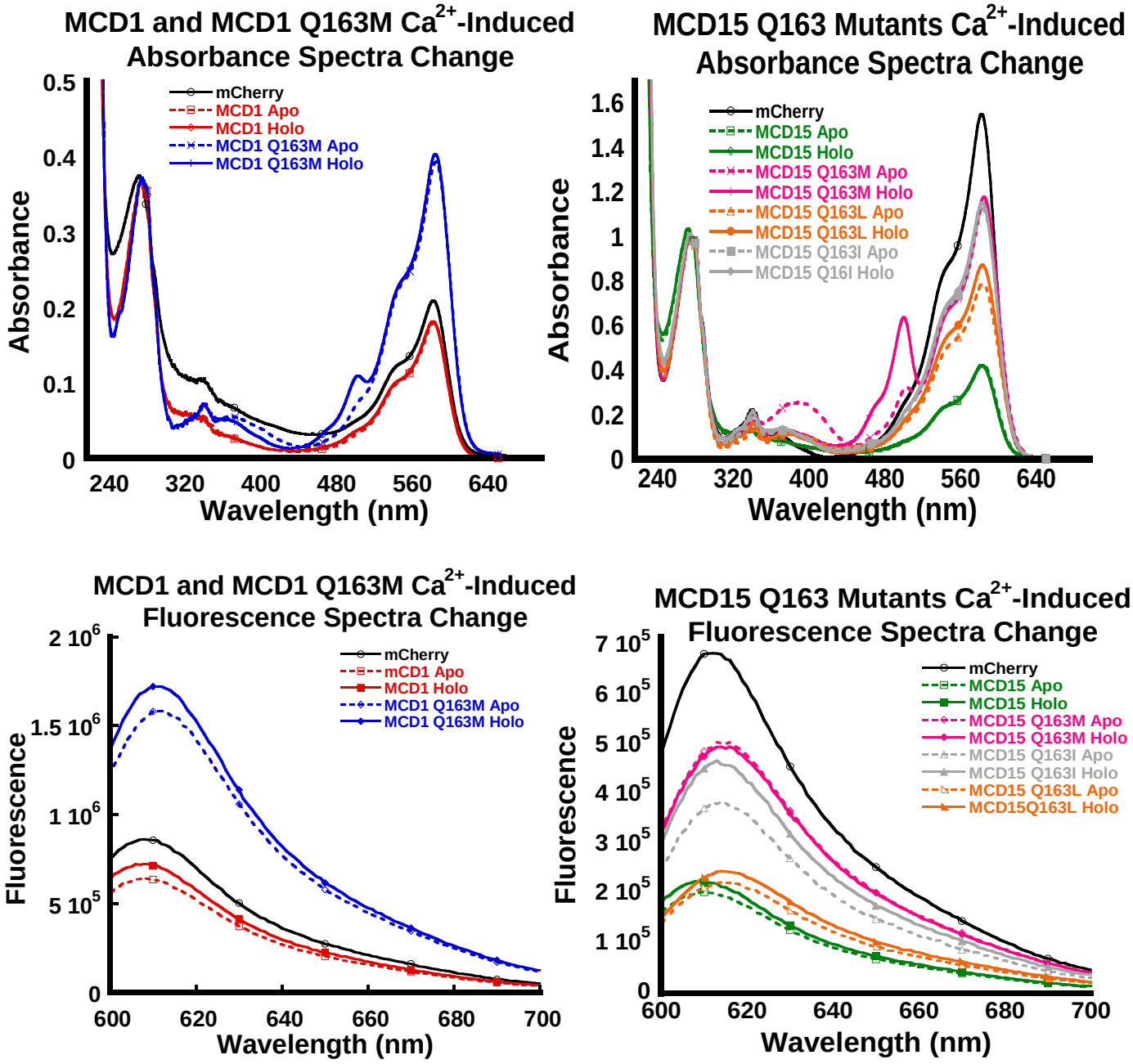

Figure 2-12 Ca^{2+}-Induced Spectral Changes

Protein samples were prepared at 10 μM concentration in 10 mM Tris (7.4 pH). A blank Tris buffer sample was used for the background in UV-VIS. The slit widths of the fluorometer were set using mCherry. The 2 μM EGTA were added to obtain the apo readings (dashed) and 10 mM Ca^{2+} was added to obtain the holo reading (solid lines).

Figure 2-13 shows the UV-VIS Ca^{2+} titration of MCD15 Q163M with the UV-VIS spectrum of mCherry as a comparison. The protein was prepared to 20 μM concentration in 10 mM Tris (pH 7.4) and the titration was carried out the same as the fluorescence Ca^{2+} titration outlined in 2.2.6.

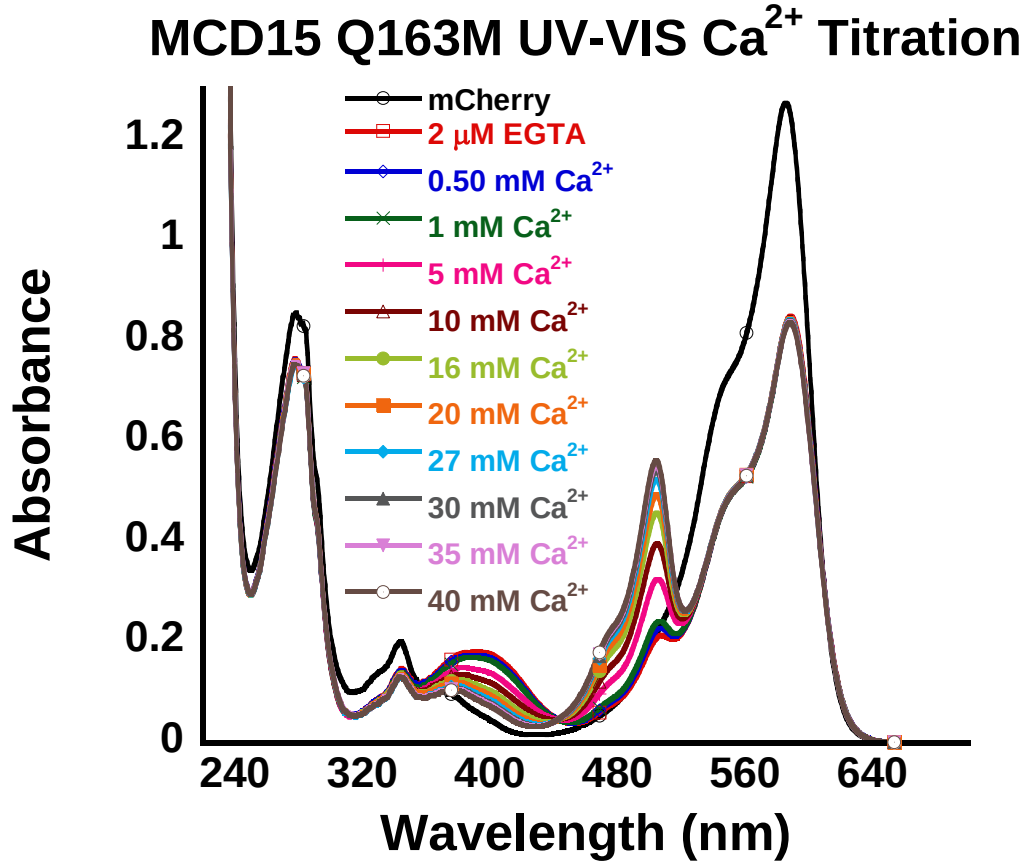

Figure 2-13 UV-VIS Ca2+ Titration

MCD15 Q163M was prepared at 20 μM concentration in 10 mM Tris (7.4 pH). A blank Tris buffer sample was used for the background in UV-VIS. A slow addition of Ca^{2+} metal was done and UV-VIS spectra taken at various increments.

The bar graph in Figure 2-14 compares the Ca^{2+}-induced change in the quantum yield of MCD1, MCD15, and MCD15 Q163M. MCD1 displayed the largest Ca^{2+}- induced change in quantum yield but MCD15 Q163M displayed greatest quantum yield values.

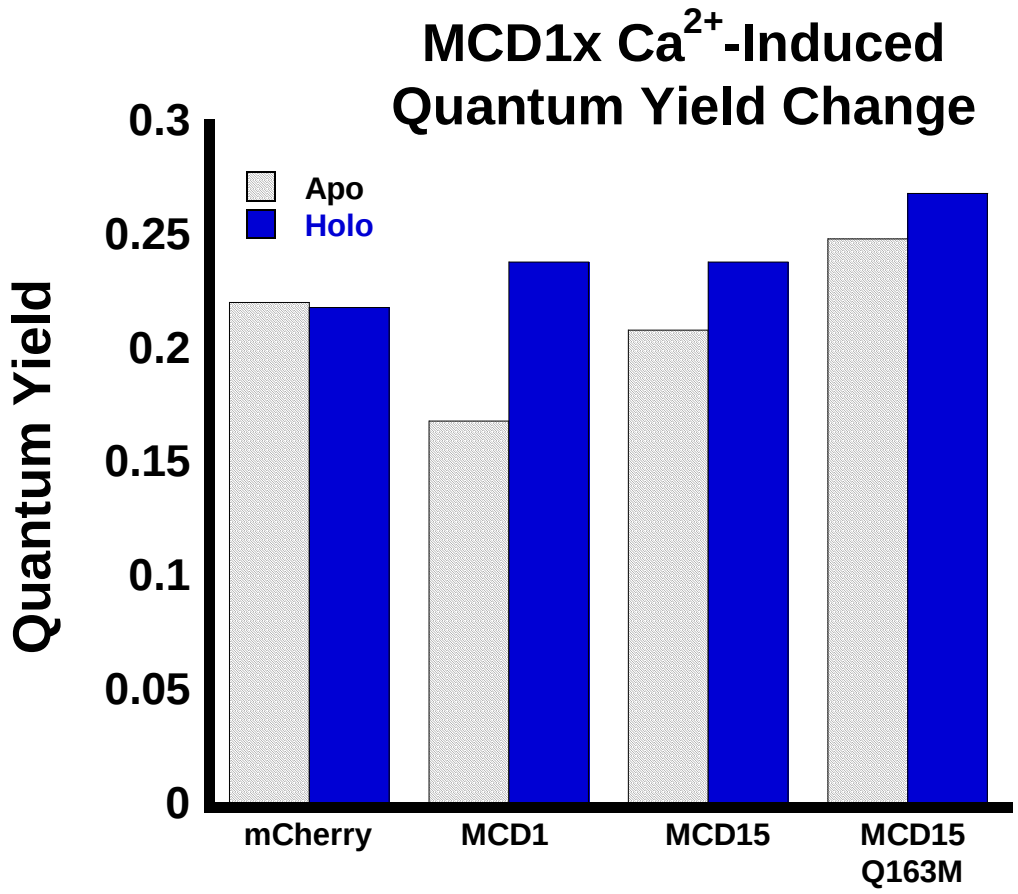

Figure 2-14 Ca^{2+}-Induced Optical Property Changes

Protein samples were prepared at five different concentrations in 10 mM Tris (7.4 pH) as outlined in section 2.2.8. A blank Tris buffer sample was used for the background in UV-VIS. The slit widths of the fluorometer were set using mCherry. The 2 μM EGTA were added to obtain the apo readings (black lined), and 10 mM Ca^{2+} was added to obtain the holo reading (blue solid). St Dev < 0.02.

2.3.6 Ca^{2+} Kd

The UV-VIS spectra and fluorescence emission spectra for the residue 163 mutants in MCD1 and MCD15 were previously shown in Figure 2-12. Figure 2-15 shows the normalized fluorescence data that gives the Ca^{2+} K_d for MCD1, MCD1 Q163M, MCD15, MCD15 Q163M and MCD15 Q163L following a Ca^{2+} titration as outlined in section 2.2.6. The proteins were made in 10 μM concentrations in 10 mM Tris (pH 7.4), and emission spectra were obtained at

various Ca^{2+} concentrations. A titration for MCD15 Q163I could not be obtained due to low protein yield.

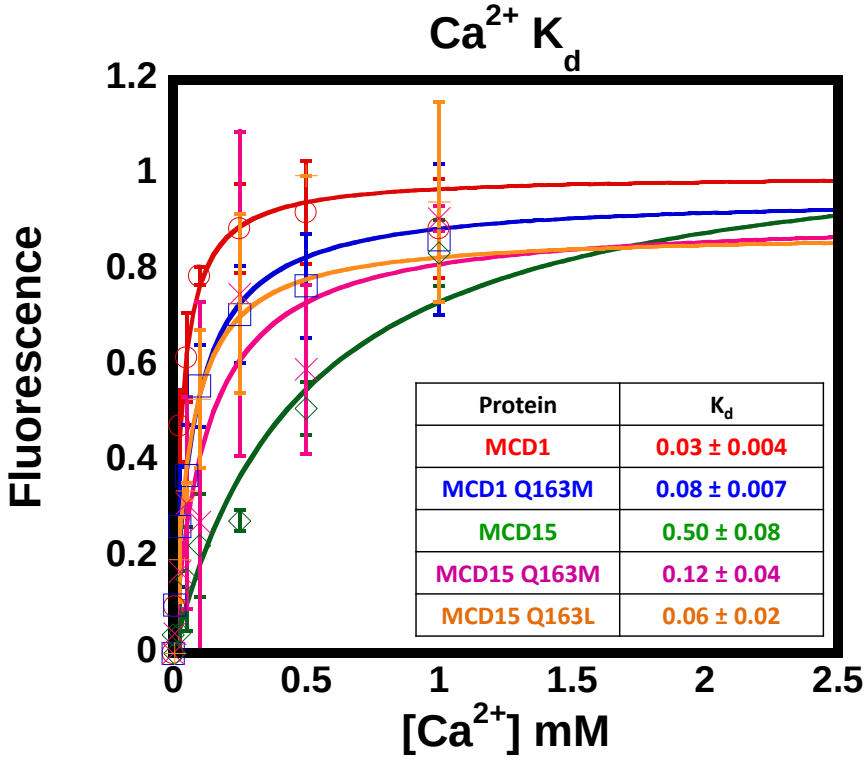

Figure 2-15 Ca^{2+} affinity of MCD1x sensors

MCD1 (red), MCD1 Q163M (blue), MCD15 (green), MCD15 Q163M (pink), and MCD15 Q163L (orange). Samples were prepared to 10 μM in 10 mM Tris (pH 7.4). Experiment was done in triplicate.

2.3.7 Fluorescence Dynamic Range

In addition to the Ca^{2+} affinity, the raw fluorescence data was used to determine the dynamic range of fluorescence of the residue 163 mutants using Eq. 2.8 in section 2.2.9. The dynamic range values for MCD1, MCD15, and MCD15 Q163M were also determined using *in vivo* imaging as outlined in section 2.2.9. These values, along with the K_d, are reported in Table 2-7.

The *in vivo* dynamic range determination data of MCD1, MCD15, and MCD15 Q163M are shown in Figures 2-16, 2-17, and 2-18 respectively. Imaging was done on the inverted fluorescence Leica microscope in C2C12 mouse myoblast cells. Cells were transfected with respective protein as outlined in section 2.2.5.

Table 2-7 Ca^{2+} affinity and dynamic range

Protein	**Ca^{2+} K_d**	***in vitro* Dynamic Range**	***in vivo* Dynamic Range**
MCD1	0.03 ± 0.01	1.118 ± 0.03	1.128 ± 0.01
MCD1 Q163M	0.08 ± 0.01	1.098 ± 0.01	---
MCD15	0.50 ± 0.08	1.089 ± 0.01	1.170 ± 0.3
MCD15 Q163M	0.12 ± 0.04	1.099 ± 0.02	1.21 ± 0.03
MCD15 Q163L	0.06 ± 0.02	1.124 ± 0.01	---

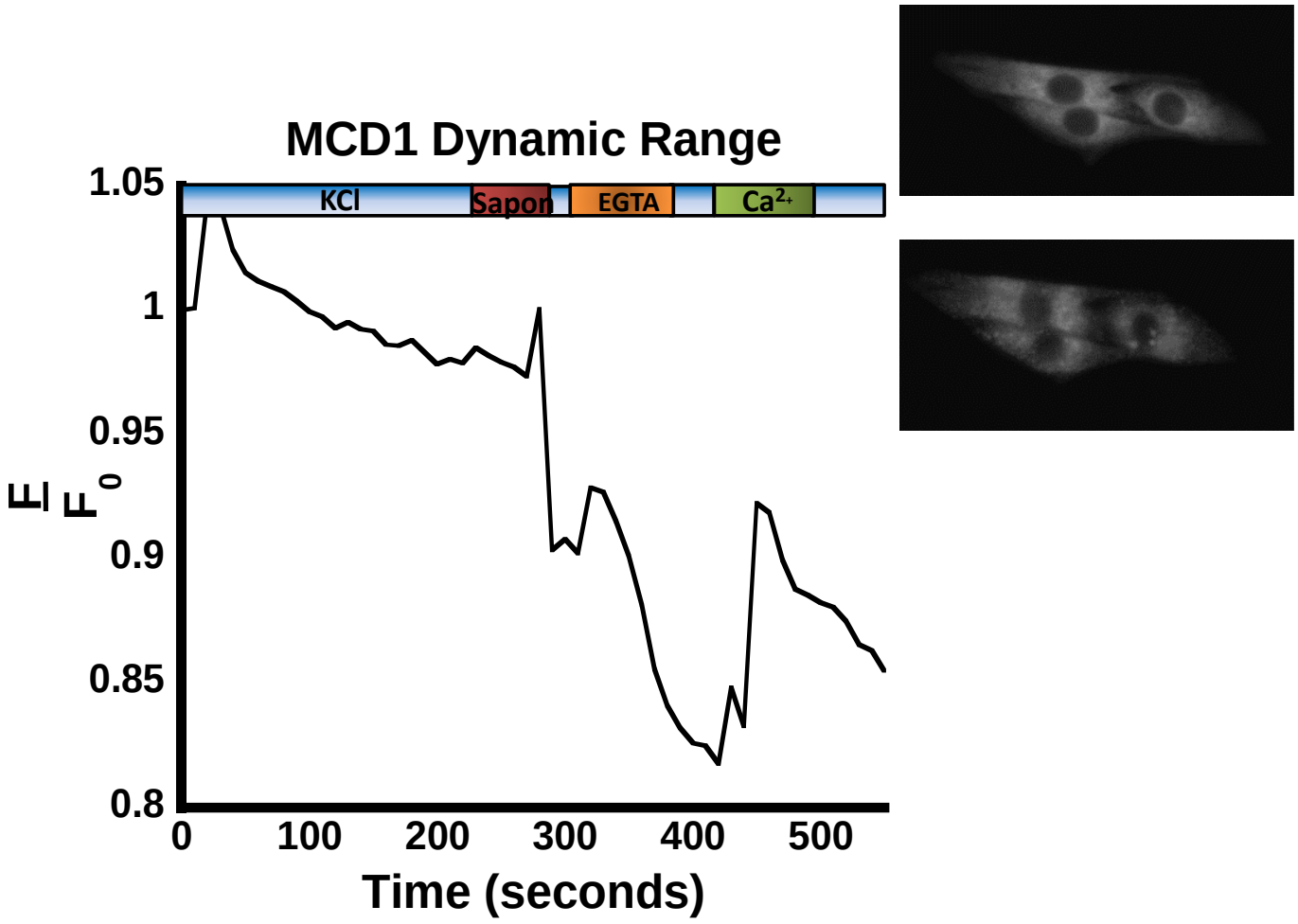

Figure 2-16 MCD1 *in vivo* dynamic range

MCD1 protein in pcDNA3.1 vector transfected in C2C12 mouse myblast cells as described in section 2.2.5. Ringers buffer (145 mM NaCl, 2.5 mM K_2HPO_4, 1 mM $MgSO_4$, 10 mM HEPES buffer, 10 mM glucose, 1.8 mM Ca^{2+}; pH 7.4), KCl rinse solution (125 mM KCl, 25 mM NaCl, 10 mM HEPES buffer, 0.2 mM $MgCl_2$; pH 7.25), 0.01% saponin, 1 μM EGTA, and 10 mM Ca^{2+} were used as described in 2.2.5. Cell images were taken before (top) and after (bottom) experiment.

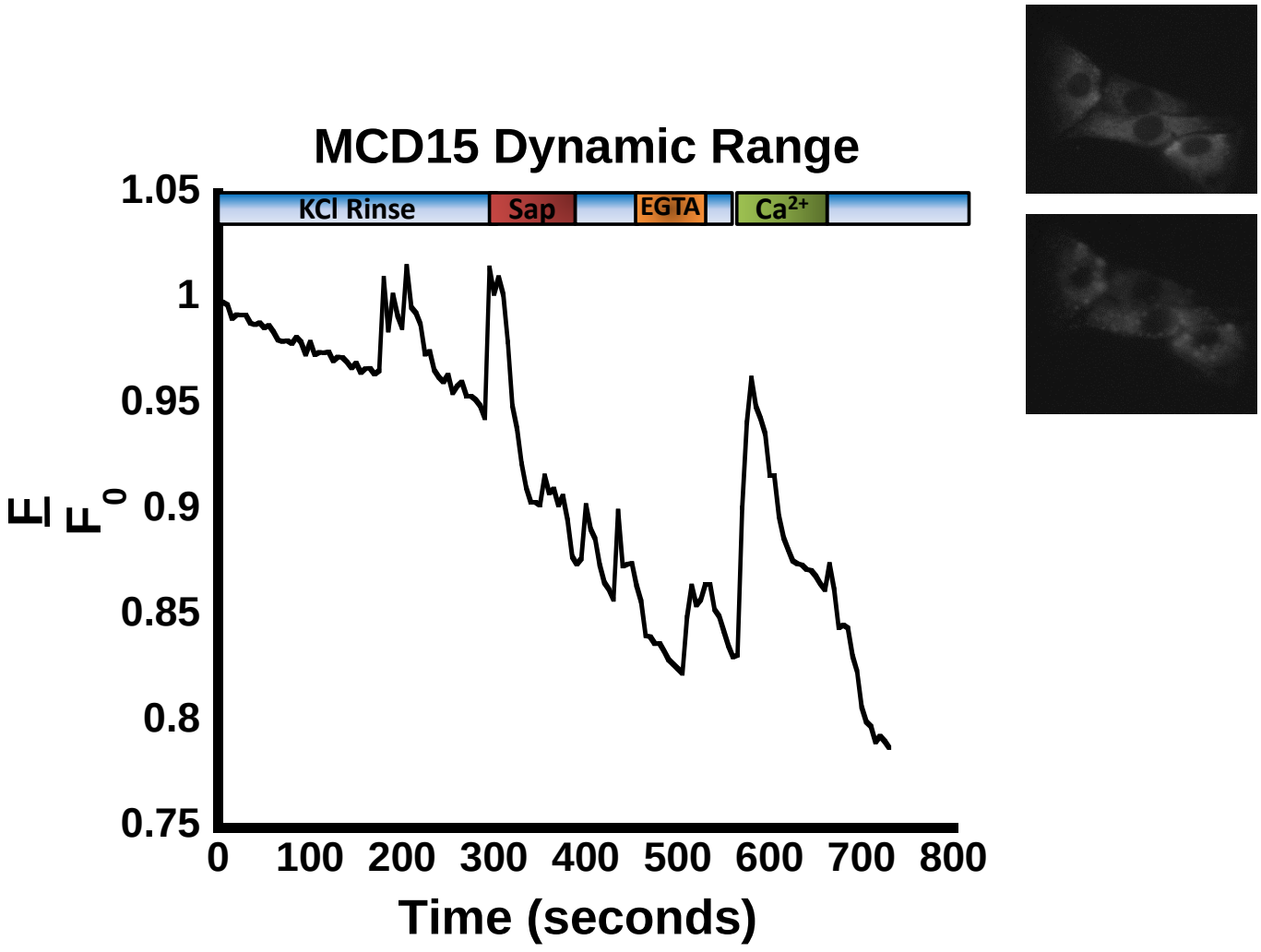

Figure 2-17 MCD15 *in vivo* dynamic range

MCD15 protein in pcDNA3.1 vector transfected in C2C12 mouse myblast cells as described in section 2.2.5. Ringers buffer (145 mM NaCl, 2.5 mM K_2HPO_4, 1 mM $MgSO_4$, 10 mM HEPES buffer, 10 mM glucose, 1.8 mM Ca^{2+}; pH 7.4), KCl rinse solution (125 mM KCl, 25 mM NaCl, 10 mM HEPES buffer, 0.2 mM $MgCl_2$; pH 7.25), 0.01% saponin, 1 μM EGTA, and 10 mM Ca^{2+} were used as described in 2.2.5. Cell images were taken before (top) and after (bottom) experiment.

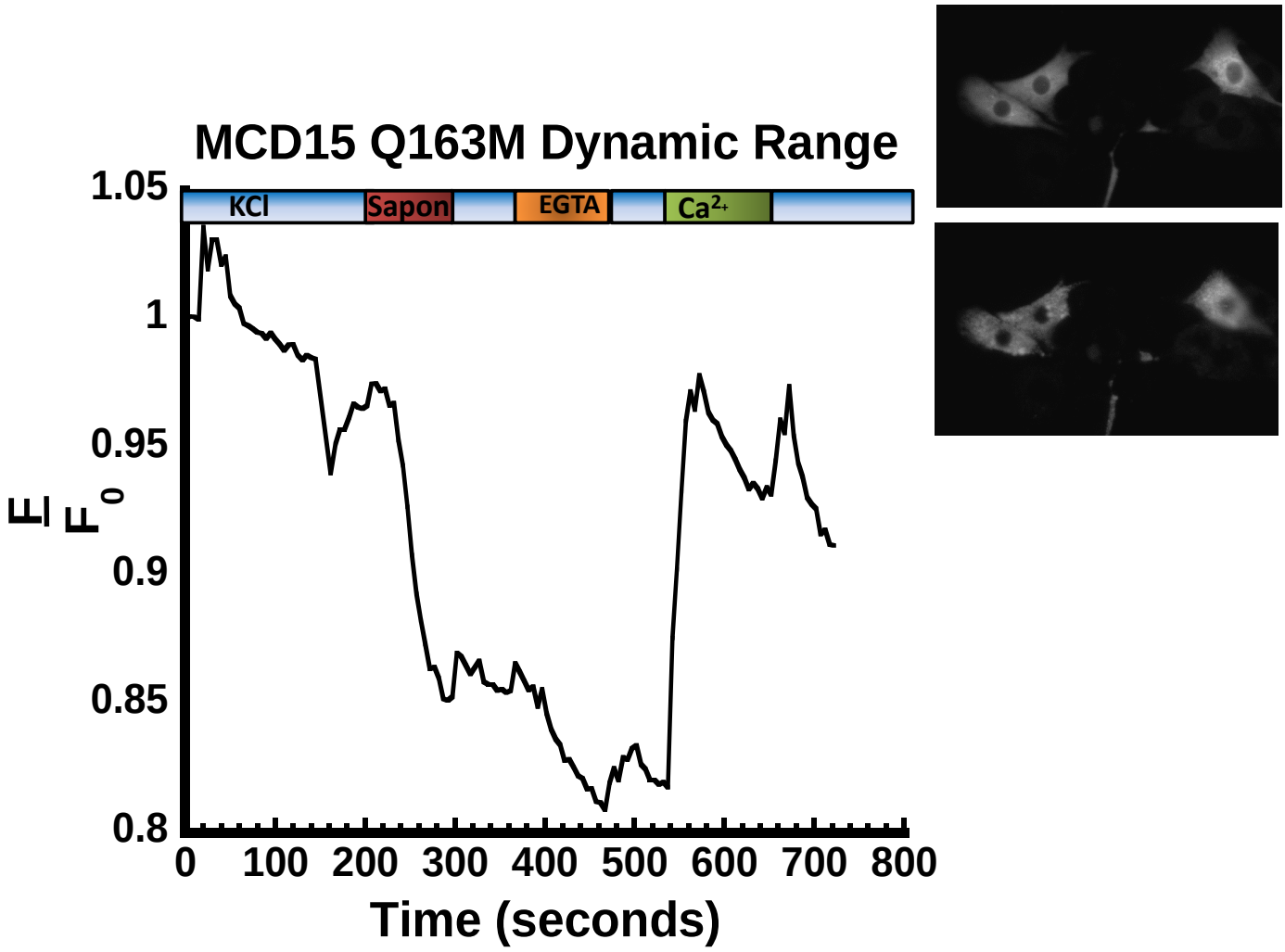

Figure 2-18 MCD15 Q163M *in vivo* dynamic range

MCD15 Q163M protein in pcDNA3.1 vector transfected in C2C12 mouse myblast cells as described in section 2.2.5. Ringers buffer (145 mM NaCl, 2.5 mM K_2HPO_4, 1 mM $MgSO_4$, 10 mM HEPES buffer, 10 mM glucose, 1.8 mM Ca^{2+}; pH 7.4), KCl rinse solution (125 mM KCl, 25 mM NaCl, 10 mM HEPES buffer, 0.2 mM $MgCl_2$; pH 7.25), 0.01% saponin, 1 μM EGTA, and 10 mM Ca^{2+} were used as described in 2.2.5. Cell images were taken before (top) and after (bottom) experiment.

2.4 Discussion

2.4.1 Chromophore Development

The 163 mutants were expressed and purified as outlined in section 2.2.4. The dialysis and desalting methods were utilized in the past to remove imidazole from the pure proteins, but these methods do not remove all of the imidazole. To eliminate as much imidazole as possible the size exclusion method through gel filtration chromatography was used. In doing this additional peaks were seen in the chromatographs that were not seen in desalting. MCD1, MCD1Q163M, MCD15, and MD15 Q163M all displayed a small peak before the large protein peak. The Q163L and Q163I mutants have less color and exhibit an increase in that first peak as well as the appearance of a third peak after the protein peak. The chromatographs of these are shown in Figure 2-3.

With an understanding of the mechanism for DsRed-like chromophore development, it is believed that the first peak, may be an immature form of the chromophore. In the samples with deep color and a high concentration after purification, this peak is very small but in those samples where the chromophore is slower or less efficiently developing this peak increases to intensities comparable to the mature protein peak. The fractions from this peak do not display any noticeable color in any of the samples, and the concentration in MCD1, MCD15, and their Q163M mutants is too low to show anything in the SDS-PAGE. The peak one samples from Q163I and Q163L do show bands in SDS-PAGE. The bands are very faint but maintain the same sizes as the protein bands in the mature protein. If the protein took the pathway branch toward the green chromophore, it would fail to have the fragment bands that are indicative of the extended conjugation into the backbone. This tells us that the possible immature protein in this peak would be in the blue intermediate form or the colorless stage before the blue intermediate.

UV-vis of this peak was obtained for MCD15 Q163M but only displayed a low peak at 280 nm, again a likely effect of low concentration. Spectra for this peak in the other mutants are being obtained to see if there are any other absorbance peaks. A native protein gel could also tell us more about this peak such as whether there is folded protein present, whether there is any dimer in the sample, and the approximate size of any protein.

The UV-vis spectra for MCD1 and MCD15 maintain the same peaks as the spectrum for mCherry. This changes with the Q163M mutation where a 3 nm red shift in the major absorbance peak from 587 nm to 590 nm occurs. There is also the appearance of a peak at 505 nm that does not appear with the Q163L or Q163I mutants. It is, however, seen in the previous RFP generations with the M163 residue. The excitation and emission spectra are shown in Figure 2-7. The Q163 mutant proteins show a 5 nm red shift in emission from the MCD1 and MCD15 templates, whose spectra are consistent with mCherry. An excitation scan was run at the peak emission, and it was noticed that there is no distinct peak at 505 nm in either Q163M mutant. Instead, the 505 nm fluorescence is observed to be an increasing part of the main 590 nm excitation peak in MCD1 and MCD15. This tells us that there is a non-emitting species made by the presence of methionine in position 163 that absorbs on its own at 505 nm. Figure 2-13 displays the UV-VIS Ca^{2+} titration of MCD15 Q163M. The 505 nm peak does have a noticeable increase with Ca^{2+}, a property that will be further studied.

The percent fluorescence intensity change of MCD1, MCD1 Q163M, MCD15, and MCD15 Q163M as compared to mCherry is shown below in Table 2-8. The values reported are for the Ca^{2+} free apo and Ca^{2+} loaded holo forms. Introducing the pocket of negative charges to mCherry to make the Ca^{2+} binding MCD1 caused a 25.3% decrease in fluorescence intensity. The additional R220E and D198E mutations made to create MCD15 caused a much larger 71.0%

fluorescence decrease compared to mCherry. This indicates that the binding pocket has a destabilizing effect on the chromophore that results in the loss of wild-type fluorescence properties.

Table 2-8 Fluorescence intensity change compared to mCherry

Protein	Apo Fluorescence Intensity Change	Holo Fluorescence Intensity Change
MCD1	-25.3%	-16.0%
MCD1 Q163M	+78.7%	+96.4%
MCD15	-71.0%	-68.2%
MCD15 Q163M	-26.1%	-27.4%

The introduction of methionine to residue 163 causes a dramatic increase in fluorescence over the wild type. The Q163M mutation caused a 78.7% increase in the fluorescence for MCD1 compared to mCherry. In MCD15 the fluorescence intensity is still 26.1% lower than mCherry, but this is a dramatic increase from MCD15 with glutamine in position 163.This implies that the interaction between the tyrosyl oxygen of the chromophore with the sulfur of methionine improves the stabilization of the chromophore dramatically. This is supported by the color intensity of the proteins compared to the wild-type and other 163 mutants. The increase in the 587 nm peaks of the absorbance spectra, an indication of the chromophore formation in a similar way to the 280 nm peak indicating protein concentration, supports the improved stabilization and formation of the chromophore.

The chromophore pK_a of each mutant was determined by incubating the protein in 12 different buffers of different pH ranging from 2 to 9 and taking fluorescence spectra. mCherry is known for having a low pK_a value of 4.5, making it insensitive to pH changes that can occur during experimentation. The creation of a Ca^{2+} binding site to form MCD1 decreases the pK_a slightly to

3.6. In MCD15 the chromophore pK_a is 4.4, nearly identical to mCherry. The addition of the Q163M mutation to MCD15 caused no change in the pK_a, leading us to believe that this mutation provides improved chromophore stability without changing the overall ionization.

The extinction coefficient and quantum yield are measurements of the strength of photon absorption and the efficiency of chromophore fluorescence respectively at a wavelength of excitation. These values are summarized in Table 2-9 below for mCherry, MCD1, MCD15 and MCD15 Q163M. The extinction coefficient for both MCD1 and MCD15 are 64 and 65 respectively, lower than the 72 of mCherry. The Q163M mutation in MCD15 brought the extinction coefficient to 88. This leads us to believe that the 163 residue plays a role in the chromophore's ability to absorb photons.

The single quantum yield of 0.22 for mCherry is lower than some of the other mFruits. The Ca^{2+} sensors display quantum yields slightly lower than the wild type. In both MCD1 and MCD15, the quantum yields come out to 0.17 and 0.21 respectively. The Q163M mutation to MCD15 restores the quantum yield to the mCherry value of 0.25. This tells us that the cluster of negative charges we introduced to create our pocket caused a decrease in both absorption strength and fluorescence efficiency but the Q163M mutation in MCD15 interacts with the chromophore in a way that it recovered the quantum yield and greatly improved the extinction coefficient. Multiplying the extinction coefficient by the quantum yield gives you the protein brightness. Proteins MCD1 and MCD15 show a respective 31% and 13% decrease in the brightness compared to mCherry while MCD15 Q163M shows a 39% increase in the brightness.

Table 2-9 Optical properties

Protein	Extinction Coefficient (ε587 (mM^{-1} cm^{-1}))	Quantum Yield (Φ)		Brightness (ε • Φ)	
		Apo	Holo	Apo	Holo
mcherry	72	0.22		15.8	
MCD1	64	0.17	0.24	10.8	15.4
MCD15	65	0.21	0.24	13.7	15.7
MCD15 Q163M	88	0.25	0.27	22.0	23.8

One explanation for the increase in properties of the Q163M mutant is hydrophobicity. As shown in Figure 2-18 the transition from glutamine to methionine increases the hydrophobicity dramatically. This drastic change in interaction is crucial for this particular residue since it is not only in the H-bond network but interacting directly with the phenolate oxygen. This increase in hydrophobicity is essentially eliminating an interaction that the oxygen was having with the nitrogen. Exactly how this change affects the conformation of the chromophore cannot be said at this time, but the ionization has been changed.

Amino Acid	Phe	Met	Ile	Leu	Val	Cys	Trp	Ala	Thr	Gly	Ser	Pro	Tyr	His	Gln	Asn	Glu	Lys	Asp	Arg
Row A	2.8	1.9	4.5	3.8	4.2	2.5	-0.9	1.8	-0.7	-0.4	-0.8	-1.6	-1.3	-3.2	-3.5	-3.5	-3.5	-3.9	-3.5	-4.5
Row B	3.7	3.4	3.1	2.8	2.6	2.0	1.9	1.6	1.2	1.0	0.6	-0.2	-0.7	-3.0	-4.1	-4.8	-8.2	-8.8	-9.2	-12.3

Figure 2-19 Amino Acid Hydrophobicity

Row A from J. Kyte and R.F. Doolittle[40]. Row B from D.A. Engelman, T.A. Steitz, and A. Goldman[41]. Hydrophobicity scales measure the degree of hydrophobicity of different amino acid side chains. It was developed based on the solubility measurements of amino acids in different solvents, vapor pressures of sidechain analogs, analysis of sidechain distributions with soluble proteins and the theoretical energy calculations.

2.4.2 Ca^{2+} Binding Properties

When looking at the Ca^{2+} affinity data in Figure 2-6 MCD1 has the greatest affinity for Ca^{2+} with a K_d 0.03 mM. MCD15 displays a weaker affinity of with a K_d of 0.5 mM. The Q163M mutation has a different effect in these two proteins, increasing the affinity for MCD15 but decreasing it in MCD1. As shown in Figure 2-1, Q163 directly interacts with the chromophore as a part of hot spot two and indirectly bonds with other residues in the network and other hotspots. MCD15 was made for improved mammalian cell expression by making the D198E and R220E mutations to MCD1. One of these residues, D/E198 of which neighbors hot spot two residue I197, affects the conformational of the binding pocket. The Q163M mutation may be working through the H-bond network with the chromophore tyrosyl and S63 to stabilize the chromophore. This stabilization is likely affecting the interactions of the imidazolinone ring with K70 and I197 to influence the binding pocket, particularly the area with residue D/E198, in a way that improves the binding affinity with the glutamate in MCD15 but decreases it with aspartate in MCD1.

In determining the other Q163 mutation affinities in MCD15, the Q163I mutant could not be accurately determined because the yield of protein was too low to perform the triplicate titration experiments. The Q163L mutant, however, gave a K_d of 0.06 mM. This is an increase in affinity compared to Q163M mutation with a K_d of 0.12 mM. The reason a nonpolar residue improves the binding affinity while the polar one decreases it is still unknown at this time.

The opposite effect occurs for the fluorescence intensity than what is seen with the affinity. As stated above in 2.4.1, the nonpolar residues decreased the fluorescence intensity of the chromophore while the polar residue increased it. The addition of Ca^{2+} induced an increase in fluorescence for all of the mutations, indicating that our binding pocket is in a position to not only influence the H-network but also affect the optical properties of the chromophore differently with

and without Ca^{2+}. The magnitude of the fluorescence intensity change from the apo to holo forms is similar in all mutants, 10.5%-12%, except for in MCD15 and MCD15 Q163L, both of which display a less that 4% change in fluorescence with Ca^{2+}.

The chromophore pK_a after Ca^{2+} binding caused an increase to 5.0 for MCD1 and a negligible increase to 4.6 in MCD15. This change in ionization retained the pH insensitivity. In the MCD15 Q163M, mutant Ca^{2+} binding caused a decrease in chromophore pK_a to a value of 3.9, making it more pH insensitive that mCherry. The mutation did not cause any change to the chromophore pK_a in MCD15 but this change in trend with the addition of Ca^{2+} further supports the theory that its presence in the H-bond network does add stabilization of the chromophore with and without Ca^{2+}. Similar results were seen with Campbell et al. (2013)[37] where a Q163M mutation into an RGECO variant maintains fluorescence at low pH.

The presence of Ca^{2+} does not appear to effect the extinction coefficient in any of the proteins. The quantum yield, however, does increase with Ca^{2+} binding in all of the variants. MCD1 and MCD15 reached values slightly larger than that of mCherry at 0.24 and MCD15 Q163M had a value of 0.25. The sensors display an increase in brightness from the apo to holo form: 43% for MCD1, 15% for MCD15, and 5% for MCD15 Q163M. Although the addition of the Q163M mutation to MCD15 made the protein 51% brighter the Ca^{2+}-induced brightness change, an indication of the dynamic range, decreased. The calculated dynamic range, from both *in vitro*, and *in vivo* experimentation, shows no change with the Q163M mutation.

2.5 Conclusion

In the goal toward creating a pH insensitive Ca^{2+} sensor capable of deeper tissue penetration we set our sights on utilizing the H-bond network of the DsRed derived mCherry. After engineering a Ca^{2+} site on the surface of the protein, we were able to obtain a sensor with

good mM affinity for the ER but with low optical properties. We hypothesized that concentrating on the hot spot residues for chromophore development could help to improve on these properties. We decided on residue Q163, located in hot spot two, and made six mutations to this residue. Q163E, Q163K, and Q163N in MCD15 showed little to no color after expression and failed to show in purification. Q163I and Q163L in MCD15 expressed with a lower efficiency than the previous generation. The Q163M mutation in MCD15 and MCD1 showed an improvement in the chromophore development and yield of the protein. This mutation improved the optical properties of our sensor including the fluorescence intensity, extinction coefficient, and protein brightness without compromising the pH insensitivity. Unfortunately, while this improved protein is much brighter in both mammalian cells and bacterial cells, the fluorescence dynamic range did not change. This leads to the conclusion that while the added chromophore stability this mutation provides raises the apo fluorescence properties above those of mCherry but the Ca^{2+} - dependent change was brought to a comparable level and thus the change between these two remains small. A new series of mutations targeted to other hot spot residues is currently being made with the hopes of further improvement.

2.6 Next Steps for Red Sensor Optimization

As mentioned in 2.1.3 the next approach to optimization is determining the effect of making single mutations to different residues in the chromophore hot spots. These mutations were chosen after a sequence comparison between mCherry and monomeric DsRed derivatives mOrange, mStrawberry, mBanana, and mTangerine. These mutations are intended to be made in the absence of and in addition to the Q163M mutation. These mutations are currently being made, and data on their characteristics is to be reported.

3 Evaluation of Charge Contributions to Optical and Metal Binding Properties of EGFP Based Calcium Sensor CatchER

3.1 Design of Intracellular Ca^{2+} Probe CatchER

3.1.1 GFP as a Biomarker

As discussed in section 1.5, green fluorescent protein (GFP) is a fluorescent protein first isolated from the jellyfish *Aequorea victoria* by Shimomura et al. in 1962. The protein was found to produce a green color after absorbing the bioluminescence from pure blue aequorin protein. GFP has an 11 strand β-barrel tertiary structure with an α-helix running through the center of the barrel. The fluorescence comes from the Ser65-Tyr66-Gly67 chromophore that lies in the center of the α-helix of the protein. The chromophore is protected from photobleaching and sensitivities of the environment. The UV-vis spectrum shows a major absorbance peak at 395 nm and a minor peak at 488 nm. These peaks are believed to be different because excitation at 395 nm gives an emission at 508 nm whereas the peak at 488 gives a peak of 503 nm. UV-vis taken in high pH conditions displayed an increase in the 488 nm peak intensity and a decrease in the 395 nm intensity, indicating that the 395 nm peak corresponds with the neutral form of the chromophore and 488 nm with the anionic form.

Different mutations to the chromophore environment of GFP yield a number of variants separated into seven classes[16]. Class 1 is the wild-type GFP protein. Class 2 contains variants with the S65T mutation to give a phenolate anion in the chromophore. The enhanced version of the wild type GFP (EGFP) belongs to this class. This mutation eliminated the neutral form of the chromophore leaving one dominant peak at 488 nm in the UV-vis spectrum. The emission of this variant sits at 510 nm. Class 3 of GFP does not have any mutations directly to the chromophore residues, but the surrounding mutations yield a neutral phenol in the chromophore with an

excitation at 399 nm. The yellow fluorescent proteins (YFP) with an S65G mutation make up class 4. This class has a phenolate anion with stacked π-electron system and redshifted excitation peaks around 510 nm. The Y66W mutation to the chromophore gives the indole chromophore group seen in the blue shifted cyan fluorescent proteins (CFP) of group 5 which absorb around 435 nm. Class 6 is comprised of the blue fluorescent proteins (BFP) that have an imidazole chromophore and blue shifted absorbance at 380 nm. The class 7 protein contains the Y66F mutation with a 360 nm excitation. All of the classes can be used to engineer biosensors. For our studies, we used EGFP in class 2 as a template.

3.1.2 Engineering CatchER and its variants

EGFP was chosen for the template to use due to its enhanced fluorescent properties over wtGFP. Statistical analysis was done for 1491 Ca^{2+} binding sites and with this knowledge, the algorithm software MUG was used to predict for Ca^{2+} binding sites on EGFP. A site on the surface was chosen, and a series of substitutions via PCR was done to engineer a negatively charged *de novo* Ca^{2+} binding pocket involving residues 147, 202, 204, 223, and 225. The variants outlined in Table 3-1 were made. Protein D11, which displayed a Ca^{2+} affinity in the mM range and the greatest Ca^{2+}-induced change in optical properties, became the Ca^{2+} sensor for detecting high concentration in the ER (CatchER).

Table 3-1 Summary of CatchER variants

Protein	Mutations	Ca^{2+} Pocket Charge
D8	S202D, F223E	-2
D9	S202D, F223E, S147E	-3
D10	S202D, F223E, S147E, T225E	-4
CatchER (D11)	S202D, F223E, S147E, T225E, Q204E	-5

While CatchER was further improved for its folding at ambient temperatures, the biophysical properties of the other variants with the lower binding pocket charge were determined to understand better what effect the increasing electrostatic interactions had on our sensor. In this chapter, we report on our work to validate our method of sensor engineering by evaluating the effects of increasing the electrostatic interactions on the protein expression and structure, the biophysical properties, the Ca^{2+}-induced changes in fluorescence, and the Ca^{2+} binding affinity.

3.2 Materials and methods

3.2.1 Transformation, Expression, and Purification in E. coli

EGFP based proteins were in the pet28a vector for bacterial expression. The bacterial expression was carried out in the BL21-DE3 E. coli competent cells. To 50 μL of the competent cells 0.5-1 μL of protein DNA was added. The solution was mixed and left on ice for 30-90 minutes. The mixture was then place in a 42 °C water bath for exactly 90 seconds. Following this heat shock step, the mixture was placed back on the ice for 2 minutes before adding 50 μL of LB media and incubating at 37 °C for 30-90 minutes. Following incubation, 50 μL of the solution was spread antibiotic treated agar plate and left to incubate overnight at 37 °C.

The next morning the transformation plate was retrieved from the incubator. Ten milliliters of LB was treated with 6 μL of 50 mg/mL kanamycin. A single colony from the transformation plate was added to the LB-antibiotic solution using an inoculation loop. The inoculate solution was left to shake at 37°C overnight. After 16-18 hours of incubation, the solution was retrieved for expression. One liter of LB media was prepared for every 10 mL of inoculate with 600 μL of 50 mg/mL kanamycin.

Two 1-mL samples of the antibiotic-media solution were taken for optical density (O.D) blanks. The 10 mL inoculate sample was then added to the flask, and a 1 mL sample was taken for an O.D. reading (600 nm). The sample was placed in a refrigerated shaker to shake at 37 ° C. A 1-mL sample was taken approximately every hour until the O.D. reached 0.6. Once 0.6 was reached, 200 μL of 1 M IPTG was added to induce expression of the polymerase and the temperature was lowered to 25 °C. The cell pellet sample taken before inoculation was saved for SDS-PAGE analysis. Approximately two more O.D. readings were taken, and the solution was left to shake overnight. The following morning one last O.D. reading was taken and the cell pellet saved for SDS-PAGE analysis of the post-induction sample. The cell pellet from the full solution was collected by centrifugation (7000 rpm for 36 minutes) and frozen until ready to purify.

The proteins were purified using a fast protein liquid chromatography (FPLC) instrument by General Electric (GE). The cell pellets were suspended in approximately 20 mL of extraction buffer (20 mM Tris, 100 mM NaCl, 0.1% Triton; pH 8.0) and vortexed to mix. The solution was sonicated for six rounds of 30 pulses to lyse the cells and then centrifuged at 17,000 rpm for 36 minutes. The supernatant was filtered using a 0.45 mm Whatman filter before being injected onto the nickel loaded 5-mL HiTrap chelating column. The Histidine-tagged protein was bound to the nickel coating the column while the impurities were washed away with buffer A (40 mM K_2HPO_4, 10 mM KH_2PO_4, 250 mM NaCl; pH 7.4). The protein was eluted off using buffer B (buffer A with 0.5 imidazole). The imidazole was removed using the dialysis method in 2 L of 10 mM Tris (pH 7.4) that was changed every 3 hours for 2-3 days. The purified protein was concentrated and stored appropriately for future use.

3.2.2 Circular Dichroism

The secondary structure of the proteins was examined using circular dichroism (CD). A 20 μM protein sample was made in 10 mM Tris buffer (pH 7.4) with 2 μM of EGTA and placed in a 400 μL CD cuvette. The N_2 tank was turned on, and the machine was purged for approximately 5 minutes to get rid of any O_2. A scan for each sample was obtained with and without Ca^{2+}.

3.2.3 Ca^{2+} Titration

To determine the calcium binding affinity, the dissociation constant (K_d) was determined by Ca^{2+} titration. One milliliter of 10 μM protein sample was prepared in 10 mM Tris buffer (pH 7.4) with 2 μM of EGTA. The absorbance spectrum was taken before experimentation to observe the calcium free apo form absorbance. A fluorescence spectrum was taken at the 395 nm and 488 nm excitation wavelengths using the fluorometer. Fifty micromoles of Ca^{2+} were added to the solution, and another fluorescence spectrum was taken at each excitation wavelength. This step was repeated as the Ca^{2+} concentration was slowly increased in the solution to 10 mM. An absorbance spectrum was taken at the end of the experiment to observe the calcium saturated holo form absorbance. The maximum value of each spectrum at the wavelength of emission was normalized with Eq. 3.1. The normalized data was graphed as normalized fluorescence versus wavelength (nm) and fitted with Eq. 3.2 to obtain the K_d. In the equations F is the fluorescence, A is the absorbance, F_0 is the lowest fluorescence value with no Ca^{2+}, F_{max} is the greatest fluorescence value at Ca^{2+} saturation, p is the protein being analyzed, and r is the reference protein.

$$f = \frac{F - F_{\min}}{F_{\max} - F_{\min}} = \frac{[P]_T + [Ca^{2+}]_T + K_d - \sqrt{([P]_T + [Ca^{2+}]_T + K_d)^2 - 4[P]_T[Ca^{2+}]_T}}{2[P]_T} \quad \textbf{Eq. 3.1}$$

$$f = \frac{(m_0 * m_1)}{(m_0 + m_2)}; m_1 = 1; m_2 = 1 \quad \textbf{Eq. 3.2}$$

3.2.4 Chromophore pKa

The pK_a of the chromophore was determined by taking fluorescence spectra of the protein in various pH conditions. A 10 μM protein sample was made in 12 different pH buffers, outlined in Table3-2, with 2 μM EGTA and incubated overnight at 4 °C. The next day the pH of each sample was determined using a pH meter to observe the calcium free apo form pH. A fluorescence spectrum was taken at the 395 nm and 488 nm excitation wavelengths using the fluorometer. The protein was saturated with 10 μM Ca^{2+}, and the fluorescence spectrum was taken again. The pH of each sample was determined using a pH meter to observe the calcium saturated holo form pH. The data was normalized with the Eq. 3.3. The normalized data was graphed as the normalized fluorescence versus pH and fitted with Eq. 3.4 to obtain the chromophore pK_a of the apo and holo forms.

Table 3-2 Buffers used for pKa determination

Buffer	Concentration (mM)	pH
Sodium Acetate (NaOAc)	500	2.0
(NaOAc)	10	3.0
(NaOAc)	10	3.5
(NaOAc)	10	4.0
2-(N-morpholino)ethanesulfonic acid (MES)	10	5.0
(MES)	10	5.5
(MES)	10	6.0
piperazine-N,N′-bis(2-ethanesulfonic acid) (PIPES)	10	6.5
(PIPES)	10	7.0
2-Amino-2-hydroxymethyl-propane-1,3-diol (Tris)	10	7.4
(Tris)	10	8.0
(Tris)	10	9.0

$$Y = \frac{Y_{\min} \times 10^{-pH} + Y_{\max} \times 10^{-pKa}}{10^{-pH} + 10^{-pka}} \quad \textbf{Eq. 3.3}$$

$$Y = \frac{1}{1 + \exp^{-\frac{(m0-m1)}{m2}}}; m1 = 1; m2 = 1 \quad \textbf{Eq. 3.4}$$

3.2.5 Quantum Yield and Extinction Coefficient

The quantum yield (Φ) and extinction coefficient (ε) are measures of the fluorescence efficiency and light absorption strength respectively of a species. The quantum yield was determined by preparing the protein at five different concentrations (15 μM, 20 μM, 25 μM, 30 μM, and 35 μM) in 10 mM Tris buffer (pH 7.4) with 2 μM EGTA. The wild-type protein was also prepared at five different concentrations (5 μM, 10 μM, 15 μM, 20 μM, and 25 μM) in 10 mM Tris buffer (pH 7.4) with 2 μM EGTA as a control and for calculations. The fluorescence spectra of the wild-type and apo protein form were obtained at excitation wavelengths 395 nm and 488 nm using the fluorometer. The absorbance spectra for both proteins were obtained using UV-vis. Ten millimoles of Ca^{2+} were added to the protein sample. The fluorescence and absorbance spectra of the holo protein form were obtained the same as the apo form. The maximum value of fluorescence at the wavelength of emission was graphed versus the maximum value of absorbance at the wavelength of excitation for each protein to obtain the fitted line slope. This value along with the literature quantum yield of the template reference protein was used in Eq. 3.5 to calculate the quantum yield.

$$\Phi_p = \Phi_r \times \frac{\frac{F_p}{A_p}}{\frac{F_r}{A_r}} \qquad \textbf{Eq. 3.5}$$

$$\varepsilon_{p\,587\,nm} = \varepsilon_{r\,455\,nm}\left(\frac{A_{p\,587\,nm}}{A_{p\,455\,nm}}\right) \qquad \textbf{Eq. 3.6}$$

$$B = \varepsilon \times \Phi \qquad \textbf{Eq. 3.7}$$

The extinction coefficient was determined using an alkali denaturation assay. The protein was prepared at five different concentrations (15 μM, 20 μM, 25 μM, 30 μM, and 35 μM) in 10 mM Tris buffer (pH 7.4) with 2 μM EGTA. The template protein was also prepared at 5 different concentrations (5 μM, 10 μM, 15 μM, 20 μM, and 25 μM) in 10 mM Tris buffer (pH 7.4) with 2 μM EGTA. The absorbance spectra of the apo protein form and holo protein form, as well as the absorbance spectra of the wild-type protein, were acquired. The proteins were then unfolded to expose the chromophore by adding 0.1 M sodium hydroxide (NaOH). After mixing the absorbance was taken. To obtain the fitted line slope the maximum absorbance value of the folded protein was graphed versus the maximum absorbance value of the denatured protein. This slope along with the literature extinction coefficient value for the template protein chromophore at the maximum absorbance in the denatured form was used in Eq. 3.6. The quantum yield and extinction coefficient can be used further to determine the brightness of the protein as shown in Eq. 3.7.

3.2.6 Fluorescence Dynamic Range

The dynamic range is a measurement of the fluorescence intensity change from the apo to the holo form of our proteins. This characteristic was determined using the Ca^{2+} free and Ca^{2+} loaded fluorescence intensities. The peak data was analyzed using Eq. 3.8 to determine the dynamic range where F is the lowest fluorescence value and F_0 is the highest fluorescence value upon Ca^{2+} saturation.

$$DyR = \frac{F_{max}}{F_0} \qquad \textbf{Eq. 3.8}$$

3.3 Results

3.3.1 Tertiary Structure

Figure 3-1 shows the Far-UV CD spectra of the EGFP and the variants D8, D9, D10, and CatchER. Ten scans of each were taken and averaged together in the program. Each protein is shown in dashed lines. The β-sheet structure has a peak at 218 nm in Far-UV CD spectrum. An overlay of the variants and template spectra show there is no deviation from this range, and the protein's secondary structure remains intact. The proteins were saturated with 10 mM Ca^{2+}, and another CD spectrum of each was taken. The results of the holo forms are in the same color as their apo forms with a solid line. As with the apo form spectra, the holo form remains in the 218 nm range with a fair amount of overlap.

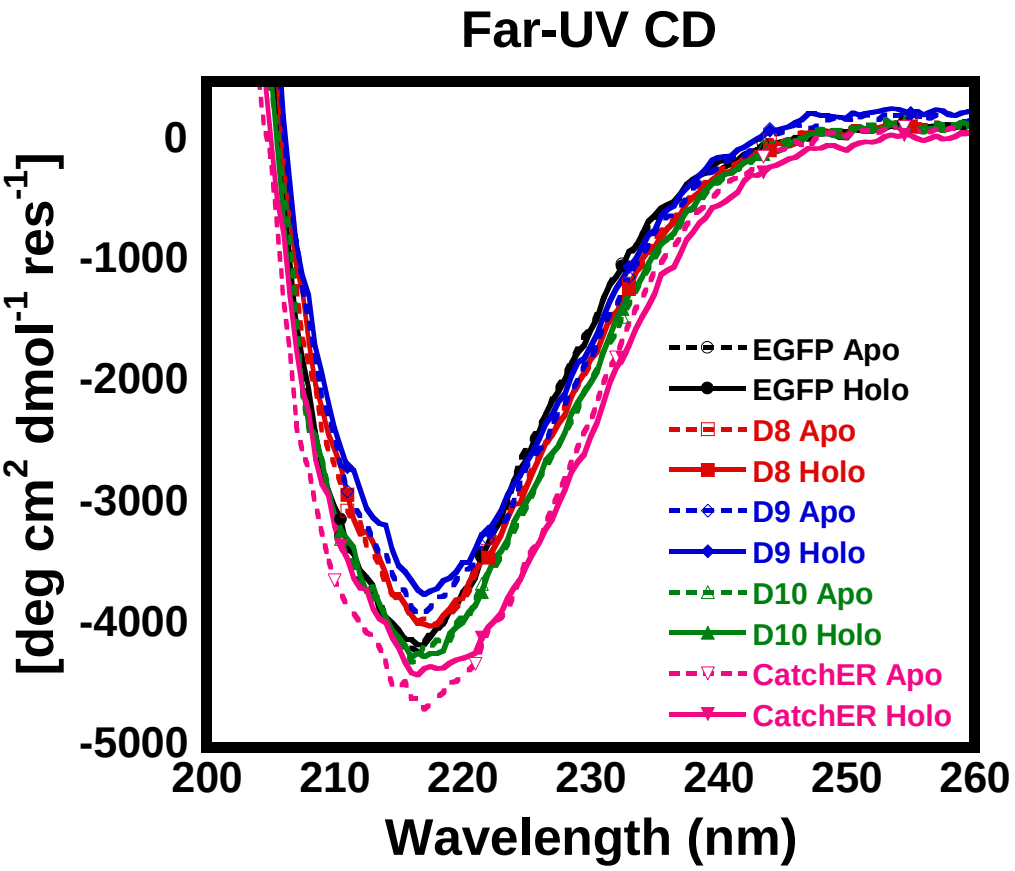

Figure 3-1 Far-UV CD of CatchER variants

Each 20 μM protein sample was prepared in 10 mM Tris (pH 7.4) with 5 μM EGTA. Spectra collected for apo (dashed line) and holo (solid line) forms.

3.3.2 Ca^{2+} Binding Affinity

The Ca^{2+} K_d was found by performing a titration as described in section 3.2.3 and normalized with Eq. 3.2 in the program KaleidaGraph. This experiment was done in triplicate. The Ca^{2+} concentration intervals are listed below in Table 3-3. Figure 3-2 shows the raw and normalized data for the titration experiments of D10. The absorbance spectra of the apo (2 μM EGTA) and holo (10 mm Ca^{2+}) forms of the protein show a consistent decrease in the absorbance of the neutral form of the chromophore at 395 nm and an increase in the absorbance of the anionic

form of the chromophore at 488 nm. The normalized curve demonstrates the saturation curve and gives the Ca^{2+} binding affinity of the protein.

Table 3-3 Ca^{2+} concentrations used for K_d determination

$[Ca^{2+}]$ (mM) in solution	**μL of $CaCl_2$ added to solution**
0	0
0.005	0.5 **(10 mM Stock)**
0.025	2.0 (10 mM Stock)
0.050	2.5 (10 mM Stock)
0.100	0.5 **(100 mM Stock)**
0.250	1.5 (100 mM Stock)
0.500	2.5 (100 mM Stock)
1.0	5.0 (100 mM Stock)
3.0	2.0 **(1 M Stock)**
5.0	2.0 (1 M Stock)
7.0	2.0 (1 M Stock)
10.0	3.0 (1 M Stock)

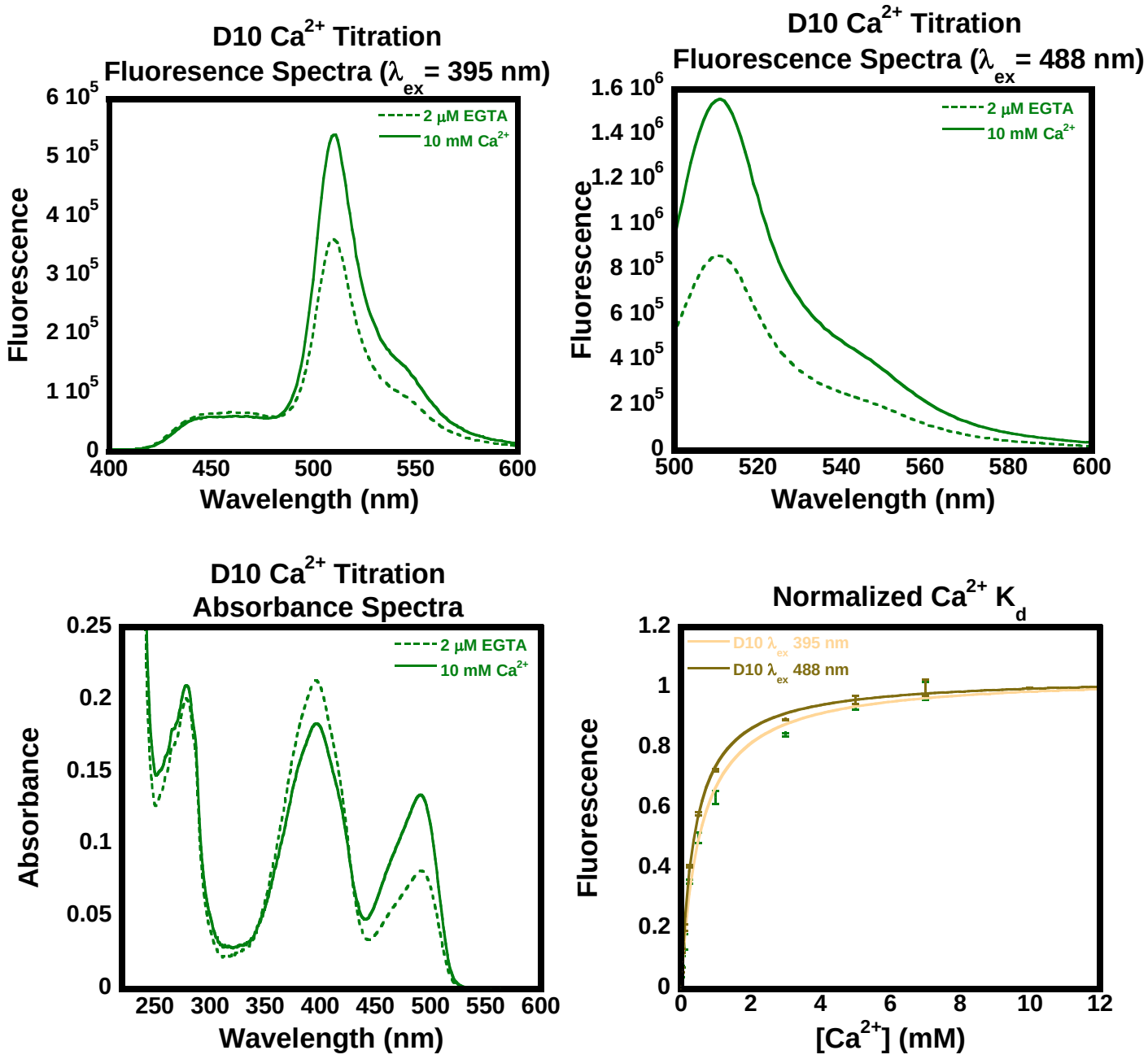

Figure 3-2 Ca^{2+} titration data for CatchER variant D10

Protein was prepared to 10 µM concentration in 10 mM Tris (pH 7.4) with 2 µM EGTA. Fluorescence spectra for the apo (dashed line) and holo (solid line) forms at 395 nm (top left) and 488 nm (top right) excitation wavelengths. Absorbance spectra (bottom left) for apo (dashed line) and holo (solid line) forms. Normalized fluorescence data (bottom right) to give the Ca^{2+} K_d at 395 nm (gold) and 488 nm (brown) excitation wavelengths.

Table 3-4 and Figure 3-3 show the normalized K_d values for D8, D9, D10, and CatchER for both 395 nm and 488 nm. The values were determined as outlined in section 3.2.3 and graphed using Kaleidagraph.

Table 3-4 Normalized Ca^{2+} K_d values for CatchER variants

Protein	D8	D9	D10	CatchER
395 nm	1.43 ± 0.01	1.89 ± 0.02	0.56 ± 0.02	0.32 ± 0.01
488 nm	1.10 ± 0.01	1.46 ± 0.03	0.40 ± 0.02	0.23 ± 0.01

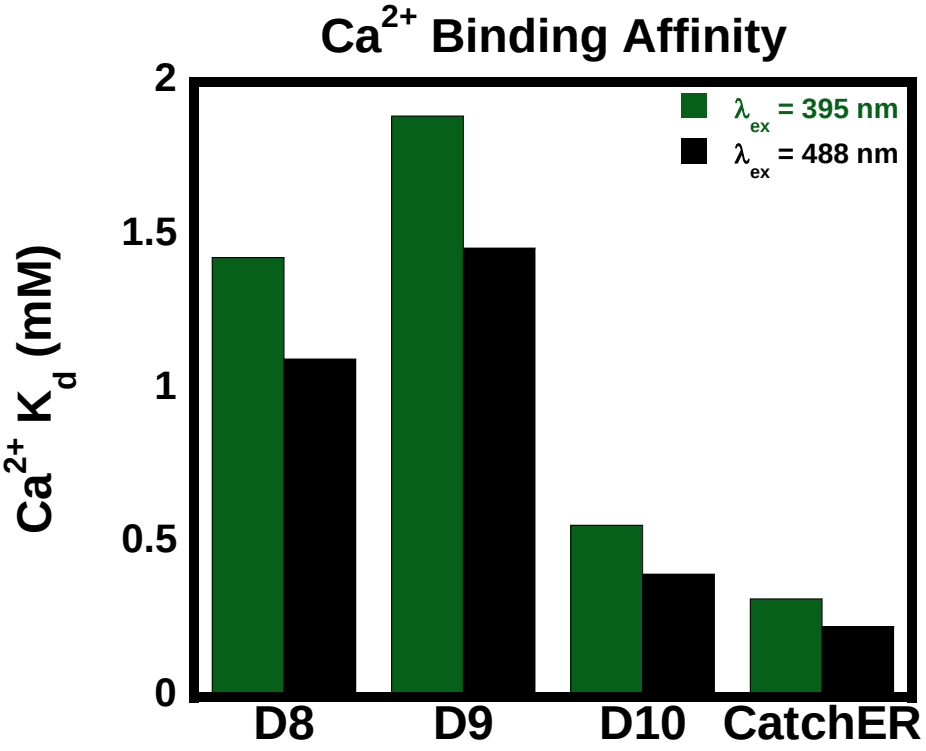

Figure 3-3 Normalized Ca^{2+} K_d values for CatchER variants

Each 10 μM protein sample was prepared in 10 mM Tris (pH 7.4) with 2 μM EGTA. Ca^{2+} K_d for the 385 nm excitation (green) and 488 nm excitation (black) in mM

3.3.3 Chromophore pK_a

The buffers used to prepare the samples for pK_a determination is outlined in Table 3-2 in section 3.2.4. The fluorescence spectra of D10 in each buffer shows that the increase in solution acidity results in increased loss of chromophore fluorescence. Normalization using Eq. 3.4 in KaleidaGraph gives the pH profile of the variants and the pK_a value, shown for D10 in Figure 3-4. There is a decrease in pKa at both 395 nm and 488 nm upon Ca^{2+} saturation. This change increases from D8 to CatchER and is larger at the 488 nm excitation. The effect of the increasing charge on chromophore pK_a is shown in Table 3-5. The chromophore pK_a increases slightly with the increase in binding pocket charge from -2 to -5. The addition of Ca^{2+} is shown to cause a decrease in the pK_a at both wavelengths of excitation. This decrease gets slightly larger going from D8 to CatchER.

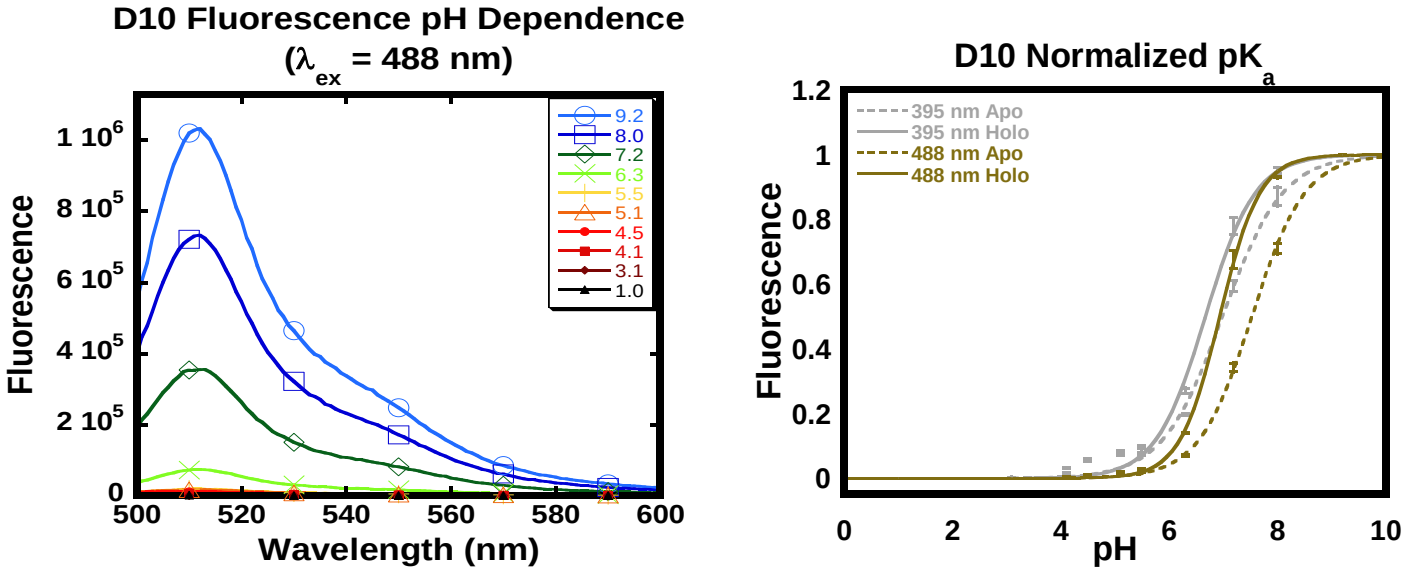

Figure 3-4 pH profiles of CatchER variants

Each 10 μM protein sample was prepared in the buffers outlined in Table 3-2 with 2 μM EGTA. Apo emission spectra of D10 in buffers of pH 1-9 (left). Normalized pH profile of D10

(right) for the apo (dashed line) and holo (solid line) forms for both the 395 nm (gray) and 488 nm (gold) excitation wavelengths.

Table 3-5 CatchER variants pKa values

Protein	395 nm		488 nm	
	Apo	Holo	Apo	Holo
D8	6.8	6.7	6.7	6.7
D9	6.8	6.8	7.3	7.1
D10	7.1	6.9	7.6	7.3
CatchER	7.1	6.9	7.6	6.9

3.3.4 Extinction Coefficient and Quantum Yield

The extinction coefficient (ε) is a measurement of absorbance efficiency while the quantum yield is a measurement of fluorescence efficiency. The extinction coefficient (Φ) was determined using the denaturation assay as described in section 3.2.5 and the quantum yield was determined by measuring the photons absorbed vs. photons emitted. Both experiments were done at 488 nm, the common wavelength used for green fluorescence in biological studies. Table 3-6 lists these values for all CatchER variants in the apo and holo forms. Figure 3-5 shows the normalized extinction coefficient and quantum yield values in the apo and holo forms.

Table 3-6 Extinction coefficient and quantum yield of CatchER variants

Protein	Extinction Coefficient (ε) mM^{-1} cm^{-1}		Quantum Yield (Φ)	
	Apo	Holo	Apo	Holo
D8	19.0	21.4	0.7	0.6
D9	13.6	19.6	0.7	0.6
D10	15.3	20.6	0.8	0.6
CatchER	7.1	15.0	0.8	0.6

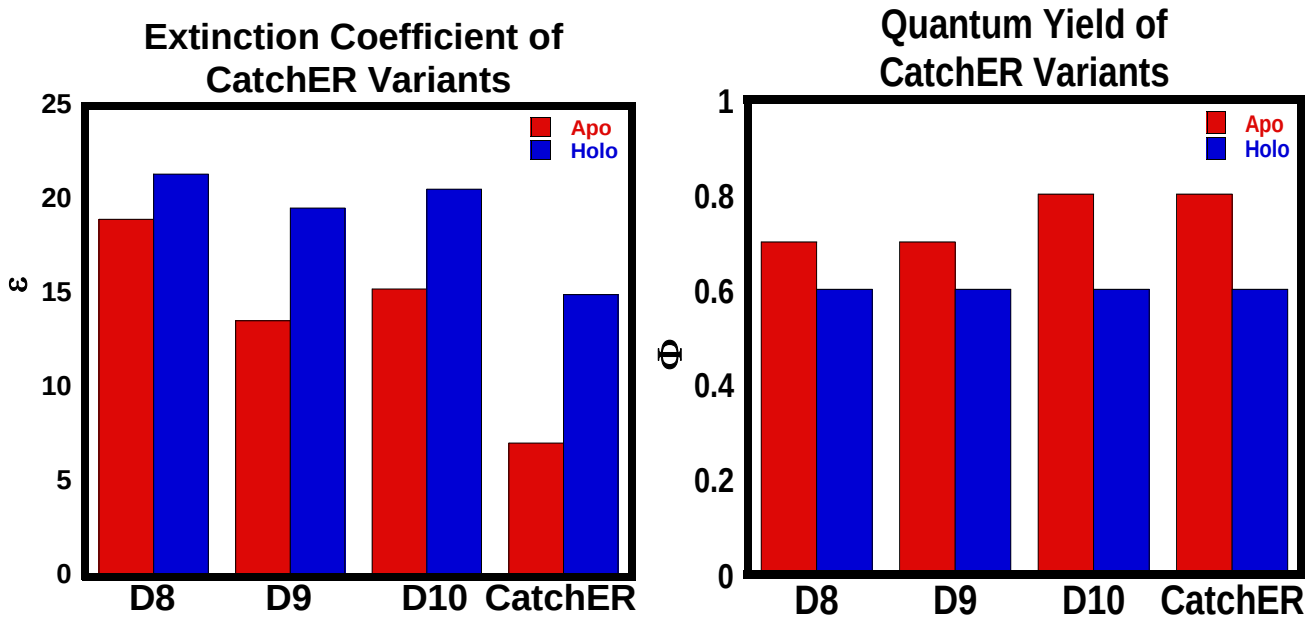

Figure 3-5 Extinction coefficient and quantum yield of CatchER variants

Five concentrations of each CatchER variant were prepared (10 μM, 15 μM, 20 μM, 25 μM, and 30 μM) in 10 mM Tris (pH 7.4) with 2 μM EGTA. Five concentrations of EGFP were prepared (5 μM, 10 μM, 15 μM, 20 μM, and 25 μM) in 10 mM Tris (pH 7.4) with 2 μM EGTA. Left: extinction coefficient comparison of CatchER variants in the apo (red) and holo (blue) forms. Right: the quantum yield comparison of the CatchER variants in the apo (red) and holo (blue) forms.

3.3.5 Protein Brightness

The extinction coefficient was multiplied by the quantum yield value to give the overall brightness of the proteins. This data is shown in Figure 3-6.

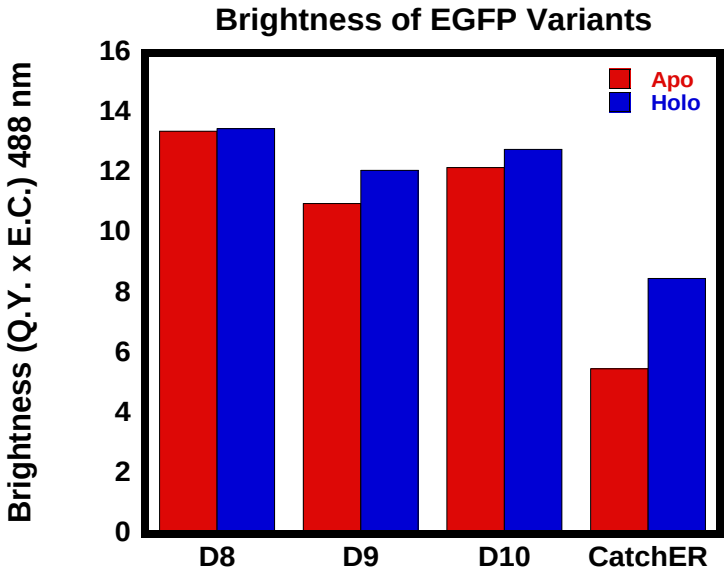

Protein	Brightness ε * Φ	
	Apo	Holo
D8	13.3	12.8
D9	9.52	11.8
D10	12.2	12.4
CatchER	5.68	9.01

Figure 3-6 Brightness of CatchER variants

Five concentrations of each CatchER variant were prepared (10 μM, 15 μM, 20 μM, 25 μM, and 30 μM) in 10 mM Tris (pH 7.4) with 2 μM EGTA. Five concentrations of EGFP were prepared (5 μM, 10 μM, 15 μM, 20 μM, and 25 μM) in 10 mM Tris (pH 7.4) with 2 μM EGTA. Left: brightness comparison of CatchER variants in the apo (red) and holo (blue) forms. Right: the brightness values of the CatchER variants.

3.3.6 High Salt Environment on Ca^{2+} Binding

The effect of increased salt ion in the environment was measured by repeating the Ca^{2+} titration experiment outlined in section 3.2.3 and adding KCl salt to the Tris buffer. This was done for 150 mM KCl, 300 mM KCl, 500 mM KCl, and 1 M KCl. The raw data and normalized spectra for this experiment are shown in Figure 3-7. Table 3-7 lists the K_d values determined from this experiment at 395 nm and 488 nm excitation wavelengths. Values listed as NB indicate there was no binding of Ca^{2+} to the protein as the normalized data could not be fitted.

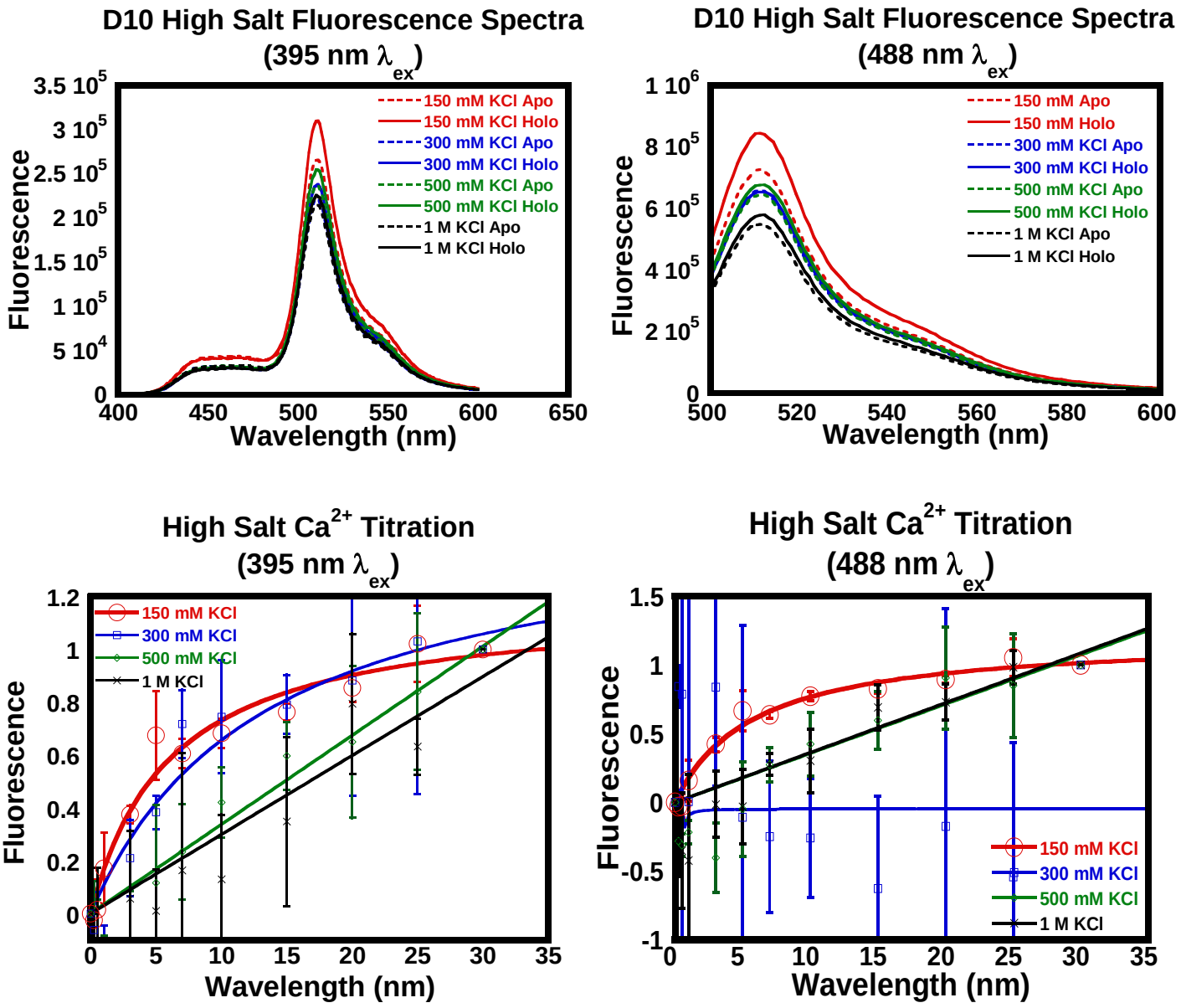

Figure 3-7 D10 high salt Ca^{2+} titration

Each 10 μM protein sample was prepared in 10 mM Tris (pH 7.4) with 2 μM EGTA and 150 mM (red), 300 mM (blue), 500 mM (green), or 1 M (black) KCl. Fluorescence spectra at 395 nm (top left) and 488 nm (top right) excitation wavelengths for the apo (dashed line) and holo (solid line) forms. Normalized fluorescence data at 395 nm (bottom left) and 488 nm (bottom right) excitation wavelengths.

Table 3-7 CatchER variants high salt Ca^{2+} K_d

395 nm λex Ca^{2+} K_d (mM)				
Protein	**150 mM KCl**	**300 mM KCl**	**500 mM KCl**	**1 M KCl**
D8	NB	NB	NB	NB
D9	NB	NB	NB	NB
D10	6.1	13.3	NB	NB
CatchER	2.0	9.74	7.1	NB
488 nm λex Ca^{2+} K_d (mM)				
Protein	**150 mM KCl**	**300 mM KCl**	**500 mM KCl**	**1 M KCl**
D8	NB	NB	NB	NB
D9	NB	NB	NB	NB
D10	5.8	NB	NB	NB
CatchER	1.0	NB	NB	NB

3.3.7 Magnesium Metal Binding

The Mg^{2+} metal binding affinity of the proteins was determined the same as the Ca^{2+} titration outlined in section 3.2.3. $MgCl_2$ stocks were used instead of $CaCl_2$ stocks in the same concentrations as shown in Table 3-3. Figure 3-8 shows the raw UV-Vis, fluorescence, and normalized fluorescence data for D10. Table 3-8 lists the Mg^{2+} K_d values for each of the CatchER variants. Values listed as NB indicate there was no binding of Mg^{2+} to the protein as the normalized data could not be fitted

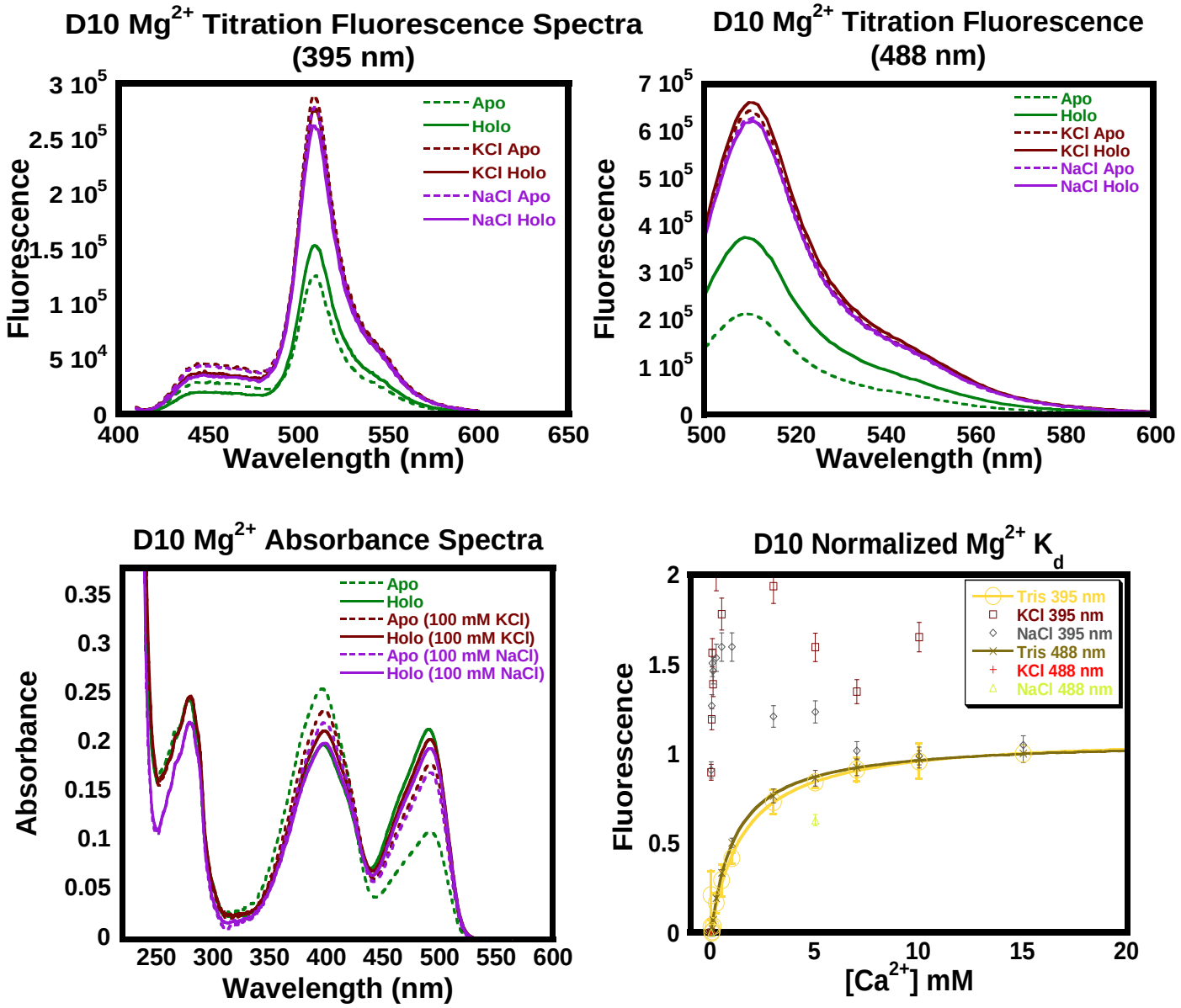

Figure 3-8 D10 Mg^{2+} titration

Each 10 μM protein sample was prepared in 10 mM Tris (pH 7.4) with 2 μM EGTA and either 0 mM salt (green), 100 mM KCl (brown), or 100 mM NaCl (purple). Fluorescence spectra at 395 nm (top left) and 488 nm (top right) excitation wavelengths and the absorbance spectra (bottom left) for the apo (dashed line) and holo (solid line) forms. Normalized fluorescence data at 395 nm and 488 nm excitation wavelengths (bottom right) with the fitted curve for no salt at 395 nm (gold solid) and 488 nm (beige solid) excitation wavelengths.

Table 3-8 CatchER variants Mg^{2+} titrations

Proteins	395 nm	488 nm
D8	4.8 ± 1.3	NB
D9	2.42 ± 0.6	2.64 ± 0.2
D10	1.6 ± 0.3	1.18 ± 0.06
CatchER	0.5 ± 0.1	0.7 ± 0.1

3.4 Discussion

The template EGFP has a stable β-barrel secondary structure. One concern with introducing a non-native Ca^{2+} binding site to its surface was that the cluster of negative charges would disrupt the tertiary structure and add instability to the protein. To examine this possibility, a CD spectrum was taken for each variant in the apo and holo form. The increase in repulsive charges made to engineer the binding pocket does not appear to have an unfolding effect on the variants as the overlay of the spectra in Figure 3-1 show the proteins remaining folded with all peaks remaining in the 218 nm range. The effect of Ca^{2+} binding on the tertiary structure was tested by saturating the proteins with 10 mM Ca^{2+} and running another CD spectrum of each. As with the apo form spectra, the holo form remains in the 218 nm range with a fair amount of overlap showing that Ca^{2+} binding does not appear to cause any structural changes to the protein. This also leads us to believe that the increase in fluorescence we see upon Ca^{2+} binding is caused by a change in the chromophore ionization and not a change in residue conformation.

The raw fluorescence spectra for the apo form of each protein at the 395 nm excitation shows the basal fluorescence intensity increasing with the increased pocket charge. Upon Ca^{2+} saturation the fluorescence of D8 and D9 both increase to the same intensity while the intensity of

D10 surpasses the lower two charged variants. At 488 nm excitation, the basal levels of all the variants are at approximately the same level while their final intensities after saturation differ. While D10 is the highest once again, D8 is the second highest and D9 the lowest. CatchER maintains the highest fluorescence among the variants for both wavelengths.

As the negative charges in the binding pocket increase, the quantum yield increases as well meaning the fluorescence of the protein becomes more efficient as you go from a -2 charge to a -5 charge. When 10.0 mM of Ca^{2+} was added to the samples, each protein experienced a decrease in the quantum yield to the EGFP value. This entails that more photons are being absorbed than emitted when Ca^{2+} is added, an assumption that is supported by the absorbance spectrum of the protein with and without Ca^{2+} where the peak at 488 nm increases when Ca^{2+} is added for all of the proteins.

While the quantum yield increased the extinction coefficient showed a non-specific trend with CatchER having the lowest value followed by D9, D10, and then D8. All four proteins saw an increase in the extinction coefficient with Ca^{2+} saturation, maintaining the order of intensity. The brightness was found to mimic the extinction coefficient trend as you increased the negative charge in the binding pocket. When Ca^{2+} was added, CatchER had a noticeable increase in fluorescence. This shows that although the proteins get dimmer going from a -2 to -5 magnitude when Ca^{2+} binds a favorable optical change useful for in vivo use is seen in the protein with the greatest charge.

The fluorescence response of each variant to calcium was observed using a fluorometer as described in section 3.2.3 with the Ca^{2+} increments described in Table 3-1 to learn the electrostatic effects on Ca^{2+} binding affinity. The K_d was calculated using Eq. 3.1 in section 3.2.3 above. When there is more metal bound protein in solution than dissociated protein and metal ions than the K_d

will be a small value. The smaller the K_d, the greater affinity the protein has for the metal. The observed trend for the variants was that the magnitude of the negative charge was directly related to the Ca^{2+} binding affinity of the protein. As the negative charge in the binding pocket was increased going from D8 to CatchER the affinity increased. This can be seen as the normalized fluorescence curve takes a tighter shape with a lower error in D10 and CatchER.

This change in binding affinity could be seen in the raw fluorescence data. As seen in Figure 3-2 at 395 nm excitation the basal fluorescence intensities increase with the increased charge. At 488 nm the basal fluorescence level is nearly the same for all of the variants. The fluorescence change upon saturation at both wavelengths of excitation is greatest for D10 and CatchER while D8 shows a greater change in fluorescence than D9.

All of the proteins maintain the pH sensitivity that is seen in GFP derived chromophores. The pKa is shown to increase slightly with the pocket charge from 6.8 to 7.1 at 395 nm and 6.7 to 7.6 at 488 nm shown in Figure_. With the addition of Ca^{2+} all pK_a values either remain the same or experience a slight decrease in value. Even with the Ca^{2+}-induced decrease, the chromophores remain pH sensitive.

After determining that the increasing pocket charge improved the affinity for Ca^{2+}, we were interested in understanding what effect increasing the electrostatic interactions of the environment would have on the binding affinity of the CatchER variants. This was done by repeating the Ca^{2+} titration experiments in conditions with increasing KCl in the Tris buffer. As shown in Figure 3-7, the intensity of fluorescence change decreases with the increasing salt conditions at both excitation wavelengths. The Ca^{2+} affinity for the already weakly binding D8 and D9 variants is eliminated at both 395 nm and 488 nm excitations in the presence of KCl. D10 and CatchER both lose binding completely after 150 mM KCl at 488 nm excitation. At 395 nm excitation D10

maintains weak binding up to 300 mM KCl and CatchER displays a nonspecific trend of weak binding up to 500 mM KCl. This lets us know that that the existence of salt ions does interfere with the sensor's ability to bind with Ca^{2+} metal.

Since all Ca^{2+} binding proteins, found natively and engineered, have been shown to bind with Mg^{2+} metal to some degree we were interested in determining the Mg^{2+} affinity of these sensors. The Ca^{2+} titration was repeated as outlined in section 3.3.2 but with $MgCl_2$ being added instead of $CaCl_2$. The trend for Mg^{2+} binding appears to be the same for Ca^{2+} binding where CatchER with the -5 charge has the greatest affinity for the Mg^{2+} metal at both wavelengths of excitation. The Ca^{2+} K_d values for CatchER are 0.32 mM and 0.23 mM for 395 nm and 488 nm excitation respectively and the respective Mg^{2+} K_d values are 0.5 mM and 0.7 mM. CatchER exhibits a stronger binding for Ca^{2+} at 488 nm and Mg^{2+} at 395 nm. The Mg^{2+} affinity is approximately two times weaker a both wavelengths than the Ca^{2+} affinity overall for both excitations.

3.5 Conclusion

One challenge in sensor engineering using the grafting method is preventing interactions between the binding site and other intracellular proteins. This can be prevented by creating a *de novo* site, as done with CatchER. This process involved increasing the negative charge of the Ca^{2+} binding pocket through mutagenesis to create CatchER with a complete -5 charge. CatchER was compared with its variants of lesser pocket charge: D8 (-2), D9 (-3), and D10 (-4). The results show that CatchER has the most significant fluorescence change with Ca^{2+} binding, improved quantum yield, and the greatest affinity for Ca^{2+}, making this an efficient method of sensor engineering.

4 Targeting of CatchER to the Membrane of the Endoplasmic Reticulum

4.1 Need for Targeting Capabilities

The Ca^{2+} homeostasis in cells is important for maintaining function (Chapter 1.1). This homeostasis is regulated by Ca^{2+} channels and pumps on the cell and organelle membranes and by buffer proteins throughout the cell. Most of the Ca^{2+} in the cell is stored in the SR/ER, and the lowest amount of free Ca^{2+} is seen in the cytosol. The intracellular organelles contain Ca^{2+} levels appropriate for their function, such as post-translational modifications in the Golgi and polypeptide degradation in the lysosomes. Ca^{2+} movement to and from the SR/ER occurs using a number of channels and pumps located on the membrane such as the inositol tris-phosphate receptor (IP_3R), ryanodine receptor (RyR), and **S**arco/**E**ndoplasmic **R**eticulum **C**a^{2+} **A**TPase (SERCA). The release of Ca^{2+} as a second messenger from the SR/ER to the cytosol, by either an action potential or Ca^{2+}-induced calcium release (CICR), activates a number of biological pathways such as muscle contraction in muscle cells and neurotransmitter release in the neurons. Malfunction of these channels and pumps can cause irregular Ca^{2+} movement and concentrations in the cell. These malfunctions could be due to mutations or expression in the channels and can lead to diseases such as diabetes, Alzheimer's disease[42], Darier's disease[25], heart disease, and Huntington's disease[8] to name a few. The field of Ca^{2+} sensor development has thus grown out of the need for tools to monitor intracellular Ca^{2+} dynamics.

There are many synthetic fluorescent dyes utilized for intracellular Ca^{2+} measurement that provide a wide range of colors, wavelengths, and Ca^{2+} affinities. The major setback of these dyes is that they lack targeting capabilities for localized Ca^{2+} measurements. The **g**enetically **e**ncoded **C**a^{2+} **i**ndicators (GECIs) are protein based with non-native Ca^{2+} binding site added by

manipulating the protein DNA sequence. DNA manipulation also allows GECIs to be targeted to specific parts of a cell with the addition of a target sequence.

For measuring Ca^{2+} flow in and out of the SR/ER a sensor could be targeted a couple of different ways. The ER targeting sequence from calreticulin and the ER retention sequence lysine-aspartate-glutamate-leucine (KDEL) could be used for sending a sensor to the lumen of the ER. Transmembrane domains, such as those from the Ca^{2+} channels, pumps, and binding proteins of the SR/ER, can also be used as targeting sequences. Transmembrane regions of an SR/ER protein are often inserted cotranslationally or post-translationally[43] into the membrane.

Our lab has already attached the first 18 amino acids of calreticulin and the KDEL retention sequence to the N and C terminals respectively to target our sensors to the SR/ER. The objective of this chapter is to develop the calcium sensor CatchER at various local SR environments to understand the key determinants important for targeting. Attaching a transmembrane sequence to one or both sides of a Ca^{2+} sensor, such as CatchER, could anchor it to various local cellular environments close to the membrane of the SR/ER and allow for local Ca^{2+} dynamic measurements.

In this chapter, we present work done to target CatchER by placing transmembrane domains from integral ER proteins RyR and calnexin to anchor the protein in the ER membrane with an intended orientation. We first identify what segments of each protein to use for the anchoring process. We then discuss the results of drug-induced Ca^{2+} release from the ER and possible protein orientation. Lastly, we discuss plans to improve the targeting of CatchER further for local ER/SR Ca^{2+} measurement.

4.2 Design of Targeted CatchER Constructs

The ryanodine receptor (RyR1) and calnexin membrane proteins of the SR/ER were chosen for CatchER anchoring constructs shown in Figure 4-1. The transmembrane proteins of the SR/ER have been found to heterogeneously express on the membrane so these constructs would be expected to express in the region of the receptor or protein from which the selected transmembrane domain (TMD) was taken. The Zorzato model[44] for the topology of the RyR1 channel was used to select which segments to use for targeting. Four constructs for anchoring CatchER to the SR/ER membrane were previously made using RyR1: CatZ5, CateZ5, CatLeZ5, and Z10Cat. These constructs were made using the 5^{th} and 10^{th} TMDs of RyR1 with CatchER having an orientation toward the cytosol.

CatZ5, CateZ5, and CatLeZ5 are all single TMD constructs. CatZ5 was made using TMD 5 (Z5) of RyR1 fused to the C-terminal of CatchER. For the construct, CateZ5 part of the loop regions on each side of Z5 were included to make an extended eZ5 targeting sequence fused to the C-terminal of CatchER. In the CatLeZ5 construct the extended eZ5 region was again used with a Ser-Leu-Pro-Ala linker was added between the C-terminal of CatchER and N-terminal of the TMD. The Kozak sequence was also added to the N-terminal of CatchER to improve the protein expression in mammalian hosts. The Z10Cat construct uses two TMD domains from RyR1. Z10Cat resembles CatLeZ5 with the addition of TMD 10 (Z10) to the N-terminal of CatchER with a single Pro amino acid linker between the two. These constructs would express on the region of the membrane with RyR1 and measure the dynamics of Ca^{2+} moving out of the SR/ER.

A fifth construct Z10CatR was designed using the same 5^{th} and 10^{th} RyR1 transmembrane domains in Z10Cat to have CatchER oriented toward the SR/ER lumen. This

construct uses CatchER with calreticulin and KDEL ER retention tags on the N and C-terminal respectively. The terminals of the TMDs were swapped to change the orientation. eZ5 followed by the single Proline linker and Kozak sequence are fused to the N-terminal before the calreticulin signaling sequence while the S-L-P-A linker followed by Z10 are fused to the C-terminal after the KDEL retention sequence.

A sixth construct CaX was made using the single transmembrane domain from calnexin (X) fused to the N-terminal with no linkers to give CatchER a cytosolic orientation. This construct would express in the mitochondria-associated endoplasmic reticulum membrane[45] (MAM) where calnexin[46, 47], a Ca^{2+} chaperone that assists with glycoprotein assembly, is expressed and be useful in measuring Ca^{2+} concentrations in this localized region of the SR/ER.

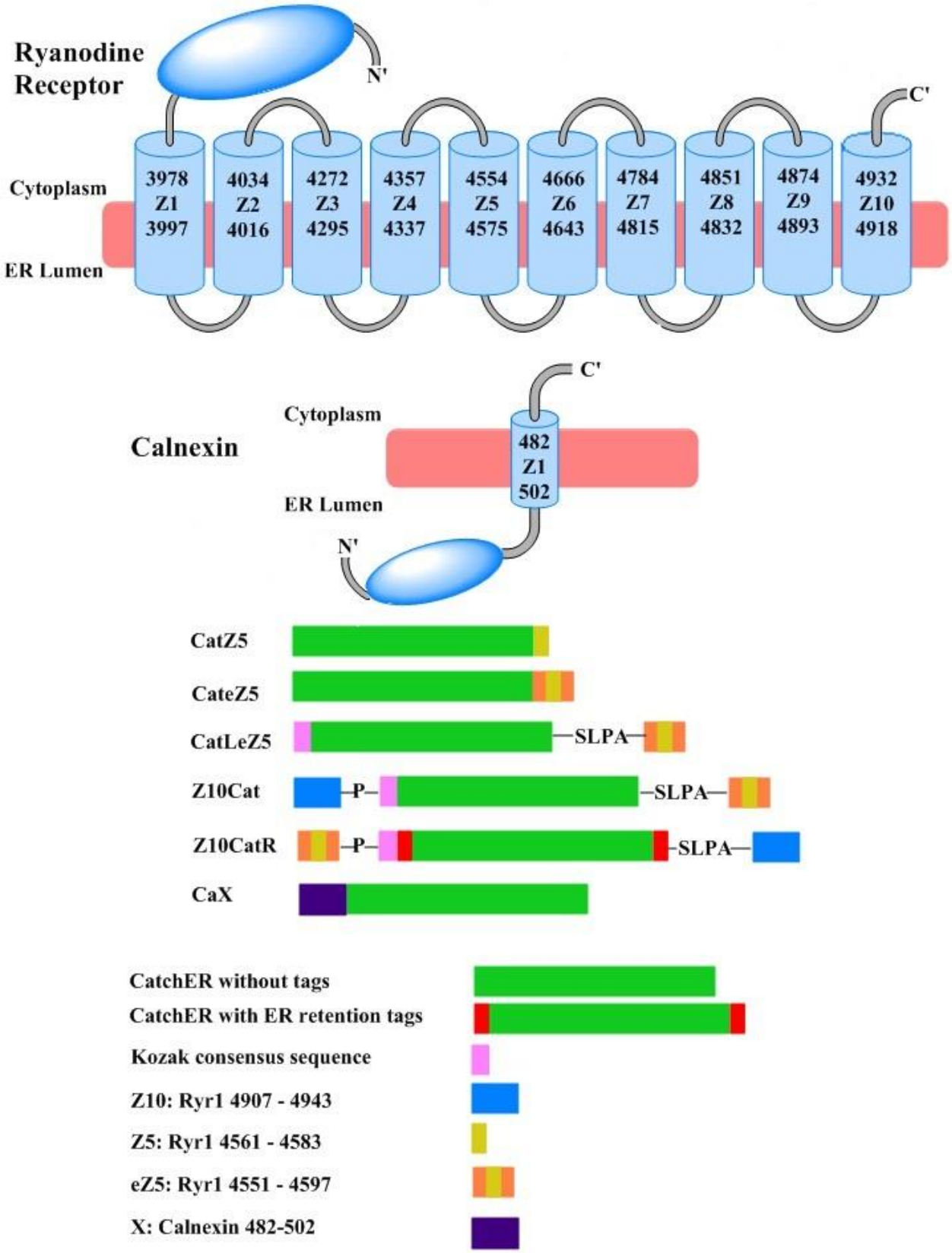

Figure 4-1 Constructs of targeted CatchER

4.3 Materials and Methods

4.3.1 PCR Sample Preparation and Process

The KOD hot start polymerase kit from Novagen was used for adding large TMDs to the proteins. For KOD a 50 μL solution was made by adding 5 μL of 10X KOD polymerase buffer, 0.1-0.2 mM of 2 mM dNTPs, 1.5-2.25 mM of 25 mM $MgSO_4$, 4 μL of 10 ng template DNA, 0.5 μL of each 30 μM primer, 1 μL of the KOD polymerase, and the rest sterile ddH_2O to a PCR tube.

4.3.2 Gel Extraction, Ligation, Inoculation, and Sequencing

DNA samples amplified using the KOD hot start polymerase were extracted using the gel extraction technique. The entire solution was inserted into 0.8-1.0% agarose DNA gel run for ~1 hour at 70 volts. The product band was cut out, and the DNA extracted using a QIAquick gel extraction kit as directed. The sample was then ligated using the rapid DNA ligation kit from Thermo Fisher Technologies according to the company protocol. The ligated sample was amplified using DH5−α E. coli competent cells. Fifteen microliters of the ligated product were added to 50 μL of competent cells and put on ice for 30-90 minutes. The mixture was then placed in a 42 °C water bath for exactly 90 seconds. Following this heat shock step, the mixture was placed back on the ice for 2 minutes before adding 200 μL of nutrient rich XYZ media and incubating at 37°C for 30-90 minutes. Following incubation, 200 μL of the solution was spread on an ampicillin-treated agar plate and left to incubate overnight at 37°C.

The plate was retrieved after 16-18 hours of incubation. Ten microliters of ampicillin were added to 10 mL of LB media in a 50 mL falcon tube for each colony selected. One colony was added to each tube using an inoculation loop, and the solution was left to shake at 37°C overnight.

After 16-18 hours of incubation the DNA was amplified using QIAprep miniprep kit as directed. The DNA obtained was sent for sequencing to Genewiz Inc. Samples with the correct sequence were expressed and used for further study.

4.3.3 Transfection in Mammalian Cells

The proteins were placed in the pcDNA3.1 vector for mammalian expression. In vivo studies were carried out in C2C12 mouse myoblast cells and HEK293 cells. The cells were cultured in high glucose DMEM buffer with 10% fetal bovine serum (FBS). The transfection reagent used to deliver the protein DNA into the cell was lipofectamine. A 1:2 μg DNA to μL lipofectamine ratio was used for EGFP based protein transfection. One milliliter of transfection solution was prepared for every dish of cells being transfected. Two tubes of 0.5 mL OPTI were prepared. The lipofectamine was added to one and the DNA to the other. The solutions were left to sit for approximately one minute at room temperature. The DNA solution was then added in its entirety to the lipofectamine solution. After using a pipette to mix the solution was centrifuged for five seconds and placed in a dark, room temperature drawer to incubate for five minutes.

For HEK293 cells the cells were previously split to the imaging slides and left to reach 40% confluency before transfection. The cells were rinsed with Hank's Balanced Salt Solution (HBSS) before adding four milliliters of OPTI buffer. After the incubation time has lapsed the transfection solution was added dropwise to the dish and left to incubate at 37 °C for four hours. The buffer was then changed to fresh DMEM and the cells left for 36-48 hours to allow protein expression.

For C2C12 cells the cells were split just before transfection. During the incubation time, the cells were rinsed with HBSS and digested in trypsin to split. The cells were transferred to the cover slips with three milliliters of DMEM buffer and one milliliter of OPTI buffer. After the

incubation time has lapsed the transfection solution was added dropwise to the dish and left to incubate at 37 °C for 24 hours. The buffer was then changed to fresh DMEM and the cells left for 36-48 hours to allow protein expression.

4.3.4 Mag-Fura-2 Cell Diffusion

Mag-Fura-2 is a high-affinity ratiometric Ca^{2+} dye designed for measurement of Ca^{2+} in the SR/ER. The acetoxymethyl (AM) ester for was used to quickly and easily load the dye into the C2C12 cells. Pluronic f-127, a nonionic compound, was used to facilitate the solubilization of the dye in the biological cell media. The cells were split onto slides and allowed to grow for 24-36 hours before dye loading. One milliliter of HBSS solution was placed in a 1-mL Eppendorf tube. To this, four microliters of 1 mM Mag-Fua-2 and two microliters of 20% pluronic f-127 was added. The dish of cells was rinsed three times with HBSS solution, and then two milliliters of HBSS added. The entire dye-pluronic-HBSS solution was added to the dish and left for incubation in a dark area for 15 minutes. The cells were gently rinsed once more and mounted for imaging.

4.3.5 Fluorescence Dynamic Range

The dynamic range is a measurement of the fluorescence intensity change from the apo to the holo form of our proteins. This characteristic was determined *in vivo* using cultured cells transfected with the tagged protein as described in section 4.3.3 or Mag-Fura-2 dye loaded as described in section 4.3.4. The slide containing the transfected cells, as outlined in section 4.3.3, was rinsed three times with 1.8 mM Ca^{2+} Ringers buffer (145 mM NaCl, 2.5 mM K_2HPO_4, 1 mM $MgSO_4$, 10 mM HEPES buffer, 10 mM glucose, 1.8 mM Ca^{2+}; pH 7.4) and mounted for imaging using the Leica microscope at 40X magnification. After ideal cells were found and focused, the experiment was carried out at 550 nm excitation in KCl rinse solution (125 mM KCl, 25 mM NaCl,

10 mM HEPES buffer, 0.2 mM $MgCl_2$; pH 7.25). The cell walls were first permeated using 25 μM digitonin. After rinsing the digitonin away with KCl rinse, 1 μM EGTA was used to empty the ER of Ca^{2+}. The cells were rinsed once more with KCl rinse and then saturated with 10 mM Ca^{2+}. The peak data was analyzed using Eq. 4.8 to determine the dynamic range.

$$DyR = \frac{F_{max}}{F_o} \qquad \textbf{Eq. 4.8}$$

4.3.6 CatchER Orientation Determination via Drug Treatment

The orientation of the membrane-targeted CatchER constructs was determined in vivo using cultured cells transfected with the tagged proteins as described in section 4.3.3. The slide containing the cells were rinsed three times with 1.8 mM Ca^{2+} Ringers buffer (145 mM NaCl, 2.5 mM K_2HPO_4, 1 mM $MgSO_4$, 10 mM HEPES buffer, 10 mM glucose, 1.8 mM Ca^{2+}; pH 7.4) and mounted for imaging using the Leica microscope at 40X magnification. After ideal cells were found and focused, the experiment was carried out at 550 nm excitation in the same 1.8 mM Ca^{2+} Ringer's solution. After the signal had become stable the cells were treated with either 200 μM 4-chloromethcathinone (4-cmc) or 400 μM caffeine, both agonist of the RyR, to induce Ca^{2+} flow out of the SR/ER. The peak was given time to recover before the agonist was rinsed off with 1.8 mM Ringer's buffer. The data was analyzed to determine the orientation of the protein.

4.4 Results

4.4.1 Dynamic Range of Mag-Fura-2 and CatchER

The Mag-Fura-2 dynamic range experiment was carried out as outlined in sections 4.3.4 and 4.3.5. No permeabilizing agent was added to this dish of cells. As shown in Figure 4-2 the

signal shows a decrease upon addition of 1 mM EGTA. After the signal baselines, the EGTA is washed off and 10 mM of Ca^{2+} is added, leading to a sharp increase in the signal. Once the signal levels off, the Ca^{2+} is washed away.

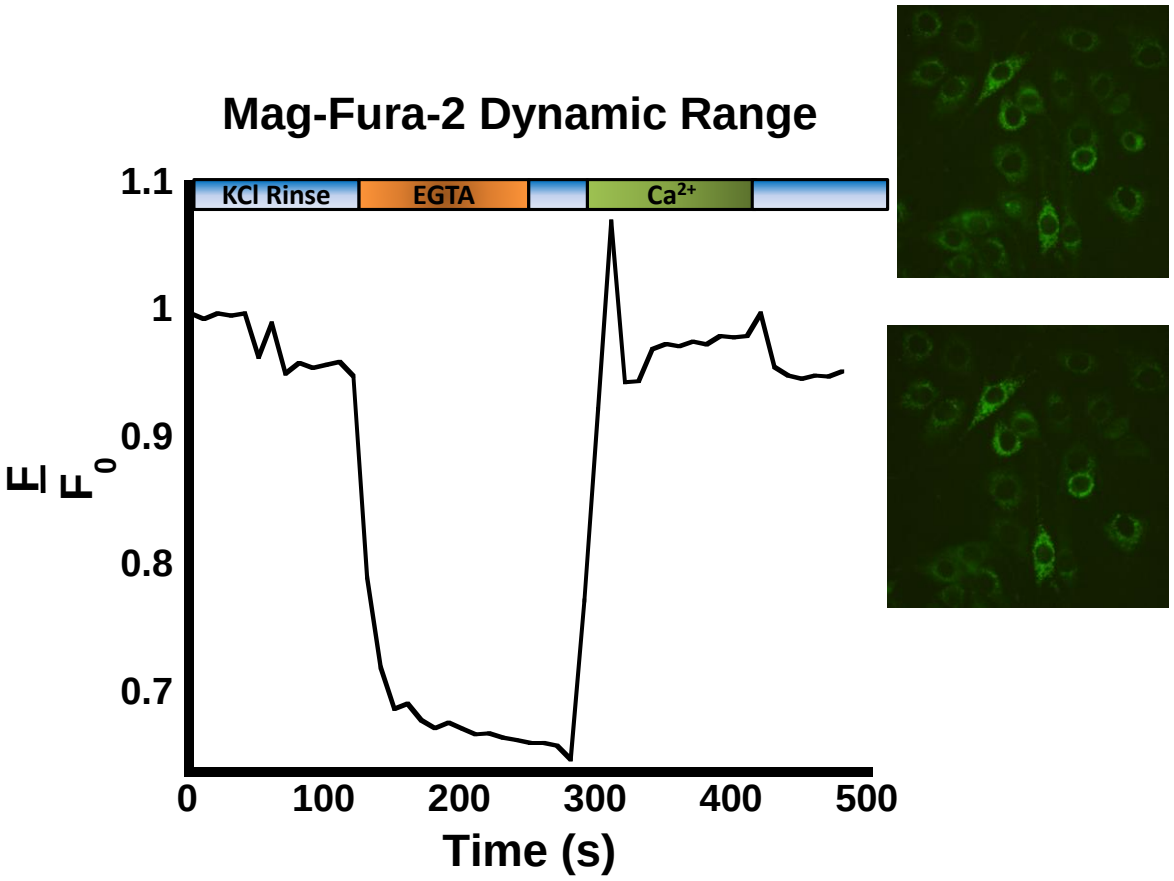

Figure 4-2 Mag-Fura-2 dynamic range

Dye was loaded in C2C12 cells using a 2:1 dye to pluoronic f-127 ratio and left to incubate in a dark space for 10 minutes. Data was obtained using the Leica inverted fluorescence microscope; 488 nm excitation; 170 gain; 0.07 exposure time. Cell images were taken before (top) and after (bottom) experiment.

The dynamic range experiment is repeated for the CatchER protein. The cells are transfected as described in section 4.3.3 with the CatchER protein being expressed at 30 ˚C instead of 37 ˚C for proper protein folding. As shown in Figure 4-3, after initial rinsing with KCl buffer the cells were permeabilized with 25 μM digitonin. The digitonin was washed off shortly

after and 1 mM EGTA was added to chelate out any free SR/ER Ca^{2+}. After rinsing off, the EGTA 10 mM Ca^{2+} was added to the cells and the signal increased.

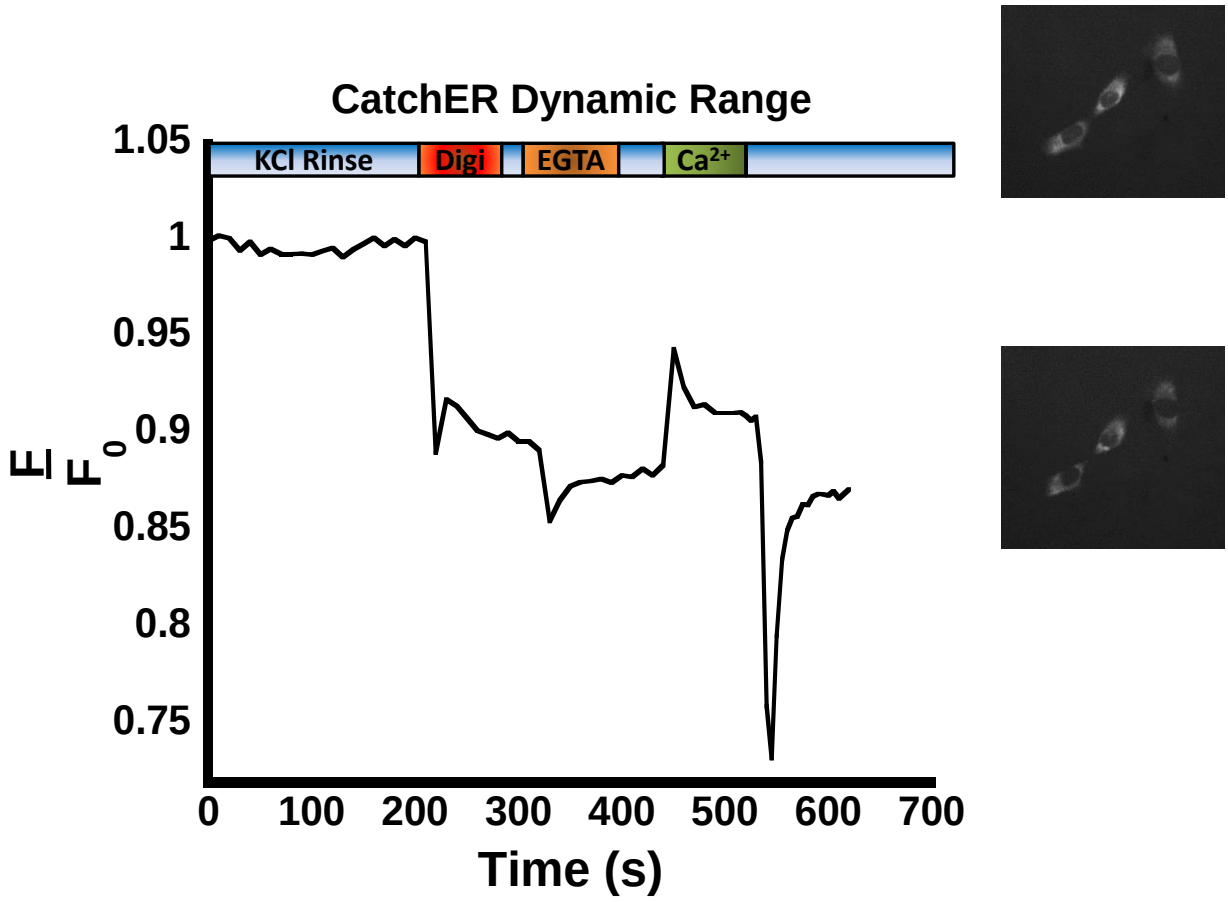

Figure 4-3 CatchER dynamic range

Protein was transfected in C2C12 cells using a 2:1 lipofectamine reagent to DNA ratio and left to express at 30 ˚C for 24-48 hours. Data was obtained using the Leica inverted fluorescence microscope; 488 nm excitation; 170 gain; 0.07 exposure time. Cell images were taken before (top) and after (bottom) experiment.

4.4.2 In Vivo Imaging of Anchored CatchER Constructs

4.4.2.1 Z10Cat in C2C12 Cells

Figure 4-4 shows the Z10Cat construct in C2C12 cells. The cells were treated first with 200 μM 4-cmc and then with 400 μM Caffeine to induce SR/ER Ca^{2+} release as described in section 4.3.5. Both drug treatments induce a decrease in the protein's fluorescence signal that recovers on its own over time.

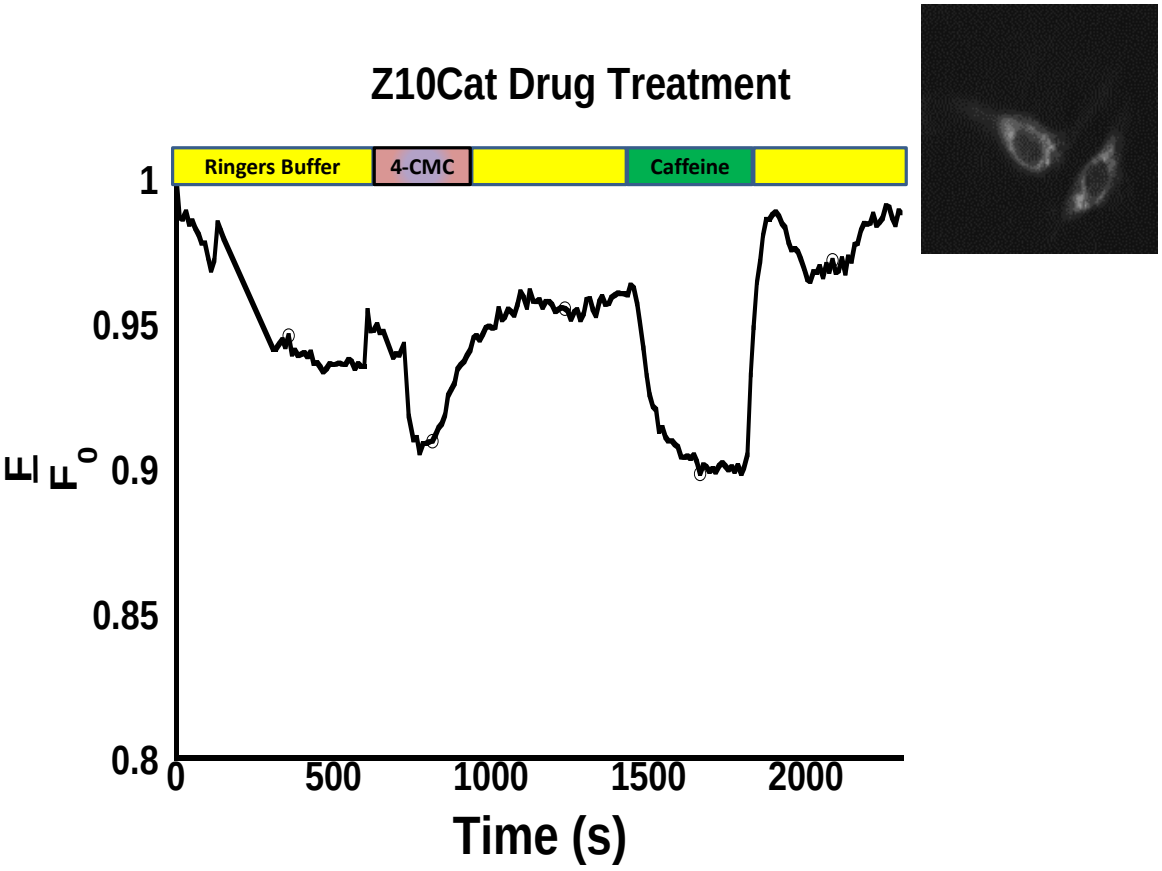

Figure 4-4 Z10Cat RyR agonist drug treatment in C2C12 cells

Protein was transfected into C2C12 cells using a 2:1 lipofectamine reagent to DNA ratio and left to express at 30 ˚C for 24-48 hours. Data was obtained using the Leica inverted fluorescence microscope; 488 nm excitation; 200 gain; 0.07 exposure time. Cell images were taken before (top) and after (bottom) experiment.

4.4.2.2 CaX in Hek293 and C2C12 Cells

Figure 4-5 shows the CaX construct in Hek293 cells and Figure 4-6 shows the CaX construct in C2C12 cells. The cells were both treated first with 200 μM 4-cmc to induce SR/ER Ca^{2+} release. Both cell types with this construct display a decrease in the fluorescence signal that partially recovers on its own over time.

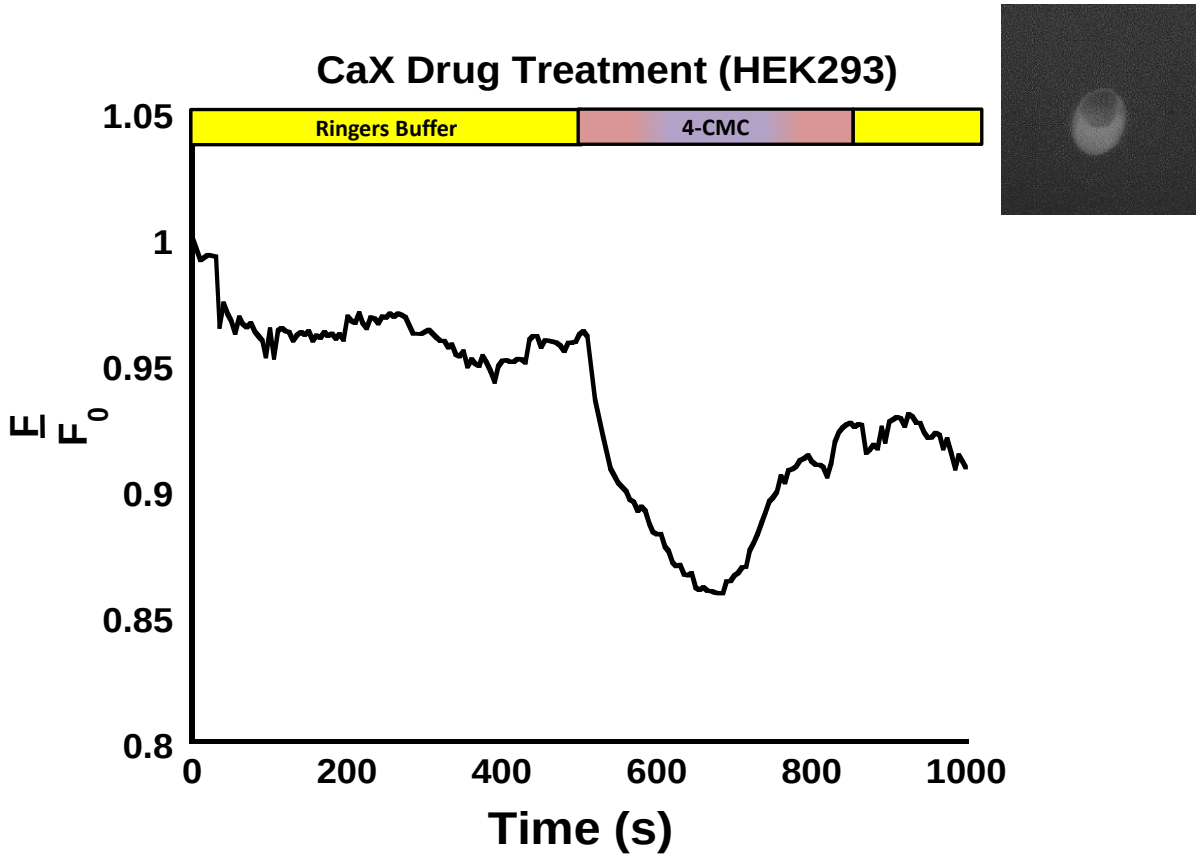

Figure 4-5 CaX RyR agonist drug treatment in Hek293 cells

Protein was transfected into Hek293 cells using a 2:1 lipofectamine reagent to DNA ratio and left to express at 30 ˚C for 24-48 hours. Data was obtained using the Leica inverted fluorescence microscope; 488 nm excitation; 200 gain; 0.07 exposure time. Cell images were taken before (top) and after (bottom) experiment.

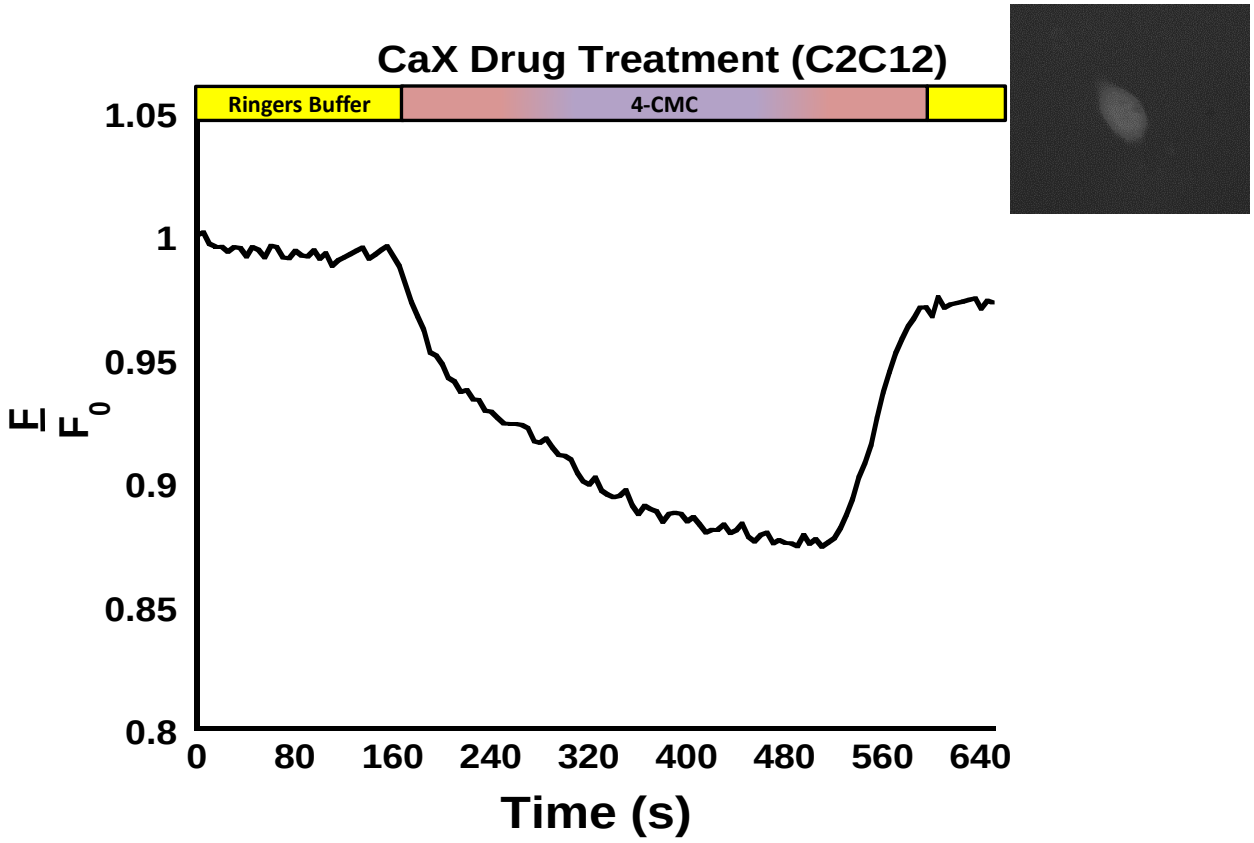

Figure 4-6 CaX RyR agonist drug treatment in c2c12 cells

Protein was transfected into C2C12 cells using a 2:1 lipofectamine reagent to DNA ratio and left to express at 30 ˚C for 24-48 hours. Data was obtained using the Leica inverted fluorescence microscope; 488 nm excitation; 200 gain; 0.07 exposure time. Cell images were taken before (top) and after (bottom) experiment.

4.4.3 Reorientation of Anchored Constructs

When making the Z10CatR construct, because the TMDs are so large four pairs of primers were needed to add them. After completing all four rounds of PCR, a DNA gel was run to determine which samples to send to sequencing. Because this construct is nearly the same in size as the Z10Cat construct, Z10Cat was used for mass comparison as shown in Figure 4-7 below. All of the samples were lower on the gel than Z10Cat, indicating that they are smaller. It was decided to send samples 1, 4, 5, and 7 for sequencing.

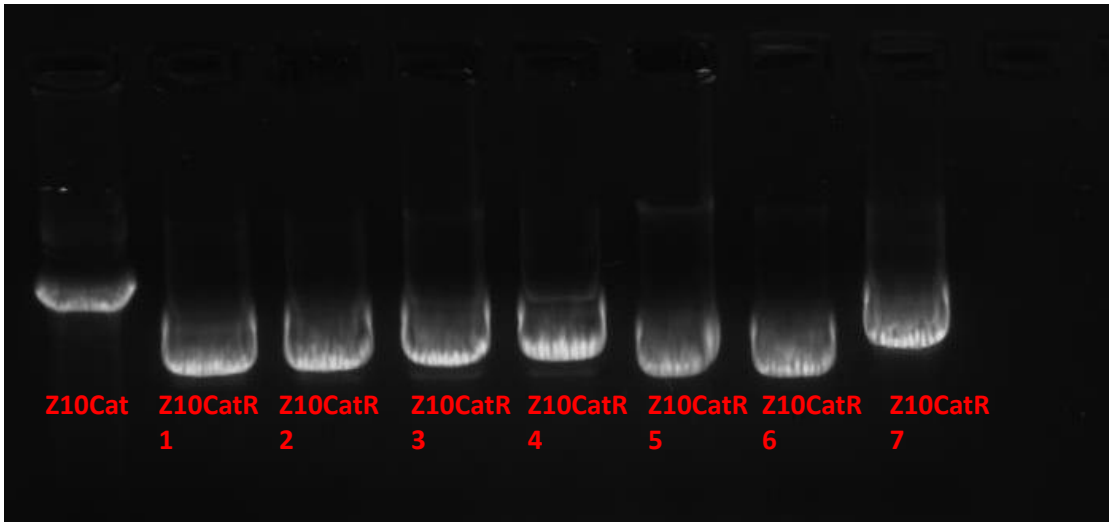

Figure 4-7 Z10CatR PCR DNA agarose gel

Ten microliters of diluted DNA from amplified PCR products of Z10CatR run in a 0.8-1.0% agarose gel. The gel was run at 70V for ~1 hour. Z10Cat was used for a size comparison.

The sequencing came back to show that half of each domain was added correctly. The second half of the domains can be added directly to these samples using the same primers. In addition to finishing this construct on CatchER, this construct will be made using the CatchER-T′ protein, an improved CatchER variant with has three thermostability mutations that allow it to express at 37 °C

4.4.4 In Vivo Imaging of Improved CatchER Variants

4.4.4.1 CatchER and CatchER-T Y49N

The RyR agonist 4-cmc was used to deplete the SR/ER Ca^{2+} store and test the response of CatchER in mammalian cells. As shown in Figure 4-8 the fluorescence signal of CatchER decreases as Ca^{2+} flows from the SR/ER into the cytosol.

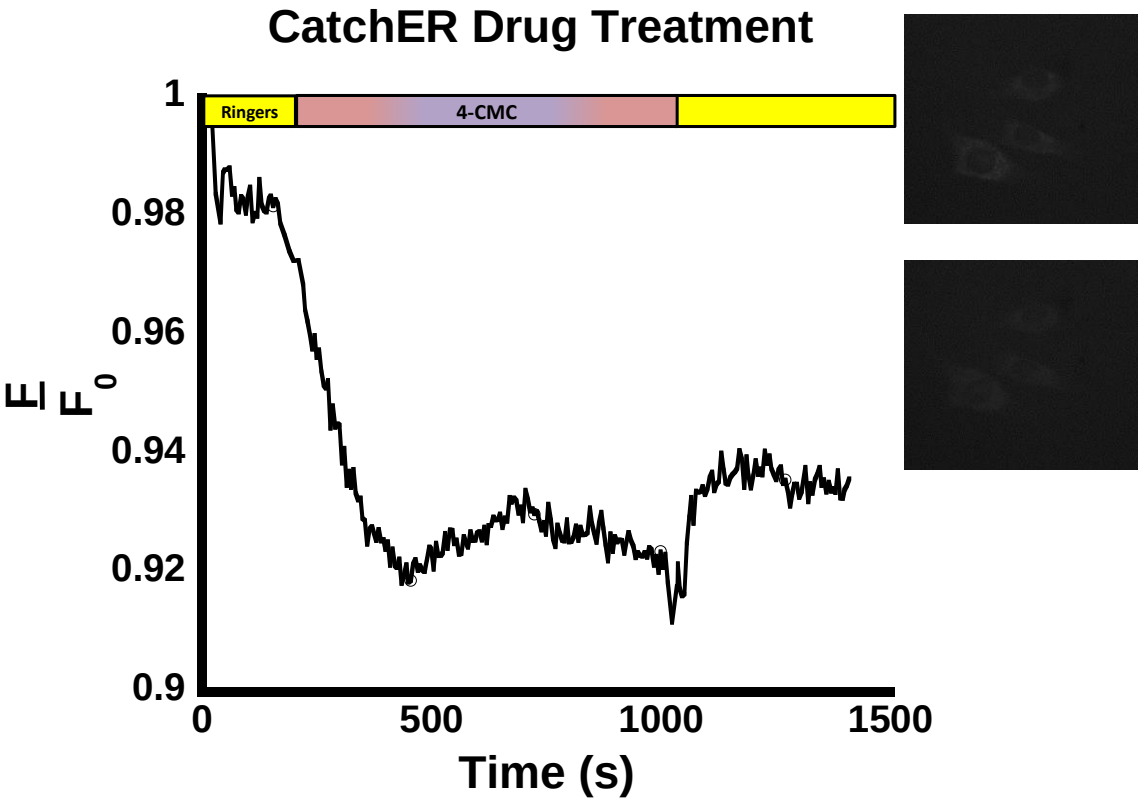

Figure 4-8 CatchER RyR agonist drug treatment in C2C12 cells

Protein was transfected in C2C12 cells using a 2:1 lipofectamine reagent to DNA ratio and left to express at 30 ˚C for 24-48 hours. Data was obtained using the Leica inverted fluorescence microscope; 488 nm excitation; 170 gain; 0.07 exposure time. Cell images were taken before (top) and after (bottom) experiment.

CatchER-T Y49N is the CatchER protein with two mutations to improve the protein's folding at 37 °C. This protein was treated with 200 μM of 4-cmc. As shown in Figure 4-9, the treatment with this drug caused a decrease in the fluorescence intensity. After ~3 minutes, the fluorescence began to recover on its own. This shows that the protein is functioning inside the ER as the decrease in the Ca^{2+} store caused a large decrease in the fluorescence intensity that began to recover as Ca^{2+} began to return to the ER. This indicates that the sensor can still function with the additional mutation.

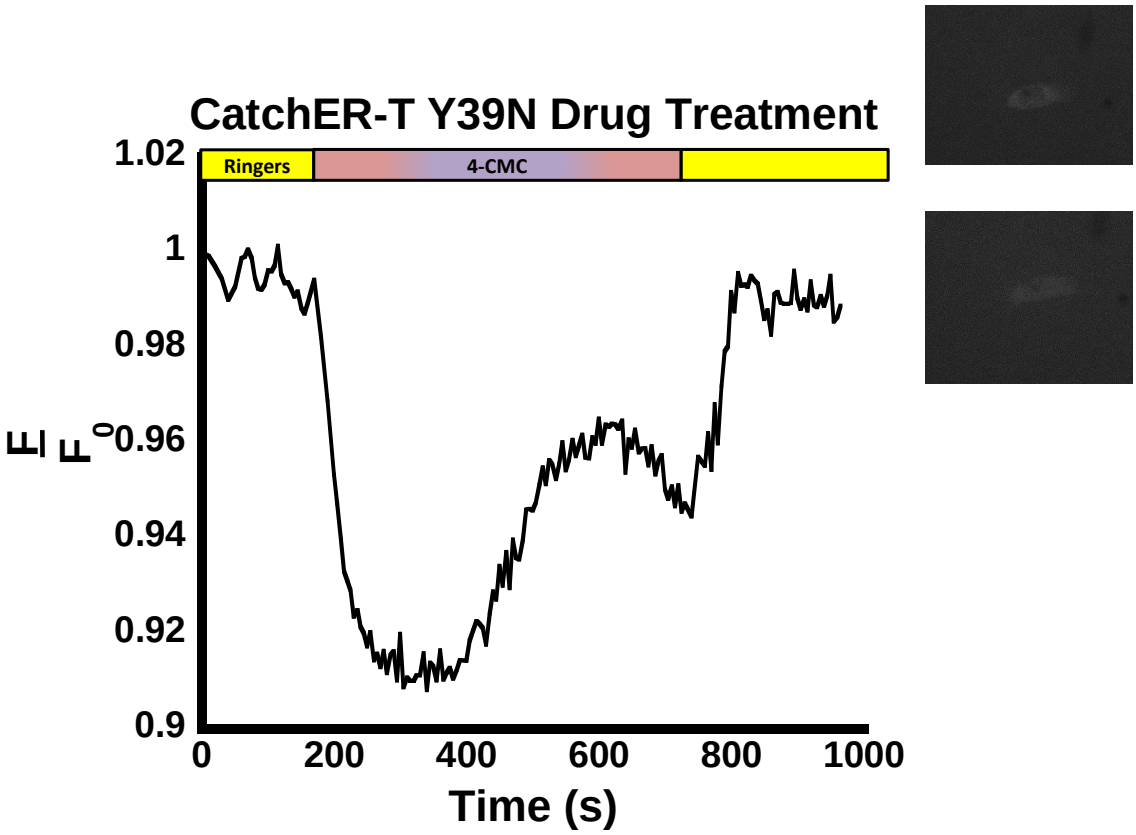

Figure 4-9 CatchER-T Y39N RyR agonist drug treatment in C2C12 cells

Protein was transfected in C2C12 cells using a 2:1 lipofectamine reagent to DNA ratio and left to express at 37 ˚C for 24-48 hours. Data was obtained using the Leica inverted fluorescence microscope; 488 nm excitation; 170 gain; 0.1 exposure time. Cell images were taken before (top) and after (bottom) experiment.

4.5 Discussion

The dynamic range conveys the change in the fluorescence of a Ca^{2+} sensor upon binding to Ca^{2+}. The larger the dynamic range, the greater the fluorescence change from apo to holo form. This value was determined for CatchER in C2C12 mouse myoblast cells by taking the fluorescence in the holo form (f_{max}) over the fluorescence in the apo form (f_{min}) as shown in Eq. 4.8 in section 4.3.5. The dynamic range for CatchER, shown in Figure 4-3, came out to be 1.04 which is 31% lower than the 1.51 of Mag-Fura-2 shown in Figure 4-2.

For the targeted constructs, designed to have CatchER anchored to the membrane of the SR/ER with an orientation toward the cytosol, the orientation was tested by transfecting the C2C12 and Hek293 cells with the targeted CatchER as described in section 4.3.3 and measuring the release of Ca^{2+} from the RyR. The RyR agonists 4-cmc and caffeine were used to induce Ca^{2+} release through the receptor from the SR/ER to the cytosol. The first construct tested was Z10Cat, which has the 10^{th} and 5^{th} TMD of RyR according to Zorzato's topology on the N and C-terminals respectively shown in Figure 4-1, in C2C12 cells. This construct is expected to express in the location of the RyR receptors and measure the expected fluorescence signal is an increase with the addition of Ca^{2+} because it should be catching the Ca^{2+} coming out of the SR/ER with the cytosolic orientation. As seen in Figure 4-4 once 4-cmc is added there is a 5% decrease that recovers after ~4 minutes. The same trend is seen with the addition of caffeine, where a 5% decrease occurs with a slower recover time of ~8 minutes.

The second construct tested is CaX, which contains the single TMD from calnexin on the N-terminal to give CatchER a cytosolic orientation, in both Hek293 and C2C12 cells. This construct is expected to express in the mitochondrial-associated endoplasmic membrane (MAM) where the calnexin protein expresses. As with Z10Cat the protein is expected to measure the Ca^{2+} present in that region after release from the SR/ER and the fluorescence signal in is expected to increase. The signal after 4-cmc treatment in Hek293 cells, shown in Figure 4-5, shows a ~10% decrease in fluorescence that partially recovers after 6.5 minutes. In C2C12 cells, Figure 4-6, there is a ~13% fluorescence decrease that recovers in 6.5 minutes as it did in Hek293. The difference between the CaX signals in these two cell lines is the amount of fluorescence recovery. In C2C12 the fluorescence recovers ~98% of the way on its own whereas in Hek293 the signal only recovers ~50% of the way.

These results indicate that there is a strong signal coming from inside the SR/ER for both anchored constructs. There are two explanations for this: overexpression of protein not yet inserted and low concentration. While these CatchER proteins do not have any ER tags on them to induce translation inside the ER, the added hydrophobic TMDs signal for translation to occur inside the ER. There are two ways that a membrane protein can be inserted into the ER membrane: post-translation where it is translated and then inserted the ER membrane and co-translation where the protein is inserted into the membrane as it is being translated. The CatchER proteins are likely being overexpressed and inserted post-translation causing a strong luminal signal. There is also the problem of low cytosolic Ca^{2+}. It was hoped that placing CatchER in the vicinity of RyR that it would be able to measure Ca^{2+} as it is released but the concentration is likely still too low for the protein's K_d. This causes the high luminal signal from the free protein to be the dominant signal we see.

Since the cytosolic constructs appear to display strong luminal signal, it was decided to change the CatchER orientation to be strictly luminal by switching the TMDs in Z10Cat so that eZ5 is on the N-terminal and Z10 is on the C-terminal, called Z10CatR. To properly add these large domains, four pairs of primers were used in four separate rounds of PCR. Primer pairs one and three add the second half of TMDs ten and five respectively. If these add correctly, then primers two and four will allow for the addition of the first half of these domains by utilizing part of the first TMD sequences as part of the annealing section. Figure 4-7 shows the DNA agarose gel for seven amplified samples after PCR with the Z10CatR construct used as a size comparison. Sequencing of four of the samples showed that half of each domain, the second half, added correctly but the first half of each did not. The PCR rounds for primers two and four are to be repeated.

In addition to testing the orientation of the targeted constructs the drug treatment experiment can also test the effect of mutations on the CatchER fluorescence. The major downside to CatchER is that it does not express well at ambient body temperature and must be expressed at 30 ˚C instead. To counteract this, mutations that have improved fluorescence in other GFP derived proteins at ambient temperature were introduced to CatchER. Dr. Shen Tang made the S175G mutation to CatchER to create CatchER-T. Florence Reddish introduced the Y39N to CatchER-T to further improve the protein folding. The fluorescence response of one of these mutants, CatchER-T Y39N, is compared to that of CatchER.

CatchER and CatchER-T Y39N, both containing calreticulin and KDEL ER retention tags on the N and C-terminal respectively, were transfected into C2C12 cells as described in section 4.3.3, 30 ˚C for CatchER and 37 ˚C for CatchER-T Y39N, and treated with 4-cmc as described in section 4.3.6. The response of CatchER to Ca^{2+} release in C2C12, shown in Figure 4-8, is compared to the response of CatchER-T Y39N shown in Figure 4-9. It is first noted that CatchER-T Y39N has fluorescence comparable to CatchER after being expressed at ambient body temperature. The fluorescence signal for both proteins decreases as expected as Ca^{2+} is released into the cytosol. For CatchER the signal decreases by ~6% and the fluorescence intensity recovers two-thirds of the way on its own. CatchER-T Y39N experiences a ~10% decrease and shows a full intensity recovery on its own. Other mutations are being made to CatchER in addition to S175G and Y39N to improve the folding and protein brightness of CatchER at 37 ˚C.

4.6 Conclusion

Once a sensor has been developed, the next step is to target it for local Ca^{2+} measurements in specific areas. For CatchER, a low-affinity Ca^{2+} sensor best suited for the

SR/ER, the target region is the membrane of the SR/ER by utilizing the TMDs of native integral proteins of the SR/ER such as RyR and calnexin. The constructs created were designed to have a cytosolic orientation but displayed luminal signal when tested with RyR agonists. This prompted a new design with a luminal orientation to be designed.

CatchER is actively being improved for its folding and fluorescence intensity at ambient body temperature as well as for membrane targeting for local Ca^{2+} measurements. The Y39N mutation to CatchER-T gave a protein with folding and fluorescence intensity at 37 ˚C that was comparable to CatchER at 30 ˚C. More mutations are being made to improve the brightness of CatchER, and these improved mutations are set to be used for the new targeting studies.

5 Significance of this work

The role of Ca^{2+} in the body is crucial for overall health and well-being. The tightly maintained dynamics of Ca^{2+} are regularly being studied and discrepancies being found to play a role in many diseases in the body. To further study how Ca^{2+} relates to these diseases the field of Ca^{2+} biosensor development has grown. This field is working to provide the need for Ca^{2+} biosensors. This work outlines the progress made to fill in the gaps that remain in the Ca^{2+} sensor field. We have worked to engineer a green EGFP based sensor for measurement of the SR/ER Ca^{2+} store and the optimize a pH insensitive red mCherry based sensor to allow for deep tissue imaging of Ca^{2+} in the SR/ER and in the more acidic organelles.

The many channelopathies of the SR/ER require a sensor with weak binding affinity and fast kinetics that has specific targeting for localization around the channel of choice. The green CatchER work includes studies on the validity of a *de novo* binding pocket creation method and work, on membrane targeting with cytosolic orientation. It was discussed in chapter 3 that a *de*

novo site could be created, eliminating the problem of intracellular protein-protein interactions seen with grafted sensors using calmodulin Ca^{2+} binding sites. Introducing negative charges into the chromophore environment to create the pocket changed the absorbance spectrum from the EGFP template spectrum to resembling that of the wtGFP spectrum with a neutral chromophore peak at 395 nm and an anionic chromophore peak at 488 nm. The amount of neutral form increased with the increasing charge while the anionic form decreased. The complete binding pocket in CatchER with the -5 charge displayed the greatest affinity for Ca^{2+} in addition to having the greatest change in fluorescence and protein brightness upon Ca^{2+} binding, making CatchER useful for intracellular measurement.

To obtain measurements for Ca^{2+} in the desired cellular environment, it is necessary to successfully target the protein to a specific organelle. Doing this would allow for Ca^{2+} dynamic measurements in the target region without interfering signal from other areas with similar Ca^{2+} concentrations. The cell already has polypeptide targeting sequences and tags for co-translation and post-translation which are commonly used for this goal, KDEL for SR/ER retention for example. These tags, however, will result in homologous expression of the protein throughout the target organelle. For disease studies, it would be useful to measure the local Ca^{2+} dynamics in the location of the suspected problem area, such as IP_3R2 in arrhythmia of atrial cells or RyR in CPVT.

Chapter 4 of this work focused on this targeting where constructs of CatchER were targeted to be anchored to the SR/ER membrane with a cytosolic orientation using transmembrane domains of RyR1 and calnexin. It was found that the constructs were displaying dominant signals from the lumen of the SR/ER when the release of SR/ER Ca^{2+} was induced with RyR agonists, possibly due to overexpression in the SR/ER and a low concentration of cytosolic Ca^{2+}

in the area of the sensor fully inserted into the membrane. Because of this, new constructs are being made to have the protein facing the luminal side of the SR/ER for Ca^{2+} measurement.

While GFP derived chromophore are commonly being used to biosensor development, they are sensitive to the pH of the environment and lack the ability to measure Ca^{2+} in the more acidic organelles such as the lysosomes. This leaves a gap in intracellular Ca^{2+} measuring capabilities. The DsRed derived mCherry protein would not have this problem with a chromophore pK_a of ~4.5 and would allow for deeper tissue penetration in imaging because of the longer wavelength excitation and emission. This protein was used to engineer a red Ca^{2+} sensor in the same way as the green CatchER. While the sensor displayed the desirable mM Ca^{2+} K_d for measurement, the fluorescent optical properties and dynamic fluorescence change with Ca^{2+} binding were weak compared to the green counterparts.

Chapter 2 describes the work to optimize these properties by attempting to change the ionization of the chromophore. It describes the effect of mutations made to residue 163 in the sensitive H-bond region of the chromophore. The Q163M mutation in both MCD1 and MCD15 sensors caused a drastic increase in both UV-Vis and fluorescence spectra for both proteins, with MCD1 Q163M surpassing the intensities of the mCherry template. The extinction coefficient and protein brightness were both greatly increased as well, showing that this mutation increased the stability and formation efficiency of the chromophore. Other mutations to this residue, including Q163L, Q163I, Q163K, Q163N, and Q163E are still being studied but do not appear to show comparable improvement in the chromophore stability. The Q163K/E/N mutations caused a loss in protein color while Q163I displayed a decrease in the protein expression yield. This project will continue with mutations in the other hot spots being made with and without the chromophore stabilizing Q163M mutation.

This work is novel in improving on fluorescent protein sensors. It provides a new method of engineering as well as strategic steps for manipulating the chromophore ionization. It is our plan to utilize the green and red sensors in new and improved ways such as local versus global Ca^{2+} measurements as well as measurements in acidic organelles of the cell.

REFERENCES

[1] Clapham, D. E. (2007) Calcium signaling, *Cell 131*, 1047-1058.

[2] Augustine, G. J. (2001) How does calcium trigger neurotransmitter release?, *Current Opinion in Neurobiology 11*, 320-326.

[3] Bers, D. M. (2002) Cardiac excitation-contraction coupling, *Nature 415*, 198-205.

[4] Whitaker, M. (2006) Calcium at fertilization and in early development, *Physiological Reviews 86*, 25-88.

[5] Gaburjakova, M., Bal, N. C., Gaburjakova, J., and Periasamy, M. (2013) Functional interaction between calsequestrin and ryanodine receptor in the heart, *Cellular and Molecular Life Sciences 70*, 2935-2945.

[6] Roderick, H. L., Berridge, M. J., and Bootman, M. D. (2003) Calcium-induced calcium release, *Current Biology 13*, R425-R425.

[7] Brzyska, M., and Elbaum, D. (2003) Dysregulation of calcium in Alzheimer's disease, *Acta Neurobiol Exp 63*, 171-183.

[8] Mikoshiba, K. (2015) Role of IP3 receptor signaling in cell functions and diseases, *Adv Biol Regul 57*, 217-227.

[9] Tsien, R. Y. (1980) New calcium indicators and buffers with high selectivity against magnesium and protons: design, synthesis, and properties of prototype structures, *Biochemistry 19*, 2396-2404.

[10] Grynkiewicz, G., Poenie, M., and Tsien, R. Y. (1985) A new generation of Ca2+ indicators with greatly improved fluorescence properties, *J Biol Chem 260*, 3440-3450.

[11] Minta, A., Kao, J. P., and Tsien, R. Y. (1989) Fluorescent indicators for cytosolic calcium based on rhodamine and fluorescein chromophores, *J Biol Chem 264*, 8171-8178.

[12] Randriamampita, C., and Tsien, R. Y. (1993) Emptying of intracellular Ca2+ stores releases a novel small messenger that stimulates Ca2+ influx, *Nature 364*, 809-814.

[13] Schultz, C., Vajanaphanich, M., Harootunian, A. T., Sammak, P. J., Barrett, K. E., and Tsien, R. Y. (1993) Acetoxymethyl esters of phosphates, enhancement of the permeability and potency of cAMP, *J Biol Chem 268*, 6316-6322.

[14] Miyawaki, A., Griesbeck, O., Heim, R., and Tsien, R. Y. (1999) Dynamic and quantitative Ca2+ measurements using improved cameleons, *Proc Natl Acad Sci U S A 96*, 2135-2140.

[15] Mank, M., and Griesbeck, O. (2008) Genetically encoded calcium indicators, *Chemical Reviews 108*, 1550-1564.

[16] Tsien, R. Y. (1998) The green fluorescent protein, *Annu Rev Biochem 67*, 509-544.

[17] Reid, B. G., and Flynn, G. C. (1997) Chromophore formation in green fluorescent protein, *Biochemistry 36*, 6786-6791.

[18] Gross, L. A., Baird, G. S., Hoffman, R. C., Baldridge, K. K., and Tsien, R. Y. (2000) The structure of the chromophore within DsRed, a red fluorescent protein from coral, *Proc Natl Acad Sci U S A 97*, 11990-11995.

[19] Shaner, N. C., Campbell, R. E., Steinbach, P. A., Giepmans, B. N., Palmer, A. E., and Tsien, R. Y. (2004) Improved monomeric red, orange and yellow fluorescent proteins derived from Discosoma sp. red fluorescent protein, *Nat Biotechnol 22*, 1567-1572.

[20] Campbell, R. E., Tour, O., Palmer, A. E., Steinbach, P. A., Baird, G. S., Zacharias, D. A., and Tsien, R. Y. (2002) A monomeric red fluorescent protein, *Proc Natl Acad Sci U S A 99*, 7877-7882.

[21] Zhou, Y., Yang, W., Kirberger, M., Lee, H. W., Ayalasomayajula, G., and Yang, J. J. (2006) Prediction of EF-hand calcium-binding proteins and analysis of bacterial EF-hand proteins, *Proteins 65*, 643-655.
[22] Zou, J., Hofer, A. M., Lurtz, M. M., Gadda, G., Ellis, A. L., Chen, N., Huang, Y., Holder, A., Ye, Y., Louis, C. F., Welshhans, K., Rehder, V., and Yang, J. J. (2007) Developing sensors for real-time measurement of high Ca2+ concentrations, *Biochemistry 46*, 12275-12288.
[23] Miyawaki, A., Llopis, J., Heim, R., McCaffery, J. M., Adams, J. A., Ikura, M., and Tsien, R. Y. (1997) Fluorescent indicators for Ca2+ based on green fluorescent proteins and calmodulin, *Nature 388*, 882-887.
[24] Romoser, V. A., Hinkle, P. M., and Persechini, A. (1997) Detection in living cells of Ca2+-dependent changes in the fluorescence emission of an indicator composed of two green fluorescent protein variants linked by a calmodulin-binding sequence. A new class of fluorescent indicators, *J Biol Chem 272*, 13270-13274.
[25] Kushnir, A., and Marks, A. R. (2010) The ryanodine receptor in cardiac physiology and disease, *Adv Pharmacol 59*, 1-30.
[26] Lehnart, S. E. (2007) Novel targets for treating heart and muscle disease - stabilizing ryanodine receptors and preventing intracellular calcium leak, *Current Opinion in Pharmacology 7*, 225-232.
[27] Filatov, V. L., Katrukha, A. G., Bulargina, T. V., and Gusev, N. B. (1999) Troponin: structure, properties, and mechanism of functioning, *Biochemistry (Mosc) 64*, 969-985.
[28] Potter, J. D., and Gergely, J. (1975) The regulatory system of the actin-myosin interaction, *Recent Adv Stud Cardiac Struct Metab 5*, 235-244.
[29] Baird, G. S., Zacharias, D. A., and Tsien, R. Y. (1999) Circular permutation and receptor insertion within green fluorescent proteins, *Proc Natl Acad Sci U S A 96*, 11241-11246.
[30] Yang, W., Jones, L. M., Isley, L., Ye, Y. M., Lee, H. W., Wilkins, A., Liu, Z. R., Hellinga, H. W., Malchow, R., Ghazi, M., and Yang, J. J. (2003) Rational design of a calcium-binding protein, *Journal of the American Chemical Society 125*, 6165-6171.
[31] Gross, L. A., Baird, G. S., Hoffman, R. C., Baldridge, K. K., and Tsien, R. Y. (2000) The structure of the chromophore within DsRed, a red fluorescent protein from coral, *P Natl Acad Sci USA 97*, 11990-11995.
[32] Verkhusha, V. V., Chudakov, D. M., Gurskaya, N. G., Lukyanov, S., and Lukyanov, K. A. (2004) Common pathway for the red chromophore formation in fluorescent proteins and chromoproteins, *Chem Biol 11*, 845-854.
[33] Subach, O. M., Malashkevich, V. N., Zencheck, W. D., Morozova, K. S., Piatkevich, K. D., Almo, S. C., and Verkhusha, V. V. (2010) Structural Characterization of Acylimine-Containing Blue and Red Chromophores in mTagBFP and TagRFP Fluorescent Proteins, *Chem Biol 17*, 333-341.
[34] Bravaya, K. B., Subach, O. M., Korovina, N., Verkhusha, V. V., and Krylov, A. I. (2012) Insight into the Common Mechanism of the Chromophore Formation in the Red Fluorescent Proteins: The Elusive Blue Intermediate Revealed, *Journal of the American Chemical Society 134*, 2807-2814.
[35] Strack, R. L., Strongin, D. E., Mets, L., Glick, B. S., and Keenan, R. J. (2010) Chromophore formation in DsRed occurs by a branched pathway, *J Am Chem Soc 132*, 8496-8505.
[36] Shu, X., Shaner, N. C., Yarbrough, C. A., Tsien, R. Y., and Remington, S. J. (2006) Novel chromophores and buried charges control color in mFruits, *Biochemistry 45*, 9639-9647.

[37] Carlson, H. J., and Campbell, R. E. (2013) Mutational analysis of a red fluorescent protein-based calcium ion indicator, *Sensors (Basel) 13*, 11507-11521.
[38] Shaner, N. C., Lin, M. Z., McKeown, M. R., Steinbach, P. A., Hazelwood, K. L., Davidson, M. W., and Tsien, R. Y. (2008) Improving the photostability of bright monomeric orange and red fluorescent proteins, *Nat Methods 5*, 545-551.
[39] Subach, F. V., and Verkhusha, V. V. (2012) Chromophore transformations in red fluorescent proteins, *Chem Rev 112*, 4308-4327.
[40] Kyte, J., and Doolittle, R. F. (1982) A simple method for displaying the hydropathic character of a protein, *J Mol Biol 157*, 105-132.
[41] Engelman, D. M., Steitz, T. A., and Goldman, A. (1986) Identifying nonpolar transbilayer helices in amino acid sequences of membrane proteins, *Annu Rev Biophys Biophys Chem 15*, 321-353.
[42] Brini, M., and Carafoli, E. (2009) Calcium pumps in health and disease, *Physiol Rev 89*, 1341-1378.
[43] Fewell, S. W., and Brodsky, J. L. (2009) Entry into the Endoplasmic Reticulum: Protein Translocation, Folding and Quality Control, *Mol Biol Intell Unit*, 119-142.
[44] Zorzato, F., Fujii, J., Otsu, K., Phillips, M., Green, N. M., Lai, F. A., Meissner, G., and MacLennan, D. H. (1990) Molecular cloning of cDNA encoding human and rabbit forms of the Ca2+ release channel (ryanodine receptor) of skeletal muscle sarcoplasmic reticulum, *J Biol Chem 265*, 2244-2256.
[45] Fujimoto, M., and Hayashi, T. (2011) New Insights into the Role of Mitochondria-Associated Endoplasmic Reticulum Membrane, *International Review of Cell and Molecular Biology, Vol 292 292*, 73-117.
[46] Williams, D. B. (2006) Beyond lectins: the calnexin/calreticulin chaperone system of the endoplasmic reticulum, *Journal of Cell Science 119*, 615-623.
[47] Schrag, J. D., Bergeron, J. J., Li, Y., Borisova, S., Hahn, M., Thomas, D. Y., and Cygler, M. (2001) The Structure of calnexin, an ER chaperone involved in quality control of protein folding, *Mol Cell 8*, 633-644.

APPENDIX

PCR program for targeting of CatchER and site mutagenesis of MCD1x mutants

Protocol for primer phosphorylation

- Spin down primer powder
- Add enough EB buffer to make 100 uM sample (for 53.4 nM use 534 μL, etc)
- Label reverse and forward tubes
- For phosphorylation of 5` end
    - PNK kit Procedure
        - Ingredients (do for each primer); total volume should be 50 μL
            - 5 μL of 10X PNK buffer
            - 1 μL of 10 mM ATP pH 7.5
            - 30 μM of Primer (for 100 □M samples: 5 μL)
            - 38 μL sterile dH_2O
            - 1 μL of PNK Enzyme
        - Incubate at 37° C for 30 minutes
        - Deactivate enzyme by putting at 65° C - 70° C for 10 minutes
- PCR procedure
    - KOD kit procedure
        - Ingredients (1 sample per PCR); total volume should be 50 μL
            - 34 μL sterile dH_2O
            - 5 μL of 10x KOD buffer
            - 3 μL 25 mM $MgSO_4$
            - 0.5 μL of each 30 μM primer (total 1 μL primer)
            - 1 μL of 10 ng/μL template DNA
            - 5 μL of 2 mM DmTP mix
            - 1 μL polymerase enzyme
    - PCR instrument
        - File and load
            - Lid- 105
            - No wait
            - 1- T = 95° C for 2 min – Hot start
            - 2- T = 95° C for 45 sec- denature cycle 1
            - 3- T = t_m -5° C for 30 sec - annealing
                - If selecting gradient
                    - Main menu-options-gradient-.02 mL tube
                    - R= 3.0° C/s (how fast)
                    - G = 4

- 4- T = 70.0° C for 3.30 min- elongation
- 5- go to step 2 – repeat 24
- 6- T = 70.0° C for 3.30 min- last elongation
- Hold at 4° C - exter
    - Exit-save yes-none, override yes
- Close lid-turn to right- hit start

- PFU kit procedure
    - Ingredients (1 sample per PCR); total volume should be 50 μL
        - 34 μL sterile dH_2O
        - 5 μL of 10x PFU buffer
        - 1 μL of each 30 μM primer (total 2 μL primer)
        - 4 μL of 20 ng/μL template DNA
        - 5 μL of 2 mM DmTP mix
        - 1 μL polymerase enzyme
- PCR instrument
    - File and load
        - Lid- 105
        - No wait
        - 1- T = 95° C for 1.5 min – Hot start
        - 2- T = 95° C for 30 sec- denature cycle 1
        - 3- T = t_m- 5° C for 1 min - annealing
            - If selecting gradient
                - Main menu-options-gradient-.02 mL tube
                - R= 3.0° C/s (how fast)
                - G = 4
        - 4- T = 72.0° C for 8 min- elongation
        - 5- go to step 2 – repeat 24
        - 6- T = 72.0° C for 8 min- last elongation
        - Hold at 4° C - exter
            - Exit-save yes-none, override yes
        - Close lid-turn to right- hit start

DNA gel -0.8% (0.8 g/100 mL)

- Make TAE buffer from 10X concentrated bottle if none made
- Need two red end pieces, clear dish, and white comb
- 35-50 mL of buffer sufficient for small holder
- Place red end pieces on either end of holder

- Prepare gel
    - Place 50 mL of 1X TAE buffer with 0.4 g of Agarose (want 0.8% - 1% so use 0.4 g - 0.5 g) in flask
    - Microwave for 50 seconds or until solution is clear
    - Add 5 μL of DNA dye(diluting 10,000 times)
    - Swirl until solution is pink and allow to cool slightly (when flask isn't hot-hot to touch)
    - Gently pour into holder and add in the white comb
    - Cover gel to cool
- Centrifuge PCR samples for a couple seconds
- To remove the gel scrape sides with syringe needle and pour on a little buffer to loosen. Remove red end piece from one end. Gently remove the white comb. Scrape other end and remove red end piece.
- Place holder in gel cassette (wells on black end) and cover to top with TAE buffer
- Make the DNA samples
    - Add dye (6X so 10 μL for the 50 μL sample). Pipette to mix
- Add 10 μL of marker (equal weight DNA) in lane 2 and each sample in lanes 4-end
- Set machine to 70 volts and start (look for bubbles on black end to ensure it's working)
- Remove once samples have reached approximately ½ way down the gel
- Check for DNA under UV light (in dark) and cut those sections out.
    - These are ~1 μg in weight
- Place in centrifuge tubes

DNA extraction

- Dissolve gel to get DNA
    - 1 tube weighs ~1 g
    - Weigh with gels in to determine the gels weight
    - Going to add 300 μL of dissolving buffer for every 100 mg of gel
    - Follow directions on kit to ligate and extract DNA
        - Typically 30 μL of solution
            - 3 μL buffer
            - ~5-15 μL DNA (however many samples)
            - 1 μL enzyme (ligase)
            - Rest water